Max-Planck Institut für Molekulare Genetik
Center for Cardiovascular Research, Charité Universitätsmedizin Berlin

Comprehensive phenotyping of two mouse mutants reveals a potential novel role of G protein-coupled receptor 30

Dissertation

zur Erlangung des akademischen Grades

doctor rerum naturalium

im Fach Biologie

eingereicht an der

Mathematisch-Naturwissenschaftlichen Fakultät I

der Humboldt-Universität zu Berlin

von Dipl.-Biologe

Luca Meoli

Präsident der Humboldt-Universität zu Berlin:
Prof. Dr. Dr. h.c. Christoph Markschies
Dekan der Mathematisch-Naturwissenschaftlichen Fakultät I:
Prof. Dr. Andreas Herrmann

Gutachter/innen:

1) Prof. Patricia Ruiz

2) Prof. Alf Hamann

3) Prof. Ulrich Kintscher

Tag der mündl. Prüfung: 03.08.2010

Ai miei genitori

Zusammenfassung

Abstract

Abbreviations

1 Introduction *1*

1.1 G protein-coupled receptors **1**
1.1.1 General considerations 1
1.1.2 G protein activation 3
1.1.3 G proteins 5

1.2 GPCRs in pharmacology **6**

1.3 G protein coupled receptor 30 **7**
1.3.1 Gpr30 signalling 7
1.3.2 Gpr30 subcellular localization and ligands 9
1.3.3 Gpr30 *in vivo* function 11

1.4 Mouse genome manipulations: transgenic and knockout mice **17**
1.4.1 Transgenic mice 17
1.4.2 Knockout mice 18
1.4.2.1 ES cells and gene targeting strategies 18
1.4.2.2 1.4.2.2 The chimera and its offspring 20
1.4.2.3 Recombinase based approaches 21

1.5 GPCR knockout mice **23**
1.5.1 Gpr30-T181 Deltagen mice 23
1.5.2 SHG17 Artemis mice 25

1.6 Phenotyping strategies **26**
1.6.1 Primary screen 26
1.6.2 Secondary screen 28

1.7 Estrogen receptors in metabolic diseases and associated cardiovascular disorders **29**

1.8 High fat diet mouse model **32**

1.9 Assessment of endocrine and cardiovascular function in mice **34**

2 Aims of the study *37*

3 Materials and Methods *38*

3.1 Gpr30 mutant mouse models **38**
3.1.1 Gpr30-T181 Deltagen mice 38
3.1.2 SHG17 Artemis mice 39
3.1.3 Genotyping of Gpr30-T181 Deltagen mice 39
3.1.3.1 Materials 39
3.1.3.2 Method 41
3.1.4 Southern Blotting 42
3.1.4.1 Materials 42
3.1.4.2 Method 43
3.1.5 RNA extraction 44
3.1.5.1 Materials 44
3.1.5.2 Method 45
3.1.6 Reverse transcription 45
3.1.6.1 Materials 45
3.1.6.2 Method 45
3.1.7 Real Time PCR 46
3.1.7.1 Materials 46
3.1.7.2 Method 46
3.1.8 SHG17 Artemis mice genotyping 47
3.1.8.1 Materials 47

3.1.8.2 Method 47
3.2 Primary screen 48
3.2.1 Microarray RNA analysis 49
3.2.1.1 Materials 49
3.2.1.2 Method 49
3.3 Secondary screen 52
3.3.1 Groups 52
3.3.2 Diets 53
3.3.2.1 Materials 53
3.3.2.2 Method 53
3.3.3 Body weight and body mass composition 54
3.3.3.1 Materials 54
3.3.3.2 Method 54
3.3.4 Intraperitoneal glucose tolerance test (IPGTT) 54
3.3.4.1 Materials 54
3.3.4.2 Method 54
3.3.5 Echocardiography 56
3.3.5.1 Materials 56
3.3.5.2 Method 56
3.3.6 Electrocardiogram (ECG) 64
3.3.6.1 Materials: 64
3.3.6.2 Method 64
3.3.7 Blood chemistry 66
3.3.7.1 Materials 66
3.3.7.2 Method 66
3.3.8 Mouse housing 66
3.4 Statistical analysis 67
3.4.1 Materials 67
3.4.2 Method 67
4 Results 68
4.1 Gpr30 mutant mouse models 68
4.2 Molecular characterization of Gpr30-T181 Deltagen mice 68
4.2.1 Genotyping 68
4.2.2 Southern blotting 69
4.2.3 Real Time PCR 70
4.3 SHG17 Artemis mice genotyping 72
4.4 Gpr30-T181 Deltagen mice phenotypic assessment 73
4.4.1 Primary screen 73
4.4.2 Secondary screen 80
4.4.2.1 Body weight and body mass composition 81
4.4.2.2 Intraperitoneal Glucose Tolerance test (IPGTT) 82
4.4.2.3 Echocardiography 84
4.4.2.4 Blood chemistry 87
4.5 SHG17 Artemis mice phenotypic assessment 92
4.5.1 Thymus gene expression 93
4.5.2 Body weight and body mass composition 94
4.5.3 Intraperitoneal glucose tolerance test 96
4.5.4 Echocardiography 97
5 Discussion 98
5.1 Gpr30 mutant mouse models 98
5.2 Primary screen 99
5.2.1 Immunological screen 99
5.2.2 Behavioural screen 102

5.3 Secondary screen **103**
5.3.1 Metabolic screen 103
5.3.2 Cardiovascular screen 104
5.3.3 Clinical chemistry 105
5.4 An estrogen receptor can do more **108**
5.5 Conclusions and outlook **110**
References ***114***
Table of Figures ***123***
List of Tables ***124***
Acknowledgements ***125***
Eidesstattliche Erklärung ***126***
Publications ***127***
Abstracts ***128***

Zusammenfassung

In den späten neunziger Jahren wurde der G Protein-gekoppelte Rezeptor 30 (Gpr30) von verschiedenen, unabhängigen Forschungsgruppen kloniert. Der Rezeptor zeigte eine hohe Homologie mit dem Interleukin Rezeptor 8. Anfangs wurde ein Chemokin als potentieller Ligand angenommen. Allerdings konnten nachfolgende Untersuchungen die Chemokinligand-Hypothese nicht bestätigen. Im Folgenden wurde in einer Genexpressions-analyse von Brustkrebszellen Östrogen als neuer potenzieller Gpr30-Ligand für schnelle Östrogen-vermittelnde Effekte identifiziert. Dieser Befund wird kontrovers diskutiert, da verschiedene Studien gegen eine Rolle von Gpr30 in der Östrogensignaltransduktion sprechen. Zudem wurde die physiologische Funktion von Gpr30 bisher noch nicht vollständig geklärt, u.a. weil nur wenige Untersuchungen *in vivo* Modelle verwenden.

Ziel der vorliegenden Arbeit war die Erforschung der Rolle von Gpr30 *in vivo*. In einer primären und sekundären Untersuchung wurde eine phänotypische Charakterisierung der Deltagen-Gpr30-defizienten Mäuse vorgenommen. Diese Mauslinie wurde generiert, indem eine β-Galactosidase-Neomycin Vektorkassette in den *open reading frame* des Gpr30 Gens eingesetzt wurde. Die primäre Untersuchung beinhaltete Analysen verschiedener Aspekte der Mausphysiologie. Gegenstand der sekundären Untersuchung war die Bestimmung eines möglichen metabolischen und kardiovaskulären Phänotyps, da Gpr30 überwiegend in den Blutgefäßen verschiedener Organe, sowie iin der Pankreas und im Magen exprimiert ist. Zu diesem Zweck wurden die Mäuse einer Hochfettdiät unterzogen und es wurden metabolische sowie hemodynamische Tests durchgeführt. Um den Phänotyp dieser ersten Mauslinie zu bestätigen, wurde eine zweite Mauslinie ohne Selektionsmarker generiert (Artemis Mäuse).

Im Rahmen der primären Untersuchung zeigte die immunologische Analyse eine Reduzierung der T-Zellen sowohl bei den männlichen als auch bei den weiblichen mutanten Mäusen. In einer Thymus-Genexpressionanalyse konnten einige Gene identifiziert werden, die möglicherweise in der Regulation der Anzahl an T-Zellen involviert waren. Auf der Grundlage dieser Ergebnisse wurde eine Erhöhung der Kalzium-vermittelten T-Zellen Apoptose hypothetisiert. In der vorliegenden Arbeit wurde erstmals eine echokardiographische Untersuchung an Gpr30-defizienten Mäusen durchgeführt und es konnte eine potenzielle Beeinträchtigung des *Cardiac Output* bei weiblichen mutanten Mäusen im Alter von sechs Monaten festgestellt werden. Da die Ergebnisse der ersten

Mausmutanten mit den zweiten, unabhängigen Artemis-Mausmutanten nicht reproduziert werden konnten, lässt sich ein Effekt der Selektionsmarker als Ursache des beobachteten Phänotyps nicht ausschließen.

In der sekundären Untersuchumg konnte aufgrund metabolischer Tests an beiden Mauslinien der Einfluss von Gpr30 auf die Glukose-*Clearance*, die Adipositas und die Regulation des Körpergewichts ausgeschlossen werden. Nach zwanzig Wochen der Hochfettdiät war das Plasmalevel von Cholesterin, *High Density Lipoprotein* und Kreatinkinase bei den weiblichen Mutanten signifikant niedriger als bei Kontrollmäusen. Dies lässt einen Einfluss von Gpr30 auf den Lipid- und Muskelstoffwechsel vermuten. Die männlichen Mutantmäuse zeigten hingegen ein signifikant niedrigeres Level der Alkalischen Phosphatase, welches möglicherweise auf eine präventive hepatische Funktion trotz der Hochfettdiät hindeutet.

Insgesamt tragen die Ergebnisse der vorliegenden Studie zu einem besseren Verständnis der Funktion von Gpr30 *in vivo* bei. Eine Rolle des Rezeptors bezüglich der Regulation des Körpergewichts konnte widerlegt werden, während ein Einfluss auf den Lipid- und Muskelstoffwechsel angenommen werden kann. Zudem wurde gefunden, dass Gpr30 für einige Östrogen-regulierende, physiologische Prozesse nicht erforderlich ist.

Abstract

Recent studies identified the G protein-coupled receptor 30 (Gpr30) as a potential new estrogen receptor. However, these findings still remain controversial and the physiological role of Gpr30 has not been clarified yet. In order to decipher the role of Gpr30 *in vivo*, we investigated the phenotype of two different Gpr30 mutant mouse lines, in a primary and a secondary screen. The first mouse line was generated by the insertion of a LacZ-neomycin cassette into the Gpr30 open reading frame. The primary screen involved different analysis in many areas of mouse physiology. It revealed a decrease of T cell levels in both male and female mutants. Thymus gene expression analysis allowed to detect some of the genes potentially involved in regulating T cell levels in these mice. On this basis a hypothesis of an increase in T cell calcium-mediated apoptosis was formulated. The secondary screen aimed at unraveling a potential metabolic and cardiovascular phenotype, being Gpr30 mainly expressed in the vasculature of several organs, as well as in the pancreas and in the chief gastric cells of the stomach. Therefore, mice were challenged with a defined high fat diet (HFD), and metabolic and hemodynamic tests were performed.

To confirm the phenotype achieved in this first mouse line, a second one was generated devoid of any selection marker. Since the results obtained in the first set of mutants could not be reproduced in the second one, an effect of the selection marker in determining the observed phenotype can not be excluded. Metabolic tests on both mutant lines excluded a role of Gpr30 in glucose clearance, adiposity and body weight regulation. After 20 weeks of HFD, total cholesterol, high density lipoprotein, and creatine kinase plasma levels were significantly lower in mutant females as compared to controls, suggesting an involvement of Gpr30 in lipid and muscle metabolism. Moreover, mutant males showed lower levels of alkaline phosphatase, potentially indicating a preserved hepatic function in these mice despite HFD.

Altogether the results achieved may contribute to a better understanding of Gpr30 function *in vivo*, disproving a role of Gpr30 in body weight regulation, suggesting a role in lipid and muscular metabolism, and providing evidence that Gpr30 may not be required for several estrogen-regulated physiological processes.

Abbreviations

AC	adenylyl cyclase
ADP	adenosine diphosphate
AMP	adenosine monophosphate
AoVel	aortic blood velocity
AP	alkaline phosphatase
BSA	bovine serum albumin
cAMP	cyclic 3´,5´-cyclic monophosphate
cGMP	cyclic guanosine monophosphate
CK	creatine kinase
Cre	cre recombinase
CSPD	cloro-5-substituted adamantyl-1,2-dioexetane phosphate
DIO	diet-induced obesity
DNA	deoxyribonucleic acid
DNase	deoxyribonuclease
dNTP	deoxynucleotide triphosphate
DPN	diarylpropionitrile
dUTP	deoxyuridine triphosphate
E2	estradiol
EDTA	ethylenediaminetetraacetic acid
EF	ejection fraction
eNOS	endothelial nitric oxide synthase
ER	estrogen receptor
ERKO	estrogen receptor knockout
FS	fractional shortening
G	G protein subunit
GDP	guanosine diphosphate
GFP	green fluorescent protein
GMP	guanine monophosphate
GPCR	G protein-coupled receptor
Gpr30	G protein-coupled receptor 30, mouse denomination
GTP	guanosine triphosphate
HDL	high density lipoprotein
HFD	high fat diet
HIV	human immunodeficiency virus
HPRT	hypoxanthine phosphoribosyl transferase
IPGTT	intraperitoneal glucose tolerance test
IRES	internal ribosomal entry site
K_i	dissociation constant
KO	knockout
LacZ	β-galactosidase gene
LDL	low density lipoprotein
LoxP	locus of crossover x in P1
LV	left ventricle
LVIDd	left ventricular internal diameter in diastole
LVIDs	left ventricular internal diameter in systole
Neo^r	neomycin resistance
NMR	nuclear magnetic resonance
NO	nitric oxide

OD	optical density
ORF	open reading frame
Ovx	ovariectomized
PCR	polymerase chain reaction
PGK	phosphoglycerate kinase
PI3K	phosphatidylinositol 3-kinase
PIP3	phosphatidylinositol 3,4,5-triphosphate
PK	protein kinases
PKA	protein kinase A
PKC	protein kinases C
PL	phospholipase
PLC	phospholipase C
PLD	phospholipase D
RNA	ribonucleic acid
RNase	ribonuclease
ROS	reactive oxygen species
SAM	significance analysis of microarrays
SDS	sodium dodecyl sulfate
SSC	saline-sodium citrate
SV40 pA	SV40 polyadenylation site
TBE	tris-borate-EDTA solution
TE	tris-EDTA
TK	thymidine kinase
Tris	tris(hydroxymethil)-aminomethane

1 Introduction

1.1 G protein-coupled receptors

1.1.1 General considerations

G protein-coupled receptors (GPCRs) are the largest known gene superfamily of the human genome accounting in particular for about 2% of the human genome (1). The characteristic feature of all known G protein-coupled receptor proteins is that they have seven hydrophobic stretches of 20-25 amino acids α-helical transmembrane (TM) domains, connected by alternating extracellular and intracellular loops. GPCRs are also known actually as seven transmembrane (7TM) receptors. There are extensive amino acid sequence similarities that divide them into several classes, each with characteristic highly conserved residues distributed throughout the molecule. An example is represented by the DRY motif at the cytoplasmic end of the third transmembrane domain and the prolines at specific positions in helices 5, 6 and 7, common characteristics to the GPCR class related to rhodopsin. All GPCRs, with the exception of the melatonin receptor are glycoproteins, and all contain at least one N-glycosilation site in the extracellular N-terminus of the receptor. In addition GPCR contain a number of conserved cysteines (Cys). There are two highly conserved Cys residues in the second and third extracellular loops of the receptors. An additional highly conserved Cys residue is found within the C-terminal tail of many GPCRs (2).

GPCR are responsible for the transduction of endogenous signals into an intracellular response. The binding of a ligand on the cell surface causes the GPCR to become active and subsequently bind and activate ubiquitous guanine nucleotide-binding regulatory (G) proteins within the cytosol. The GPCR protein's association with the heterotrimetic G-protein complex causes the GDP bound to the Gα subunit to be exchanged for GTP. The Gα-GTP complex then dissociates from the Gβγ subunit, freeing the Gα subunit to couple to an effector enzyme. An extremely heterogenous set of molecules can act as GPCR ligands including ions, hormones, neurotransmitters, peptides, and proteins. Sensory GPCR can also be activated by stimuli such as light, taste or odour. More than one type of GPCR can interact with more than one kind of G-protein creating a complex system involving a variety of mechanisms. GPCRs control and/or affect physiological processes as diverse as neurotransmission, cellular metabolism, secretion, cellular differentiation, and inflammatory responses. Based on sequence homology and functional similarity GPCRs can be grouped into 6 classes: class 1 or

A: rhodopsin like receptors, class 2 or B: secretin receptor family, class 3 or C: metabotropic glutamate receptors, class 4 or D: fungal mating pheromone receptors, class 5 or E: cAMP receptors, class 6 or F/S: frizzled/smoothened receptors. Class A receptors account for over 80% of all GPCRs and represent the largest class of human receptor. There are at least 286 human non-olfactory class A receptors, the majority of which bind peptides, biogenic amines, or lipid-like substance (2). The binding of endogenous peptides has an important role in mediating the effects of a wide variety of neurotransmitters, hormones, and paracrine signals. Receptors that bind biogenic amines e.g., norepinephrine, dopamine, and serotonin, are very commonly modulated by drugs. Pathological conditions, including Parkinson´s disease, schizophrenia and drug addiction, are examples of where imbalances at the level of biogenic amines cause altered brain function. Class B receptors bind the large peptides such as secretin, parathyroid hormone, glucagons, glucagons-like peptide, calcitonin, vasoactive intestinal peptide, growth hormone-releasing hormone, and pituitary adenylyl cyclase (AC) activating protein. Metabotropic glutamate receptors (mGluRs), a type of glutamate receptors, are activated through an indirect metabotropic process. Like all glutamate receptors, mGlusRs, bind to glutamate, an amino acid that functions as an excitatory neurotransmitter. In humans, mGluRs are found in pre- and postsynaptic synapses of the hippocampus, cerebellum and cerebral cortex, as well as in other parts of the brain and peripheral tissues. Class 4 receptors bind pheromones, used by organisms for chemical communication. cAMP receptors are part of chemotactic signalling systems. Frizzled receptors are necessary for Wnt binding while the smoothened receptors mediate hedgehog signalling. The six different classes can further be divided into families and sub-subfamilies based on the function of the GPCR and the specific ligand that it binds (3-6).

Along with the elucidation of the human genome in 2001 many new members of the 7TM GPCR target family became “visible” at the DNA sequence level, and advanced gene-expression analysis and bioinformatics methods became available for function and classification purposes. A recent comparative analysis of the human and mouse non-olfactory/non-sensory GPCRs (endo-GPCRs) repertoire, revealed 367 humans and 392 mouse GPCRs; 343 were found to be common to both species (7). Of the 367 human GPCRs, 284 belong to the rhodopsin-like class A, 50 to secretin receptor like class B, 17 to class C and 11 to the frizzled-smoothened receptors class. Among the 392 mouse GPCRs, 313, 47, 17 and 10 belong to classes A, B, C and F/S respectively. Two hundred twenty four human and 214 mouse GPCRs have a known ligand. The remaining 143 human and 178 mouse GPCRs have

no known ligands and are therefore considered orphan receptors. Among the orphan receptors, 98 human and 136 mouse receptors belong to class A, 34 human and 31 mouse receptors belong to class B, six receptors belong to class C in both species, and none belongs to class F/S.

1.1.2 G protein activation

Heterotrimeric G proteins are composed of three subunits, α, β and γ, and their switching function depends on the ability of the G protein α-subunit (Gα) to cycle between an inactive GDP-bound conformation, primed for interaction with an activated receptor, and an active GTP-bound conformation modulating the activity of downstream effector proteins. In humans, there are 21 Gα subunits encoded by 16 genes, 6 Gβ subunits encoded by 5 genes, and 12 Gγ subunits. Heterotrimers are typically divided into four main classes based on the primary sequence similarity of the Gα subunit: $G\alpha_s$, $G\alpha_i$, $G\alpha_q$ and $G_{\alpha 12}$ (8). Many crystal structures of these proteins have been resolved in various conformations providing the framework for understanding the biomechanics of G protein signalling (9, 10). In addition to bovine rhodopsin, the crystal structures of other three G-protein-coupled receptors such as β1 and β2-adrenergic receptor, and the A_{2A} adenosine receptor have been solved, providing high-resolution structural data on the transmembrane bundle of any GPCR (11-13). The structures of the Gα subunit reveal a conserved protein fold that is composed of a GTPase domain and a helical domain. The GTPase domain is conserved in all members of the G protein superfamily, including monomeric G proteins and elongation factors. This domain hydrolyses GTP and provides the binding surfaces for the Gβγ dimer, GPCRs and effector proteins. The Gβ subunit has a seven–bladed β propeller structure that is composed of seven WD40 sequence repeats. The N-terminus of Gβ adopts an α–helical conformation that forms a coiled-coil with the N terminus of Gγ. Although most of Gβ subunits can interact with most Gαγ subunits not all of the 72 possible dimer combinations occur (14). Additionally several Gβγ dimers can interact with the same Gα isoform (15).

Receptors are a physical conduit for the transmission of chemical signals across the cell membrane. Agonists bind to the extracellular surface of a GPCR and induce a conformational change that leads to G protein activation. Receptors bind ligands in various different ways (16). The small molecules that activate some rhodopsin family members bind deep within the transmembrane helix bundle, peptide ligands bind both within the transmembrane helices and on the extracellular loops. Large glycoproteins hormones, such as thyroid-stimulating

hormone, bind to the large N-terminal leucine-rich repeat domain, which positions the appropriate ligand to interact with the extracellular loops. Regardless of the mode of ligand binding, the common result is a conformational change in the cytoplasmic domain of the receptor.

Two opposing models have been presented to explain how G proteins encounter activated receptors. In the "collision coupling" model, these interactions occur as a result of free lateral diffusion within the plasma membrane, wherein G proteins only interact with activated receptors (17). The alternative model suggests that G proteins can interact with receptors before agonist binding so that they are "pre-coupled". Much of the recent data in favour of the pre-coupling receptor hypothesis comes from Fluorescence Resonance Energy Transfer (FRET) studies (18, 19). Whether the first or the second proposed model is the right one is not yet clarified. Further complexity is provided by the accumulating evidence that rhodopsin family GPCRs may form homo- and hetero-dimers (20, 21). Dimerization has also been demonstrated in glutamate family receptors; in particular the γ aminobutyric acid type B ($GABA_B$) receptor was one of the first GPCRs shown to function as a heterodimer (22). However, the importance of receptor dimerization in G protein signalling remains a contentious issue. Relatively few types of G proteins transduce signals from a vast number of GPCRs, and so each member of the G protein family must be able to interact with many different receptors. Indeed different agonists can affect which G proteins are activated by a given receptor (23).

The complexity of GPCR signalling is particularly enriched by the mechanisms underlying the GDP release phase. Some models for instance identify in the interaction between Gα and Gβγ a crucial role in G protein activation. It has been shown that mutations in the C-terminus of Gγ increase receptor-catalysed nucleotide exchange (24). Physiologically, the receptor–G protein complex is transiently due to rapid binding of GTP, whose cellular concentration exceeds that of GDP several fold. Binding of GTP to the Gα subunits causes a structural rearrangement of Gα (GTP), Gβγ and the receptor, which allows the dissociation from the receptor and the interaction with the effector. Indeed the kinetics of G protein activation can be different depending on the G proteins involved. It is known for instance that G_t turnover rates compared with other signalling systems is markedly faster (10).

1.1.3 G proteins

G proteins are activated to engage effectors and stimulate cascades resulting in diverse biological responses. The G_s family includes G_s and the olfactory G_{olf} which are both constitutively activated by cholera toxin through ADP ribosylation of their α subunit. Common to G_s family member is their capability to activate AC, and thereby causing an increase in intracellular 3´,5´-cAMP. The G_i family is most diverse, and consists of $G\alpha_{i1}$, $G\alpha_{i2}$, $G\alpha_{i3}$, $G\alpha_o$, $G\alpha_{t\text{-}r}$, $G\alpha_{t\text{-}c}$, $G\alpha_g$, and $G\alpha_z$. Rod transducin $G\alpha_{t\text{-}r}$, cone transducin $G\alpha_{t\text{-}c}$ and gusducin $G\alpha_g$ are involved in the transduction of visual and taste signals. All G_i family members are sensitive to inhibition by pertussin toxin via ADP ribosylation of their α subunit except $G\alpha_z$. This prevents their coupling to GPCRs, and hence their activation. $G\alpha_{1\text{-}3}$, $G\alpha_o$ and $G\alpha_z$ inhibit the activity of AC. The sensory G_i protein $G\alpha_g$ activates PLC-β and induces the increase of intracellular Ca^{2+}, whereas $G\alpha_{t\text{-}r}$ and $G\alpha_{t\text{-}c}$ activate the cyclic cGMP-dependent phosphodiesterases (PDE) 8, causing a decrease in intracellular cGMP and hyperpolarization of photocells via cGMP-gated ion channels. The G_q family includes $G\alpha_q$, $G\alpha_{11}$, $G\alpha_{14}$ and $G\alpha_{15/16}$. All members lead to the activation of the four PLCβ isoforms ($PLC\beta_{1\text{-}4}$) and hence cause activation of PKC and intracellular Ca^{2+} mobilization. $G\alpha_q$, $G\alpha_{11}$ are ubiquitously expressed, whereas the expression of $G\alpha_{14}$ is more restricted. $G\alpha_{15}$ and $G\alpha_{16}$ are solely found in hematopoietic cells. The $G\alpha_{12}$ family consists of the ubiquitously expressed $G\alpha_{12}$ and $G\alpha_{13}$ proteins. Both activate the small GTPase Rho, which can cause downstream activation of c-Jun N-terminal kinase (JNK) and PLD (25, 26). The activity of Gα proteins is regulated by protein modification, such as phosphorylation, N-terminal myristoylation ($G\alpha_i$ proteins) and internal palmitoylation (26). Effectors regulated by Gβγ dimers are PLCβ, ACs, phosphoinositide 3-kinase (PI3K), and G protein-inwardly-rectifying K^+ channels (GIRKs).

1.2 GPCRs in pharmacology

The ability of GPCRs to mediate the signalling of a wide and extremely differentiate range of molecules makes this kind of protein involved in the physiological regulation of virtually every cell and tissue. GPCRs are actually a privileged target for therapeutic agent development (Fig. 1.1). They are used in the treatment of many different diseases in every major organ of the body including the central nervous, cardiovascular, reproductive, respiratory, metabolic and urogenital systems. In relation to the metabolic and cardiovascular systems along with related diseases (e.g. diabetes, or heart failure) some of the most successful drugs targeting GPCRs include: β-blockers acting at cardiac β1/2 adrenergic receptors to treat cardiac failure, hypertension and coronary heart disease; angiotensin-receptor 1 (AT1) antagonists able to prevent diabetes-induced renal damage, hypertension, and heart failure; cannabinoids-receptor 1 (CB1) antagonist rimonabant to treat obesity; glucose-dependent insulinotropic polypeptide 1 (GLP1) analogues (e.g. exenatide) used in the treatment of diabetes type 1 and 2 (27).

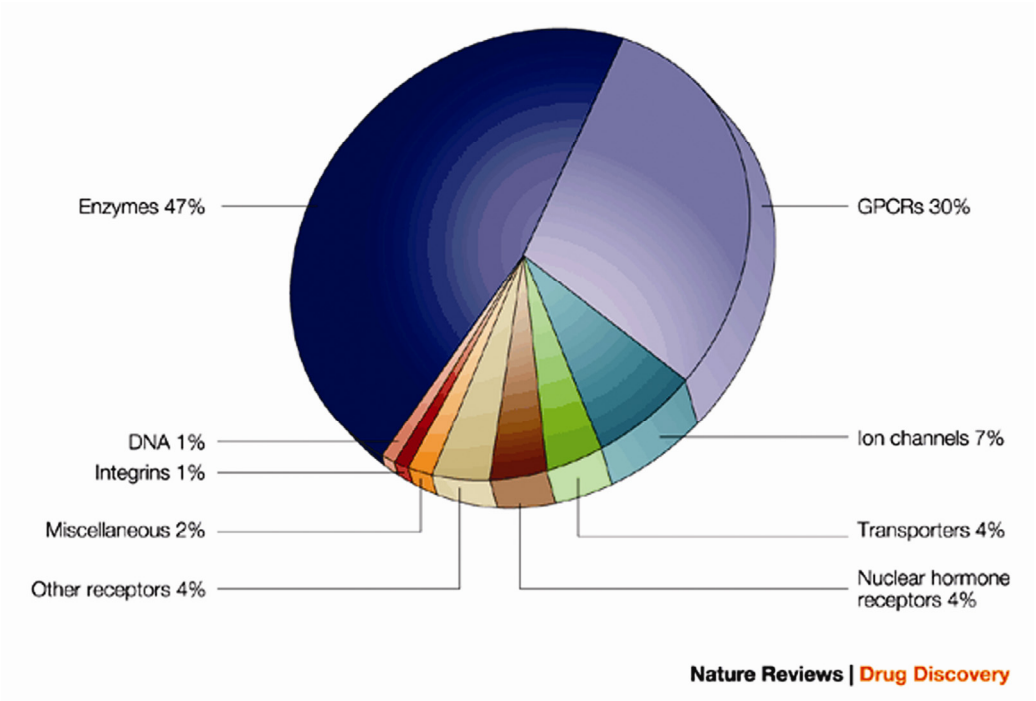

Figure 1.1: GPCRs in pharmacology

30% of marketed small-molecule drug targets are represented by GPCRs. Adapted from Hopkins and Groom (28).

1.3 G protein coupled receptor 30

In the late 1990s G protein-coupled receptor 30 (Gpr30) was independently cloned by four different groups (29-32). Since no ligand was known for the receptor, Gpr30 was classified at the beginning as an orphan receptor. Subsequently in different studies Gpr30 has been proposed as a new estrogen receptor able to mediate rapid signalling exerted by estrogen stimulation (33, 34) (see also Gpr30 signalling).

Gpr30 gene is localized on chromosome 7 in humans (map position 7p22.3) and on chromosome 5 in the mouse genome (map position 5 G1). Both the human and the mouse Gpr30 genes are characterised by the presence of three exons. Three main different splicing variants are known for the human transcript of Gpr30 differing in the 5´ UTR and encoding a protein of 375 amino acids with a molecular weight of 42 KDa (NM_001039966.1, NM_001098201.1, NM_001505.2). There is only one mouse transcript variant of Gpr30 encoding a protein of 375 amino acids and with a molecular weight of 42 KDa (NM_029771.2). Gpr30 is belonging to the class of rhodopsin-like receptors (class A). Based on a phylogenetic analysis of a vast number of GPCRs, Gpr30 turned out as a typical but distant member of the subfamily A2 (chemokine receptors) (35). Gpr30 protein has considerable homology with different chemoattractant receptors. In particular it shows 30% homology with interleukin 8-receptor (IL-8R). The common motif of the amino acid residues SCLNPLIY(A/S)F is found in the trans-membrane domain 7 (TM VII) (29). Subsequently an alternative name adopted for Gpr30 was also chemokine receptor-like 2 (CMKRL2).

1.3.1 Gpr30 signalling

Gpr30 has been proposed to represent a new estrogen receptor able to mediate non-genomic and rapid effects exerted by estrogen. Gpr30 main transduction mechanism works through G_i/G_o family coupling. The secondary transduction mechanism involves coupling with G_s protein family members. Gpr30 estrogen stimulation has been shown to promote mitogen-activated protein (MAP) kinases Erk1/2 activation via epidermal growth factor (EGFR). Subsequently also the activation of an AC was reported in response to Gpr30 estrogen stimulation (36, 37).

Filardo and colleagues proposed a signalling model in which Gpr30 activation by estrogen leads a Gβγ subunit to promote a non-receptor tyrosine kinase (Src)-mediated matrix

metalloproteinase (MMP) dependent cleavage, and the release of heparin bounding (HB) – EGF from the cell surface, resulting then in the activation of Erk-1/-2 pathway. In a sort of compensatory pathway, a Gα protein would be able to stimulate AC that in turn leads over time to a PKA-mediated suppression of EGF-induced Erk-1-/-2 activity. It was indeed observed that not only estrogen would be able to act as an agonist for Gpr30 determining the described Erk-1/-2 balanced pathway, but also antiestrogen molecules as fulvestrant (ICI 182,780) and tamoxifen. These conclusions were questioned by a paper of Levin and colleagues reporting EGFR activation exclusively mediated by estrogen receptor α (ERα) (38). Yet Revankar and colleagues could show in monkey kidney fibroblasts (COS-7 cells) transfected with ERα or Gpr30 both conjugated to GFP, an estrogen-mediated intracellular calcium mobilization in both cases at 17β-estradiol concentrations below 0.1 nM, with an EC50 value of approximately 0.5 nM (34). Indeed the authors showed that EGFR inhibitor AG1478 was able to inhibit calcium mobilization only in cells transfected with Gpr30. Estrogen activation of Gpr30 resulted also in the synthesis of phosphatidylinositol 3,4,5-triphosphate (PIP3) in the nucleus through the PI3K. Interestingly in a brest cancer cell line missing both nuclear ERs (SkBr3 cells), estrogen-mediated signalling showed the same characteristics found in COS-7 cells transfected with Gpr30.

In addition it has been shown that Gpr30 promotes estrogen-mediated inhibition of oxidative stress-induced apoptosis, by promoting the B-cells lymphoma 2 gene (Bcl-2) expression (39) as well as cell growth by the stimulation of cyclin D expression (40). Upregulation of C-fos by estrogen and phytoestrogens through Gpr30 was observed in SkBr3 cells (41). Estrogen and tamoxifen proliferation Gpr30-dependent was revealed in endometrial and thyroid cancer cells (42, 43).

Despite the tendency in recognizing Gpr30 as new estrogen receptor (G protein-coupled estrogen receptor, Gper, has been proposed as a new alternative name for the protein) part of the literature demonstrates controversial results concerning the effective nature of Gpr30 ligand and signalling (44). A report from Otto and colleagues shows that radioactive 17β-estradiol does not bind Gpr30 in a specific way (45). In the absence of ERα or ERβ Gpr30 has been also shown to be unable to mediate estrogen signalling (46). Furthermore silencing of Gpr30 did not compromise effects mediated by estrogen (46, 47). In analogy to the sphingosine-1 phosphate receptor EDg-3, also a 7TM receptor, involved in estrogen signalling (48), Levin recently proposed for Gpr30 a function in estrogen signalling actually

subordinated to membrane localized ERα (44). Gpr30 therefore may participate in the complex signalling mediated by ERα, constituting one of the many possible links between estrogen and downstream effectors. The hypothesis is supported by the observation that if it is often true that the rapid effects attributed to Gpr30 in response to estrogen require ERα (43, 49, 50) the opposite does not seem always to occur (47). Indeed in cells from a transgenic mouse model, expressing only a functional E domain of the ERα at the plasma membrane (MOER model), Erk and PI3K activation by estrogen was rescued as opposed to cells lacking any ER. A remarkable limitation of these results identifying Gpr30 as a new estrogen is the scarce information about the *in vivo* function of Gpr30. Moreover even these do not always confirm the role of Gpr30 as a new estrogen receptor, e.g. regarding the expected estrogen effects in classical estrogen target tissues such as mammary gland and uterus (45) (see also Gpr30 *in vivo* function).

1.3.2 Gpr30 subcellular localization and ligands

Based on the homology of Gpr30 with IL-8 receptor, the ligand of Gpr30 was at the beginning thought to be a peptide. Different peptides or proteins were tested including: the chemotactic IL-8 peptide, the melanoma growth stimulatory activity alpha peptide (GRO-α), the monocyte chemotactic proteins 1 and 3 (MCP-1 and MCP-3 respectively), the macrophage inflammatory protein 1-alpha-P (MIP-1 α) and others. Experiments were also performed with conditioned media from cell lines known to produce cytokines. No increase or decrease of cAMP levels as well as of intracellular calcium was registered (31). Only later in a gene expression analysis of SkBr3 cells, estrogen was also proposed to function as a Gpr30 ligand. However, the nature of the ligand is up today still controversial (see Gpr30 signalling). The cellular localization of Gpr30 also represents a critical issue, whose determination has proceeded along with all the efforts in understanding the nature of the ligand. This aspect has undoubtedly important implications for the function of the receptor itself. An intracellular localization implicates for instance that the ligand has to be membrane permeable, defining a relevant chemical characteristic of the putative ligand. Although most of the GPCRs are expressed on the cellular membrane some studies show Gpr30 to be expressed on the endoplasmic reticulum (34, 51). The idea that a GPCR may be located in intracellular compartments has been already contemplated (52). Yet two studies claimed Gpr30 to be expressed on the extracellular membrane, even though no staining of subcellular markers was provided, and the localization of Gpr30 fusion protein seemed to depend on the cell-type analysed and the tag used (53, 54).

In order to determine the subcellular localization of Gpr30 Revankar and colleagues purified two estrogen derivatives conjugated to Alexa dyes, the resulting products being known as E2-Alexa 546 and E2-Alexa 633 or fluorescent estrogens, able to bind ERα, ERβ and Gpr30. Moreover confocal fluorescence microscopy revealed that E2-Alexa 546 staining colocalized with Gpr30-GFP expression in the endoplasmic reticulum and that this binding could be competed by an excess of 17β-estradiol. A direct linear correlation was observed between receptor expression levels and specific Alexa-633 binding staining of COS-7 cells transfected with ERα, ERβ, or Gpr30 conjugated to GFP. Competition binding assays of E2-Alexa 633 with 17β-estradiol showed a K_i of approximately 6.6 nM for Gpr30 (34). Otto and colleagues reached the same conclusion as Revankar and colleagues in terms of subcellular localization, detecting Gpr30 in the endoplasmic reticulum. However using radioactive estradiol they could observe specific saturable binding of estradiol only to ERα but not to Gpr30 (51). A first approach to uncover Gpr30 ligand has been a molecular-dynamics-simulated annealing using the hydrophilic cyclopeptide EMTOVENOGQ, derived from alpha-fetoprotein, an inhibitor of estrogen-stimulated proliferation of human breast cancer (55). Later, combining virtual and biochemical screening techniques aimed at sift through a vast numbers of compound candidates as GPCR ligands, Bologa and colleagues identified a new molecule able to bind selectively and with high affinity to Gpr30. The compound is a substituted dihydroquinoline, and was denominated Gpr30-specific compound 1 (G1) (56). Using fluorescent estrogens the authors performed competition binding assays for Gpr30 in COS-7 cells, and found a dissociation constant (K_i) of 11nM for G1. Furthermore they could confirm the localization of Gpr30 on the endoplasmic reticulum by immunohistochemistry approaches. Indeed G1 stimulation of COS-7 cells led to intracellular calcium mobilization and PIP3 nuclei accumulation. The same results were found in SkBr3 cells as well as in a human breast adeno-carcinoma cell line, MCF7 cells, supporting the ability of G1 to activate also endogenously expressed Gpr30. Conflicting results with those reported by Bologa and colleagues were described by Otto and co-workers who were not able to show calcium current in response to G1 in several cellular lines transiently transfected with Gpr30 (e.g. MDA-MB231, HEC50, MCF-7 and COS-7 cells). A long-last stimulation of calcium currents was detected as expected when agents such as ionomycin were applied (45). Nevertheless in a recent paper Dennis and colleagues following the same approach used to identify the G1 agonist for Gpr30 could select a new molecule as the first selective antagonist of Gpr30, G15 (57). The authors conducted competitive binding assay experiments and reported an affinity of G15 for Gpr30 of about 20 nM. G15 displayed little binding to ERα and ERβ at concentrations up to 10μM.

Moreover they performed assays for intracellular calcium mobilization in SkBr3 cells, showing that G15 alone was not able to induce calcium mobilization but pre-incubation with G15 reduced in a dependent dose manner the response to G1 or to estrogen. Like for G1, G15 was tested in COS-7 cells in response to estrogen or G1 mediated PI3K activation after transfection with Gpr30, ERα or ERβ. G15 could inhibit PIP3 accumulation in response to G1 stimulation, but was unable to exert the same inhibitory effects in cells transfected with ERα or ERβ and stimulated with estrogen. The specificity of G15-Gpr30 binding was proved by its inability to interfere with ATP calcium mediated mobilization.

One aspect of great interest in the field of Gpr30 ligand studies is certainly represented by the interaction between 4-hydroxytamoxifen (a selective estrogen receptor modulator, SERM), fulvestrant (a pure ERα antagonist) and Gpr30. Any of them have been discussed to represent Gpr30 agonists (54). Transactivation of EGFR through Gpr30 leading to epithelial proliferation, has been proposed to be the molecular mechanism explaining the onset of endometrial cancer in women treated with tamoxifen (34, 58, 59). However so far the distinct roles of ERα and Gpr30 in transactivating EGFR have not been properly clarified and a subordinated role of Gpr30 to ERα could not be excluded (38).

1.3.3 Gpr30 *in vivo* function

So far most of the functional studies of Gpr30 were based on cell-assays, and only few publications have reported *in vivo* approaches. An overview of the most relevant results from these studies is shown in the Table 1.1. Most of the approaches were aimed to clarify the potential role of Gpr30 as an estrogen receptor: for this scope E2, G1 compound, ICI 182,780, and the newly identified G15 have been used in the different *in vivo* studies. Wildtype rats and Gpr30 knockout (KO) mice were the animal models used. In particular so far four different Gpr30 KO mouse models have been generated (45, 60-62) and the following functional categories identified: immunology, neurology, reproduction, metabolic and cardiovascular function, inflammatory mechanisms. The approaches are disparate and often the results conflicting.

Table 1.1: Gpr30 *in vivo* function

Animal model	Method	Main phenotype reported	Proposed or excluded Gpr30 function
Gpr30 KO mice PD1-KO mice	EAE induction and G1 treatment	enhanced suppressive activity of CD4(+)Foxp3(+) T regulatory cells through a Gpr30- and programmed death 1-dependent mechanism	Protective effect of Gpr30 against EAE (69)
Gpr30 KO mice Rats	G1 infusion, BP and BW measurements	Reduction of MAP in rats. Obesity in Gpr30 KO mice	Gpr30 estrogen mediates effects of protection from cardiovascular diseases and obesity (68)
Ovx Gpr30 KO female mice	E2 treatment	E2 treatment did not effect femur length in Ovx Gpr30 KO females mice	Gpr30 is required for a normal estrogenic response in growth plate (220)
Gpr30 KO mice	Morphological metabolic and hemodynamic studies (e.g. GTT, BP measurements)	In females mice: impaired glucose metabolism, reduced BW, increased blood pressure, reduced bone growth	Gpr30 is required for normal bone growth, glucose homeostasis, and blood pressure in female mice (61)
Gpr30 KO mice Ovx Gpr30 KO female mice	Continuous mating studies E2, E2+P treatment	Gpr30 KO mice have normal: fertility, development of reproductive organs, and responses to E2 or E2+P in the uterus and mammary gland	Gpr30 is not involved in estrogenic response in reproductive organs (45)
Ovx Gpr30 KO female mice	G1 treatment	G1 has not impact on estrogenic responses in the uterus and the mammary gland (epithelial cell proliferation, endbud formation, target gene induction)	Gpr30 is not involved in estrogenic response in reproductive organs (51)
Gpr30 KO mice	E2, G1 treatment: assessment of the thymic atrophy and thymic apoptosis	E2-induced apoptosis in TCR $\beta^{-/low}$ DP thymocytes was significantly attenuated in Gpr30 KO mice. G1 treatment in WT mice, similar to E2, induces apoptosis	Gpr30 is indispensable for E2-induced thymocyte apoptosis and consequent thymus atrophy (along with Erα–mediated DN thymocytes development blockage) (62)
Ovx female and ICR male mice	E2, G15 injections G1 and G15 administration in tail suspension test	Epithelial cell proliferation E2 or G1- induced, reduced by G15 in a dose dependent manner. G1 and E2 antidepressant effects inhibited by G15	Gpr30 estreogen mediated effects of epithelial cell proliferation and regulation of depression (antidepressant effect of G1 inhibited by G15) (57)
Ovx female rats	5HTP injection to induce VH	Lost of VH when ovx rats were treated with antisense oligodeoxynucleotide against Gpr30	Gpr30 estrogen-mediated VH (73)

Gpr30 *in vivo* function. 5HTP: 5-hydroxytryptophan; BP: blood pressure; BW: body weight; E2: estrogen; EAE: experimental autoimmune encephalomyelitis; GTT: glucose tolerance test; KO: knockout; MAP: mean arterial pressure; Ovx: ovariectomized; P: progesterone; VH: visceral hypersensibility.

Analysis shown in the first paper was conducted in rats, using a trauma-hemorrhagic shock (THS) model based on a mechanical and controlled bleeding followed by a pharmacological resuscitation. The animals were treated with E2 or E2 conjugated to BSA and hepatic injury was based on plasma α-glutathione S-transferase (αGST) levels. E2 and E2-BSA administration after THS were both able to reduce αGST levels. Indeed the authors showed in hepatocytes PKA inhibition of the anti-apoptotic Bcl-2 gene, in response to E2 or E2-BSA stimulation. The authors concluded that hepatic injury may be attenuated in response to estrogen through a Gpr30 mediated anti-apoptotic signalling (63). In this study there was no difference in using E2 or E2-BSA, the latter being a membrane-impermeable compound. Its presumed effects mediated by Gpr30 are however in contradiction with strong evidences for Gpr30 being located on the endoplasmic reticulum (see Gpr30 subcellular localization and its ligands). Other studies also provided evidence for a pro-apoptotic function of Gpr30 (62, 64).

A recent paper reports that Gpr30 is required for E2 stimulation of the primordial follicle in the hamster ovary suggesting a potential role of Gpr30 in reproduction (65). On the other hand Otto and colleagues showed that Gpr30 is not involved in estrogenic response in reproductive mouse organs (45). They used ovariectomized (ovx) Gpr30 KO female mice treated with E2 alone or in combination with progesterone (P) to simulate pregnancy status. They found that the lack of Gpr30 did not affect endbud or sidebranches formation in mammary gland, as well as uterine growth (weight) and epithelial cell proliferation. Uterine genes expression as Hspa5, S100a10, and Wnt4, claimed to be induced by estradiol in an Erα independent manner, were also not influenced by Gpr30 lack (66, 67). Moreover mating studies showed Gpr30 KO mice to be fertile and that follicles from all stages of development were present as well as corpora lutea. A similar experimental approach using also G1 *in vivo* led to the same results. The authors therefore concluded that no impairment of the hypothalamic-pituitary-gonadal axis in female mutant mice was observed and they excluded a general involvement of Gpr30 estrogen response in reproductive organs (45, 51). In a recent paper however Dennis and colleagues (2009) showed an increase of epithelial proliferation in ovx female mice treated with E2, reverted by the pre-treatment with G15.

Another study on Gpr30 KO mice claimed an involvement of Gpr30 in the regulation of glucose metabolism and blood pressure, with a sexual dimorphism (61). The authors found that deletion of Gpr30 was associated with hyperglycemia and impaired glucose tolerance, reduced skeletal growth and increased blood pressure in female mice. Glucose impaired

tolerance was associated with reduced glucose-stimulated insulin release. Indeed female Gpr30 KO mice exhibited an age reduced body weight as well as increased mean arterial pressure (MAP) at 9 months of age, probably due to events of arterial remodelling such as an increase in the media-to-lumen ratio. In the same year Haas and co-workers claimed a role of Gpr30 in the metabolic and cardiovascular system, but reported results contrasting with those from Martensson concerning magnitude, direction, and sexual dimorphism in body weight and blood pressure (68). Infusion in rats of G1 resulted in an acute reduction of MAP, being the phenotype sex independent. Using pressurized rat mesenteric resistance arteries, they found that G1 was able to promote acute dilatation of preconstricted arteries, and the dilator effect was abrogated in the carotid artery of Gpr30 KO mice. G1 but not E2 turned out to be able to abrogate serotonin-calcium increase after intracellular (but not extracellular) injection of the compound. Haas and co-workers proposed a model wherein Gpr30 is involved in mediating acute vasodilatation through a pathway antagonizing calcium release. Moreover the authors showed that both males and females Gpr30 KO mice have a higher body weight compared to their wildtype littermates.

An immunological role of Gpr30 was proposed by Wang and colleagues (62). The authors investigated the mechanisms of thymic atrophy occurring in response to estrogen exposure. The maturation of T cells can be divided in different stages in relation to the expression of CD4 and CD8 receptors: double negative (DN: $CD4^-/CD8^-$), double positive (DP: $CD4^+/CD8^+$) and single-positive (SP: $CD4^+/CD8^-$; $CD4^-/CD8^+$) stages. DN T cells can further be found at different levels of maturation depending on their expression of CD44 and CD25 receptors (DN1-4). E2 treated Gpr30 KO female mice showed alleviated but not completely reversed thymic atrophy. The atrophic effect resulted rather abrogated in α-ERKO mice. Still the authors could distinguish between the contribution of Gpr30 and ERα in mediating thymic atrophy since the apoptosis in TCR $\beta^{-/low}$ DP thymocytes was significantly attenuated in Gpr30 but not in ERα depleted cells; concerning the role of ERα, they observed that E2-induced accumulation of DN1 and DN2 thymocytes was only blocked in α-ERKO mice.

Recently the same authors proposed a possible involvement of Gpr30 and ERα in autoimmune diseases protection (69). Using a multiple sclerosis mouse model, experimental autoimmune encephalomyelitis (EAE) induced in wildtype mice was partially rescued by G1 as well as by E2 treatment, whose protective effect, through ERα has been formerly proven (70-72). In order to distinguish between the contribution of Gpr30 and ERα in attenuating

EAE, the authors investigated ex vivo the role of a T regulatory cells fraction ($CD4^+$ $FoxP3^+$ Treg cells) potentially expressing the programmed death 1 (PD-1) receptor. The expected PD-1 receptor up-regulation mediated by estrogen was abolished in Gpr30 KO PD-1^+ splenocytes. Indeed G1 administration *in vivo* failed to protect PD1-KO mice from EAE. The authors concluded that G1 may suppress EAE by up-regulation of the PD-1 signalling pathway in $CD4^+$ $FoxP3^+$ cells. However E2 treatment of α-ERKO mice as opposed to Gpr30 KO mice did not attenuate EAE, detecting ERα as the main factor in this process (70).

Other studies provide evidence indicating a role of Gpr30 in mediating distinct phenomena of nociception. Lu and colleagues (2009) recently investigated the role of Gpr30 in estrogen induced visceral hypersensitivity (VH). VH is a factor involved in the pathogenesis of irritable bowel syndrome, and can be mimicked in rats through injections of 5-hydroxytryptophan (5HTP, a precursor of serotonin). The entity of VH was assessed *in vivo* using a colorectal distension procedure and measurements of electromyogram (EMG) levels, accounting for the visceromotor reflex. Pre-treatment of ovx rats with the presumed selective Gpr30 agonist G1 and not with ERα or ERβ agonists, namely propylpyrazole-triol (PPT) and diarylpropionitrile (DPN), increased EMG levels following 5HTP sensitization. Pre-treatment with the ER antagonist fulvestrant in the presence of estrogen led to the same results. Since the use of antisense oligodeoxynucleotides against Gpr30 could prevent the 5HTP induced VH events, the authors concluded that Gpr30 mediated visceral pain in the described *in vivo* model (73). Starting from the observation that gonadal hormones may influence pain, Kuhn and colleagues investigated the involvement of Gpr30 in an estrogen induced nociception rat model (74). Previously the same group demonstrated that injection of estrogen into the hind paw of male rats induced a PKCε dependent mechanical hyperalgesia. Kuhn and colleagues questioned whether this mechanism could have been mediated by Gpr30. Injecting 10 ng of G1 in the hind paw of male rats and measuring the nociceptive flexion reflex, they found significant increase of hyperalgesia. Hundred ng as well as 1 μg led to the near-maximal mechanical hyperalgesia. Same results were obtained using a fulvestrant and both effects were abrogated by the use of a specific PKCε inhibitor. Ten nM estrogen was the minimal concentration required to observe activation of PKCε in neurons *in vitro*, but plasma levels of estrogen in male rats has been estimated in 1.1 nM (a value closer to K_i values of ERα and Erβ), therefore the authors hypothesized that a Gpr30 mediated nociception model may require high locally restricted estrogen levels, hypothesis not yet proved.

A role of Gpr30 in estrogen related effects in depression has been recently proposed by Dennis and co-workers. The authors showed the ability of G1 as well as E2, in a method for screening antidepressants in mice (tail suspension test), to replicate the effects determined by the antidepressant drug desipramine. This effect was then shown to be partially reverted by G15 treatment. Once more the role of the nuclear estrogen receptors could not be completely excluded, since not only G1 but also E2 led to the same results in the tail suspension test. Moreover the effects of ERα or ERβ antagonist were not analysed (57).

1.4 Mouse genome manipulations: transgenic and knockout mice

1.4.1 Transgenic mice

Transgenic and knockout mice are a powerful and invaluable tool to dissect the function of individual components of complex biological systems. Transgenic technology was developed in the early 1980s and precedes gene targeting technology. The latter is based on homologous recombination in embryonic stem cells (ES cells), and its development aimed at overcoming the limits of the random insertions that transgenic technology involves. The first transgenic experiments have been published about 30 years ago following infection of mouse embryos with viruses or retroviruses (75, 76). Pronuclear injection of mouse oocytes with naked DNA is the technique at the base of transgenic mice generation (77). The technique allows the use of transgenic constructs of several 100 kb in size, using for example yeast artificial chromosomes (YACs), P1-derived artificial chromosomes (PACs) or bacterial artificial chromosomes (BACs) (78). Often mini-gene constructs up to 10-15 kb are used. They consist of a regulatory sequence, a carefully selected promoter sequence and a coding sequence (cDNA) with polyadenylation sites. In order to obtain a large number of mature follicles female mice are treated with gonadotropic hormones to induce super-ovulation. F1 hybrid mouse strains are often used, as for example B6D2F1 mice, with a C57BL/6 mother and a DBA/2 father (79). Fertilized oocytes (zygotes) are collected when the paternal and maternal nucleus (pronucleus) are not fused yet and the transgene construct injected into the pronucleus of the zygotes. The microinjected oocytes are subsequently implanted into the oviducts of wildtype pseudo-pregnant mice previously obtained by mating them with vasectomised males. Through random recombination events the fusion gene construct becomes integrated into the genome. The integration normally occurs in a “head-to-tail” orientation and in a variable range number of copies verifiable through analysis by PCR and a southern blot (80). When the transgene inserts into the genome before the first cellular division, the embryo develops with the “foreign” gene (i.e. the transgene) in every somatic cell and germ-line, and the mouse that will develop from this embryo will constitute the founder of a transgenic line, able to transmit the genetic modification to its offspring. Alternatively the embryo may develop as a genetic mosaic. The founders are heterozygous for the transgene. The heterozygotes are subsequently mated to obtain the other possible genotypes.

Transgenic technology is an efficient and well established approach. Despite that it shows some important drawbacks: 1) the copy number of the integrated transgene is highly variable

and the integration site can strongly influences transgene expression; 2) the injected DNA does not contain necessary all regulatory elements, often not reflecting the complexity of the genome since these elements are sometimes located at large distance from the coding sequence or within introns of complex genes; 3) transgenes with a trans-dominant lethal phenotype cannot be studied (81). Some of these limitations have been overcome through new approaches and a variety of gene transfer methods, are today also available, many of them based on ES cell or lentiviral vectors (82). But independently of the technique used, pronuclear injection, gene transfer into ES cells or lentivirus-mediated gene transfer, the insertion of the transgene remains random, and its expression not linked in most cases to the endogenous locus. In contrast knockout technology achieves a specific genetic modification at a given gene locus.

1.4.2 Knockout mice

1.4.2.1 ES cells and gene targeting strategies

Knockout or gene targeting technology derives from a combination of ES cell culture techniques and homologous recombination strategies aimed at introducing a specific mutation in a specific gene. ES cells are pluripotent cells isolated from the inner cell mass of pre-implantation blastocysts and can contribute to both somatic and germ-line tissues after reintroduction into blastocysts (83, 84). The genetic background of the majority of available ES cell lines is 129, a mouse strain from which ES cell lines can easily be established (85). The principles of homologous recombination were first established in yeast where recombination between a DNA vector and genomic DNA occurs through the specific recognition between homologous DNA regions. In the mammalian cells such an event is much more infrequent (81). In particular, experiments of gene targeting in ES cells, namely the technique to delete or specifically inactivate a gene trough homologous recombination, was first realized for the hypoxanthine phosphoribosyl transferase HPRT gene locus, a selectable gene (86, 87), and then for the int-2 and the c-abl gene loci, two non-selectable genes (88, 89). These experiments paved the way for the construction of the first knockout mouse in 1989 (90). A schematic representation of a knockout mouse generation approach is shown in Fig. 1.2. The first step in a gene targeting experiment is to isolate the genomic clones containing the gene of interest, and the best approach involves the use of both ES cells and genomic clone from the same genetic background (i.e. isogenic DNA). The vectors can be classified as either replacement or insertion vectors. A replacement type vector, present in a linearized form, is inserted into the genomic locus by a double crossover that leads to the

ejection of the genomic DNA fragment. An insertion type vector enters the target locus as linearized vector that leads to the duplication of genomic sequences. Most often replacement vectors are used. In any case the vector has to contain a gene that allows a positive selection strategy, able to confer e.g. a precise antibiotic resistance to the transgenic ES cells, as for instance neomycin resistance (neo^r). Alternatively other gene cassettes may render resistance against hygromycin, puromycin or histidinol (91-93). To enrich the clones that have undergone homologous recombination a second gene allowing a negative selection of sensitive ES cells is usually added to the construct, often a cassette encoding thymidine kinase (TK). Those cells that have undergone homologous recombination have lost the TK gene, on the other hand the cells that have still kept the genes will result exposed to the toxic effect of an agent such as gancyclovir and consequently be eliminated. Altogether the system is known as negative-positive selection strategy (88). Another negative selection marker used with success was the diphteria toxin A (DT-A) gene fragment (94). Some approaches combine directly a positive selection strategy with homologous recombination technology. Therefore the vector is designed in such a way that when a homologous recombination event occurs regulatory elements of a given selection marker necessary are reconstituted (88, 89, 95).

It has been described that several factors can affect the rate of homologous recombination in ES cells: 1) the locus per se, likely reflecting the variable organisation of chromatin structures; 2) the extent of the homology region between the targeting vector and the targeted locus, being 10 kb the empirical optimal value (96); 3) the genetic background of the targeted ES cells, since isogenic DNA increases the efficiency of homologous recombination (97).

Other technical improvements have enriched and refined the strategy of gene targeting (98, 100, 101). In designing a targeting vector often the possibility of introducing a β-galactosidase gene (LacZ) in frame with the targeted protein has been considered. On the other hand this strategy leads to fused proteins of LacZ and the transgene, e.g. LacZ-neo^r. Alternatively one could introduce an internal ribosomal entry site (IRES) sequence in order to drive the translation of LacZ protein alone. The main advantage of both approaches is to use LacZ expression able to report the expression pattern of the gene protein of interest, providing therefore an invaluable knowledge. Indeed in the present study was used such a model, aiming at the functional characterization of a rather unknown gene locus, Gpr30.

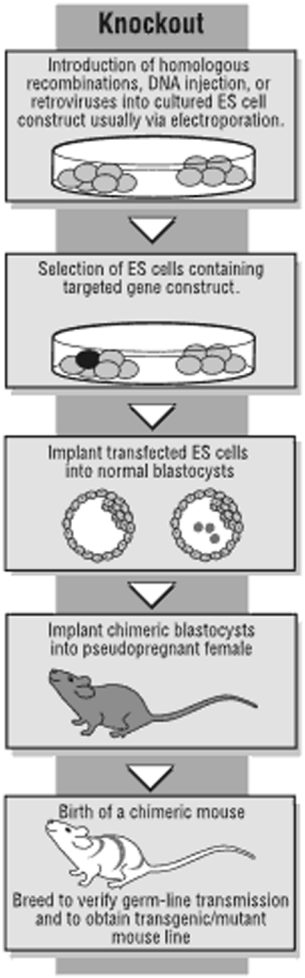

Figure 1.2: Schema of a KO mouse generation

Selected ES cells for the mutation are implanted into a normal blastocyst. The blastocyst is implanted in a pseudopregnant mouse that will generate chimeric mice, bred to verify germ-line transmission of the mutation. Adapted from Crawley JN (99).

1.4.2.2 The chimera and its offspring

Competent ES cells are subsequently injected into a blastocyst of wildtype pseudopregnant mice, preliminary collected from superovulated female mice, often the C57BL/6 strain. Collection is usually performed at embryonic day 2.5, when the blastocyst is at early stage of development (79). A fine-gauge needle is used to microinject cultured, single ES cells into the central hollow of the blastocoele of the blastocyst. The injected blastocysts are then implanted into pseudopregnant female recipients. The adoptive mothers can be of any strain, usually C57BL/6. When ES cells carrying a dominant allele of Agouti as A^w (white-bellied agouti, from a substrain of 129) are injected into mouse blastocysts of the strain C57BL/6 (a non-agouti), mice containing both C57Bl/6 and 129-derived cells can easily be identified by coat color chimerism. In this case the pups (chimeras) have typically a greyish brown colour. If

manipulated ES cells have also colonized germ-line organs, the resulting chimeras will be able to transmit the mutation.

To detect germ-line transmission, crossings are conducted. Chimeras are bred to wildtype mice such as C57BL/6 or 129/Sv. The F1 offspring of these crosses are then analysed for the expression of the mutation. Southern blots or PCRs are performed on small tissue sample from the tail of the offspring, to identify positive heterozygotes. Heterozygotes are then mated with each other to produce a F2 generation. Homozygous mutants may not survive, providing evidence for an autosomal recessive mutation and the embryonic lethality as the result of the gene ablation. Heterozygous mutant may express half of the gene product, reflecting the presence of half gene dosage, or may also express variable amounts. PCR and western blot are usually used to evaluate the absence of the specific mRNA and protein.

A critical and essential issue to be considered is the genetic background of the mutant mice (102). The majority of targeted mouse mutants have been generated using ES cells derived from 129 substrains (85) and the 129-derived chimeras are bred with C57BL/6 females since 129 strains are poor breeders. Such a strategy leads to mixed genetic background of the mutant mice. Moreover targeted mutations can render very different phenotypes when studied on different genetic backgrounds (103). To eliminate confounding effects caused by a mixed genetic background a mutation should be studied on a pure genetic background. One possibility is breeding chimeras with mice of the same genetic background of the original ES cells used to generate the mutation. A valid alternative may also be systematic backcrosses between the mutant and the standard inbred mice (e.g. C57BL/6, 129/Sv, CD-1 etc.)(104).

1.4.2.3 Recombinase based approaches

A breakthrough in gene targeting technology was achieved with recombinase-based approaches, leading to the second generation of conditional KO mice. This strategy is based on the use of the Cre/LoxP recombination system. This technique involves the use of the site-specific recombinase Cre from the phage P1 that recognizes and binds to a 34-bp long, partially palindromic sequence called LoxP (locus of crossover x in P1). The Cre-recombinase protein has the ability to excise any sequence placed between two LoxP-sites. In particular if the LoxP-sites are positioned in the same orientation the recombinase will lead to the excision of the sequence. If the two LoxP-sites are in a tail to tail orientation the insertion will result a Cre-mediated genomic inversion. The first process is more efficient than the second one and it is broadly used in generating a non-selectable mutation in the mouse

genome (81). In principle the approach consists in the use of a cassette including the mutated locus of interest along with a neo^r marker gene for a positive selection, properly flanked by two LoxP sites. The ES cells selected for homologous recombination are transiently transfected with a Cre recombinase vector that leads to the excision of the neo^r gene. A negative selection allows to enrich the culture for those cells containing exclusively the mutated locus. As an alternative to Cre/LoxP system the Flp/Frt recombinase system from yeast has been used in ES cells as well as in transgenic mice (105, 106).

The general main advantage of this strategy is that the selection marker gene and its potential "side effects" on the generated mutant mouse can be opportunely removed. However the KO mice generation as described above is preferentially achieved establishing two mutant mouse lines. A first main line contains LoxP-sites flanking the genomic region to be deleted, properly inserted by homologous recombination in ES cells. The second one is a transgenic mouse carrying one copy of the Cre-recombinase gene. Mating these two lines leads to the generation of a Cre-and LoxP-double positive transgenic offspring. In these mice, the targeted gene is disrupted by Cre/LoxP-mediated deletion of the target chromosomal gene segment. An advanced generation of knockout vectors possesses LoxP sites at the 5´ and 3´ of a pivotal portion of the locus of interest (e.g. the start codon) and additionally in order to specifically remove the selection marker the neomycin cassette is flanked by Frt sequences recognized by Flp recombinase. A mouse carrying a LoxP/Frt vector is crossed with a transgenic mouse expressing Cre and Flp recombinase in germ cells so that the neomycin resistance gene is removed. Moreover if Cre is expressed under the control of a tissue specific promoter, or in an inducible manner, the resulting mutant will be a conditional knockout, potentially showing a reversible phenotype (107-109).

1.5 GPCR knockout mice

Transgenic techniques as well as constitutive and inducible gene targeting strategies have been extensively used for dissecting GPCR function *in vivo* (110). There are many examples of GPCR knockout mice generated by gene cassettes targeting based on replacement vectors, often in combination with reporter gene cassettes. These include members of adrenergic, dopaminergic, serotonergic, endothelin, thrombin, mGlu receptor, angiotensin II, bradykinin, and histamine receptor families (111).

As already mentioned Gpr30 is a member of chemokine receptors showing high homology with IL-8R (CXCR1). Several chemokine receptors KO mice have been generated (112). These mice present often impaired host defence inflammatory response and macrophage function, evidencing a role for these receptors in immune response. In particular IL-8R KO mice have been shown to be extremely susceptible to an urinary tract infection (UTI) model. These mice showed a dysfunctional neutrophil response to UTI, being these cells unable to cross the epithelial barrier and causing tissue destruction (i.e. kidney scarring) (113, 114).
So far there are four different Gpr30 mutant mouse models. In the present thesis we focused in particular on two different mutant mouse lines, Gpr30-T181 Deltagen mice and the SHG17 Artemis mice.

1.5.1 Gpr30-T181 Deltagen mice

Gpr30-T181 mice were generated at Deltagen (San Carlos, USA) through a homologous recombination approach in ES cells from 129/Sv strain. In synthesis a LacZ-neo^r cassette was used to disrupt the open reading frame (ORF) in the exon 3 of the Gpr30 gene. The insertion deleted 349 bp of the ORF encoding the first two transmembrane domains and the first intracellular loop. The inclusion of the reporter LacZ gene within the targeting construct served a dual purpose: 1) to disrupt the gene of interest and 2) to allow the assessment of receptor expression pattern. The use of reporter genes in conjunction with disruption schemes has been demonstrated for other GPCR as the mGlu1 receptor and the angiotensin type 1A receptor (AT1) (115-117). Using LacZ reporter assays on a variety of several Gpr30-T181 tissues and co-immunolocalization experiments we could identify tissues and cell types expressing Gpr30 (60).

We found Gpr30 expression in endothelial cells of small arterial vessels of several tissues such as kidney, heart, peritoneum, and genital tract; in smooth muscle cells and pericytes in the brain; in a neuronal subpopulation in the cortex as well as in the polymorph layer of the dentate gyrus; in the intermediate and anterior lobe of the pituitary gland and in the medulla of the adrenal gland. Indeed Gpr30 was expressed in gastric chief cells of the stomach. RT-PCR experiments performed at Deltagen detected also high expression levels of Gpr30 in the stomach and the pancreas (Fig.1.3).

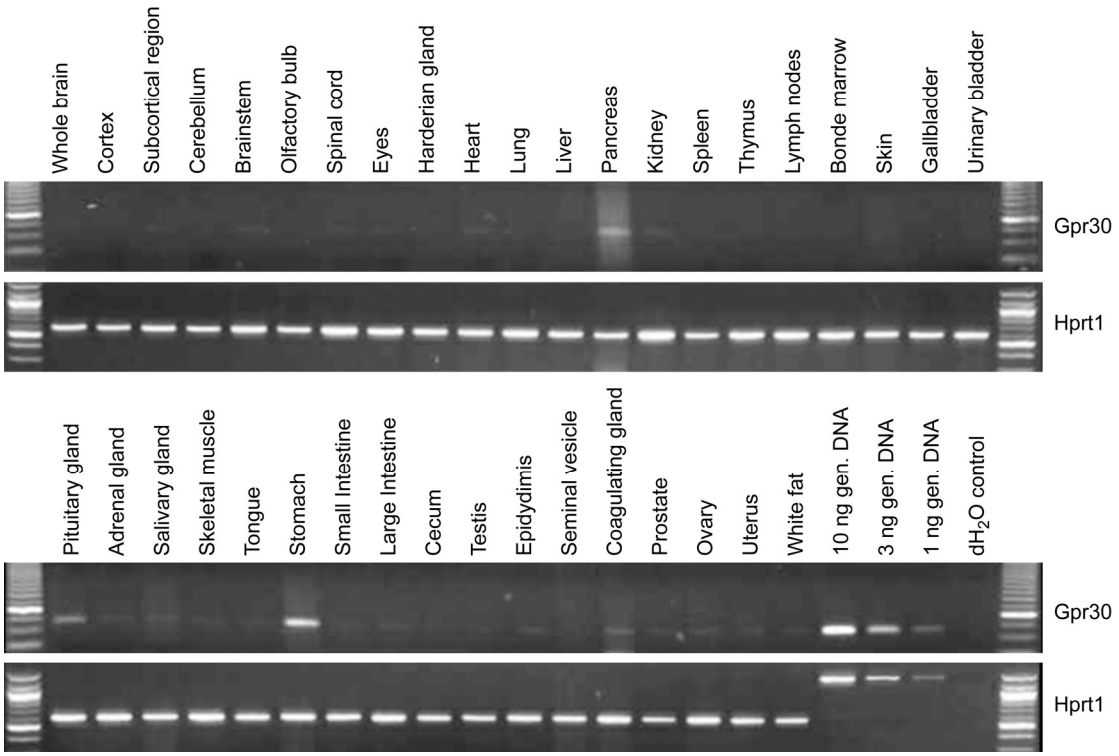

Figure 1.3: RT-PCR analysis (Deltagen)

Using different tissues from Gpr30-T181 mice shows a predominant Gpr30 expression in stomach, pancreas and pituitary gland.

In a preliminary screen, however performed on a small cohort of animals (Deltagen), and consisting in physical, histological, clinical chemistry, haematology, aging and fertility examinations Gpr30-T181 mice did not show any obvious phenotype. The only observation reported as potential phenotypic change concerned higher serum levels of low density lipoproteins (LDL) in mutant female mice.

1.5.2 SHG17 Artemis mice

SHG17 Artemis mice were generated using a Cre-recombinase based approach (45). The inactivation of Gpr30 was obtained deleting exon 3 from the murine genome which encodes the complete ORF of the Gpr30 protein. SHG17 Artemis mice were found at the expected mendelian ratio and a gross histopathological analysis did not show any aberrant phenotype of Gpr30 deficient mice. Still a slight but significant decrease in liver relative weight was only found in mutant females compared to their wildtype littermates. Moreover in mating studies SHG17 Artemis mice showed a normal fertility.

1.6 Phenotyping strategies

Animal models are essential for understanding the genetics and pathogenetics of human diseases. Several reasons underline such a statement: 1) the genome is 90% identical to the human genome; 2) modifying the mouse genome is a well established approach and of relatively easy access; 3) manipulating mouse genome allows to produce animal model diseases or altering the normal function of organs, systems or behaviours allowing to gain insights into the mechanisms underlying a normal organ, system or behaviour; 4) mouse models can be used for drug screening and testing of therapies (118). Once the mouse model is generated an appropriate and rigorous phenotype analysis is required.

The phenotype is defined as an observable characteristic or biochemical tract of an organism that results from the interaction between environment and genotype (119). A phenotypic analysis of a mutant mouse can be developed at different levels. A first level includes a comprehensive and standardized phenotyping of the mouse line of interest (primary screen). A second level includes approaches focussed on specific organ systems and their function, based for instance on mutation "challenging" strategies (secondary screen). Limiting the analysis to one level of investigation might lead to miss unexpected phenotype alterations, therefore the two strategies can be combined in a global "pyramidal" phenotyping approach (119). Gpr30 mutant mice, whose phenotype study is here presented and discussed, underwent both an extended primary screen and in parallel a mutation challenging strategy based on a specific theoretical background, as clarified in the following paragraphs.

1.6.1 Primary screen

The German Mouse Clinic (GMC) at the Helmotz Centrum and German Research Center for Environment and Health in Munich provides a comprehensive phenotyping of mouse models, structured in different areas of investigation. A first line screening bundles screens which can be carried out at relatively high-throughput and applied in a comprehensive manner to a significant number of mice. The "standards operating procedures" (SOPs) are divided in two categories: 1) primary protocols that are simple to apply and require little special equipment, 2) primary extended protocols that give further information on the phenotype but require more specialized skills or equipments.

The phenotyping platforms at the GMC cover several research areas. 1) In the dysmorphology screen mice are analysed for morphological abnormalities in different organ systems. The aim of the screen is to detect mouse models for human skeletal diseases like osteoporosis or others diseases connected to the bone and the cartilage. The screen is essentially based on morphological observations, e.g. x-ray and bone density analysis. 2) The cardiovascular screen aims at the assessment of cardiovascular parameters and involves hemodynamic studies as electrocardiograms (ECG) or non-invasive measurements of blood pressure (tail-cuff) and atrial-natriuretic peptide (ANP) plasma levels analysis. 3) The metabolic screen focuses on the determination of food and energy uptake under *ad libitum* conditions concerning food access and metabolic adaptations during food restrictions. Body weight, energy uptake metabolizable energy and body temperature are measured. 4) Clinical chemistry and hematologic primary investigations aim at detecting haematological changes, as well as changes in metabolic pathways and electrolyte homeostasis. Several parameters are measured as various enzymes activities or specific substrates and electrolytes. 5) Assessment of morphological alterations of the eye is realized evaluating anterior segment abnormalities by slit lamp biomicroscopy as well as posterior segment abnormalities by funduscopy. The axial eye is measured by laser interference biometry. 6) For lung function analysis spontaneous breathing patterns during rest and activity are studied. The technique involves a chamber that allows measurements of pressure changes which arise from inspiratory and expiratory, temperature and humidity fluctuations during breathing. 7) The molecular phenotyping screen is based on RNA expression profiling of different tissues. 8) A potential behavioural phenotype is explored by evaluation of exploratory drive, reactivity to novelty and emotionality (Open Field Test) of the mice as well as prepulse inhibition in response to acoustic stimuli: a neurological phenomenon whose deficit is linked to abnormalities in sensorimotor gating (a predictor of schizophrenia and others psychiatric diseases in humans). 9) In the primary neurological screen different parameters are evaluated to assess muscle, motor neuron, spinocerebellar, sensory and autonomic functions. 10) Nociceptive screen is based on the evaluation of the somatosensory responsiveness to thermal pain. 11) For a first immunological profile leukocyte populations of the peripheral blood and immunoglobulin levels in blood plasma are measured. 12) To detect a potential tendency to develop allergy total plasma immunoglobulin E is measured, since several immune disorders are IgE mediated (e.g. allergic asthma, allergic rhinitis, and atopic dermatitis). 13) Steroid metabolism plays a key role in controlling differentiation and the proliferation processes of cells and tissues, such as regulation of apoptosis and bone remodelling. The steroid metabolism screen

is focussed on steroids dehydroepiandrosterone (DHEA) and testosterone plasma levels assessment. 14) A pathology screen is realized by histological analysis of several organs (e.g. skin, muscle, brain kidney et cetera) (120).

1.6.2 Secondary screen

In parallel to the comprehensive analysis of the phenotype performed at the GMC, we decided to challenge Gpr30-T181 mice with high fat diet (HFD). Several reasons justified this approach. LacZ assays conducted in Gpr30-T181 mice showed that Gpr30 protein was mainly expressed in endothelial cells of small vessels, but also in the stomach and the pancreas (45, 60). A first phenotypic preliminary screen (Deltagen) showed that female mutant mice may have higher serum values of LDL. Therefore our work hypothesis was that the lack of Gpr30 may lead to a metabolic and cardiovascular imbalance set off by a challenge such as HFD.
Moreover in order to exclude a gene targeting strategy effect potentially responsible for the resulting Deltagen mice phenotype, Artemis mice, generated on a pure C57BL/6 background and devoid of any targeting vector at genomic level were used.

1.7 Estrogen receptors in metabolic diseases and associated cardiovascular disorders

Obesity results from a prolonged imbalance of energy intake and energy expenditure. Co-morbidities associated to obesity include hypertension, dyslipidemia and cardiovascular diseases, which significantly reduce life expectancy. In this context type 2 diabetes mellitus (T2DM) also represents a growing health threat. Indeed metabolic diseases and associated complications are becoming progressively object of study of an emerging gender-medicine community, since the evidence for gender disparities regarding glucose and lipid metabolism, as well as body weight regulation (121).

In some cases these differences may partially be related to circulating levels of sexual hormones and to the sex-dimorphic effects of these hormones. Testosterone has gender dimorphic effects on the incidence of T2DM: high levels of testosterone may be protective against T2DM, but have opposite effects in women. Estrogen deficiency may affect glucose regulation and may also increase insulin resistance in estrogen-resistant males or in postmenopausal women (122, 123). However, it has been reported that ERα seems beneficial for glucose homeostasis stimulating the expression of glutamate transporter 4 (GLUT4). Moreover in this mechanism seems to play an important role the ERα/ERβ ratio (122). Androgen receptors play a more significant role in visceral and estrogen receptors in subcutaneous fat tissues respectively. The different obesity patterns in women and in men, who tend to accumulate adipose tissue prevalently at abdominal or gluteal levels respectively, may reflect the pronounced antilipolytic effects of ERα in subcutaneous fat tissue (121, 122). In fact the perimenopause women frequently become obese developing a male pattern, which is termed also android obesity and that is per se linked to an increased cardiovascular mortality (124).

The role of estrogen receptors in regulating energy and glucose homeostasis has been studied in estrogen receptor knockout models. α-ERKO mice are obese and insulin resistant and the absence of ERα produces adipocyte hyperplasia and hypertrophy in the white adipose tissue (125). ERα deficient mice store increased amount of fat in retroperitoneal and gonadal fat pads and show higher levels of insulin free fatty acids and total cholesterol (126). Also aromatase knockout (ArKO) mice that lack the enzyme responsible for converting androgens

in estrogens show the same characteristics (125, 127). GLUT4 expression is drastically reduced in α-ERKO, unaffected in β-ERKO mice, and increased in ArKO mice (128).
Despite the reported evidence of a protective role of estrogen in humans as well as in animal models, whether estrogen actually plays a positive or negative role in the development of insulin resistance and T2DM is still unclear and currently under debate. In particular estrogen levels out of a physiological range are related to a higher incidence of insulin resistance (129) and high levels of estrogen in postmenopausal women have been related to T2DM (130). Mice treated with estrogen or bisphenol A (the environmental estrogen) showed insulin resistance after 4 days of treatment (131). In addition to the classical estrogen nuclear receptors, non-classical membrane estrogen receptors have also been hypothesised to play a role in the control of energy balance (129). Estrogen may also act binding other receptors or ion channels (132, 133).

Cardiovascular diseases associated to the metabolic syndrome show remarkable gender differences (124). Interaction of hyperinsulinemia and sexual hormones may explain the elevated predisposition of patients with diabetes to the development of cardiovascular diseases. Insulin resistance is associated with a greater relative cardiovascular risk in women compared to men (134). Diabetic patients have a greater risk to develop myocardial infarction, and diabetic women show a higher increase in early and late mortality compared with diabetic men (135). Diabetes impairs the microcirculation and the cardiac energy level, hence it represents one of the most important factors in the onset of diastolic dysfunction, a form of cardiac dysfunction that seems to be more frequent in postmenopausal women than in men (136). The frequency of atherosclerosis in premenopausal women is lower compared to postmenopausal women and it can be partially reversed through hormone replacement therapy (137, 138).

In reaction to vascular injury and development of atherosclerosis estrogen has important effects on vascular protection by regulating for instance lipid and cholesterol levels. ERα gene polymorphisms are associated to increased high density lipoprotein (HDL) levels in postmenopausal women with coronary disease in response to estrogen therapy (139). In addition, ERβ gene polymorphisms are associated with reduced LDL cholesterol levels in premenopausal or postmenopausal women exposed to estrogen therapy (140). Mice lacking the apolipoprotein gene E (ApoE knockout mice) develop spontaneous atherosclerotic lesions, a phenotype attenuated by estrogen treatment. The mechanism seems to be mediated mainly

by ERα, since ApoE KO mice crossed with α-ERKO mice are not responding to estrogen treatment (141-143).

Estrogen does not exert only indirect cardiovascular protective effects through lipid regulation, but also acts directly on blood vessels through non-genomic effects. These occur in a short time and do not require gene expression changes, so that they are not related to nuclear ERα or ERβ. Estrogen mediated vasodilation represents a good example of such an effect. In several studies it has been shown that estrogen membrane receptor isoforms mediate rapid effects of estrogen in endothelial cells, in which estrogen interacts with p85α, the regulatory subunit of PI3K. Stimulation with estrogen produces a stronger activation of ERα-associated PI3K, recruitment and activation of Akt protein kinase, resulting downstream in the activation of endothelial nitric oxide (NO) synthase (eNOS) (144-146).

1.8 High fat diet mouse model

HFD fed mice represent a robust model for obesity and early type 2 diabetes. This model was initially described by Surwit and colleagues (147). In general two types of macroscopic responses have been observed when rodents are given a HFD: some species and strains gain weight but others do not. Among the different mouse strains the C57BL6/J one positively responds to HFD and is often used as a diet-induced obese (DIO) mouse strain (148). SWR/J and A/J mice are obesity resistant whereas BALB/cByJ, C3H/HeJ and C57L/J mouse strains are intermediate (149). Moreover it has been shown that HFD in C57BL6/J mice results over time in a stable hyperinsulinemia indicating a progressive worsening of insulin resistance. After already one week of HFD feeding, mice have been shown to display elevated plasma glucose and insulin levels, a reduced glucose clearance and an impaired insulin secretion. Indeed characteristic for impaired glucose resistance and type 2 diabetes are insulin resistance and islet dysfunction (150). The DIO model along with obesity and insulin resistance is also characterized by dyslipidemia, namely hypertriglyceridemia with low blood HDL levels, hyperleptinemia, hypoadiponectinemia, central adiposity and elevated triglycerides levels. These factors are component of the metabolic syndrome.

The metabolic syndrome is defined as a clustering of hyperglycemia/insulin resistance, obesity and dyslipidemia. Moreover all these events may lead to micro and macro vascular injury, hypertension and atherosclerosis. In particular the impairment of vessel function, known as endothelial dysfunction (ED), is considered as the final common pathway between cardiovascular risk factors and the development of atherosclerosis (151). Notably HFD insulin resistance and visceral adiposity have been associated to ED. Adiponectin, which normally exerts a protective role on vessel function, is downregulated upon HFD. Hyperinsulinemia stimulates endothelial and vascular muscle cell proliferation, causing vasoconstriction, and an increase of the adrenergic system tonus, leading to pathological angiogenesis (152). In visceral fat, leptin resistance increases the generation of toxic reactive oxygen species (ROS). Indeed free fatty acids may contribute to ED by a combination of different mechanisms (151).

Obesity is considered an independent risk factor for cardiac diseases (153) and has been associated with left ventricle (LV) hypertrophy, lipid cardiomyopathy and heart failure in human patients (154). Hypertension, tachycardia, LV hypertrophy, increased collagen deposition, reduced cardiac contractility and increased end-diastolic pressure are some of the

cardiovascular alteration observed in various DIO animal models (155, 156). However in studies conducted in rats, similar effects were not reported (157, 158). HFD has already been used in rodents to induce and study cardiac dysfunction (159). A study from Park and colleagues showed that ventricular fractional shortening of mice fed with HFD progressively declined between 10-15 weeks (160). The differences in the effects of HFD presumably account for species, diet type, age of the animals and time feeding, but in general do not diminish the experimental value and the usefulness of the DIO models.

1.9 Assessment of endocrine and cardiovascular function in mice

Metabolic and endocrine disorders can be evaluated with many different tests of high variable complexity. The direct and close observation of mouse behaviour may be the first source of information, e.g. nervousness may be associated with hyperthyroidism (161). Such apparent organ abnormalities may easily be detected in a primary screen such as a dysmorphology analysis (162). Body weight monitoring represents another simple but high informative test, providing an initial assessment of metabolic homeostasis. The direct measurement of adipose mass by nuclear magnetic resonance (NMR) allows to measure directly the amount of fat mass *in vivo* and to analyse potential differences in terms of fat mass deposition even without changes in total body weight. NMR was established to be more precise and rapid than other available measurements such as dual energy x-ray absorptiometry (DAX) or chemical post mortem analysis (163). It allows a non-invasive measurement of total adipose mass and skeletal muscle of unanesthetized mice.

Insulin resistance develops when an increase of insulin is required to inhibit hepatic gluconeogenesis and for stimulating glucose uptake from fat and muscle tissues. To keep stable the levels of blood glucose, the pancreas reacts producing progressively more insulin; this phenomenon leads to pancreas dysfunction and onset of T2DM. Glucose impaired clearance is an indicator of insulin resistance which can be assessed by a glucose tolerance test. This test indicates altogether the efficiency of the liver in concentrating and storing glucose, the capacity of the pancreas to produce insulin, and the sensitivity of the cells to respond to it. After assessing baseline values of blood glucose concentrations, glucose is administered by intraperitoneal injection (IPGTT) or by oral gavage (OGTT). Plasma glucose concentrations are then measured at regular intervals of 2 hours and plotted against the time. The calculated incremental area under the curve (AUC) indicates the insulin sensitivity, so that an increase in the area shows a decreased glucose tolerance and vice versa.

One important aspect in establishing a metabolic disease model is to investigate lipid metabolism. The main serum lipid parameters such as LDL, HDL, triglycerides (TG) and total cholesterol are assessed. Lipoproteins are molecular complexes consisting of lipids and proteins, whose main function is to transport non-polar lipids from the site of synthesis to those of their utilization. The non-polar lipids are membrane components and play a relevant function since constitute a transportable metabolic energy pool, and participate in hormone

synthesis. Lipoproteins transport is mainly based on three pathways: exogenous, endogenous and reverse (164). In the exogenous pathway dietary–derived lipids are absorbed and packaged into large TG rich particles called chylomicrons and subsequently delivered to the various cells of the body. In the endogenous pathway very low density lipoproteins (VLDL) are synthesized by the liver for TGs transport. In the reverse pathway cholesterol esters in mature HDL particles are selectively taken up by the liver through HDL receptors.

Along with lipids analysis, a wider clinical chemistry profile may be fundamental to find potential alterations in a mutant mouse model. For instance enzymatic deviations from physiological ranges of alanine amino transferase, alkaline phosphatase, α-amilase, creatine kinase, lactate dehydrogenase may indicate skeletal, pancreas, liver, cardiac or muscle disease. Other substrates of interest are normally represented by bilirubin, creatinine and urea. Increased values of bilirubin may indicate icterus, elevated values of creatinine may underlie heart insufficiency, kidney diseases, or urinary tract disorders; alternatively reduced values of creatinine may indicate cachexia. An increase of urea may be associated with heart insufficiency or kidney disease and a decrease with defects in protein catabolism (161).

There are different approaches to assess cardiac function in mice. They are based on ventricular catherization, radiolabed microspheres or thermodilution. However they constitute invasive techniques and do not allow to analyse physiological changes in a serial manner, a condition required for instance in a longitudinal study. Echocardiography represents a valid alternative to characterize cardiac phenotypes. It allows the measurement of physiological parameters in adult, neo-natal and embryonic rodents. Echography is a technique that uses high frequency broadband sound waves in the megahertz range that are reflected by the tissues producing three-dimensional images. Briefly a transducer in a real-time micro-visualization (RMV) scan-head is used to transmit ultrasound pulses into the animal through a coupling medium such as water or ultrasound gel. The transducer detects the back-scatter or ultrasound echo returning from the animal. The echo is used to build up a single digital ultrasound image. As the transducer moves over the object multiple ultrasound lines are acquired and combined in a so-called B-Mode image. B-Mode imaging is essentially a method of acquiring ultrasound data and creating two-dimensional images. There are at least other two different methods besides B-Mode: the M-Mode and the Doppler-Mode. The different systems of acquiring and elaborating data serve different scopes. M-Mode is a method of acquiring data in order to generate an image of a single ultrasound beam over time.

M-Mode images are for instance used to measure chamber dimensions at various time-points throughout the cardiac cycle, e.g. left ventricle internal diameter in diastole or in systole (LVIDd, LVIDs). LV fractional area shortening (FS) and ejection fraction (EF) are the most commonly used indices of LV systolic performance, even though more sophisticated indices have been introduced and developed (165). EF is the fraction of blood pumped out with each heart beat. FS measures the change in the diameter of the left ventricle between the contracted and relaxed states (for the formulas see Materials and Methods).

Following the formulas established in human echocardiography left ventricular systolic function parameters and left ventricular mass can also be calculated in mice (166-171). For instance B-Mode imaging allows the acquisition of two-dimensional images necessary to visualize the area of interest for the measurements in M and Doppler-Mode. Doppler images allow to examine the velocity of flow within a region of interest (e.g. aorta) (171). Moreover in some studies precise two-dimensional echo measurements replaced M-Mode measurements to assess LV volume, ejection fraction or cardiac output, allowing to build three dimensional models (172). Altogether echocardiography in mice has reliably assessed LV mass, chamber dimensions and wall thickness, LV systolic and diastolic function as well as vascular properties (165). Indeed a systematic methodology for *in vivo* transthoracic cardiac imaging has substantiated these results obtained using echocardiography by magnetic resonance (173).

One of the limits of echocardiography conducted in mice is the effects of anaesthetics on cardiac function (174). Many different regimens of general anaesthesia have been used such as ketamin-xylazine mixtures, tribromoethanol barbiturates or inhalation of isoflurane and halothane. Among the various approaches isoflurane anaesthesia was the most reliable one in terms of reproducible fractional shortening values and end-diastolic dimensions (165). A second problematic aspect is the poor resolution of the right ventricle. To overcome this challenge transesophageal echocardiography has been established as a reproducible method for assessing size and function of the right ventricle (175).
To validate echocardiography results electrocardiogram (ECG) may provide a second system to measure heart rate (HR). ECG is a tool that records the electrical activity of the cardiac system providing an additional standardized procedure.

2 Aims of the study

Estrogen (E2) regulates gene expression via nuclear estrogen receptors, ERα and ERβ, acting as a ligand-activated transcription factor exerting an important role in a wide variety of biological processes including energy and glucose homeostasis (129, 176). Several studies suggest that in addition the G-protein coupled receptor 30 (Gpr30) binds E2 with high affinity and mediates rapid estrogen signalling in tissue culture (34, 36, 37). The presumed ability of Gpr30 to bind estrogen and its intrinsic nature as G protein-coupled receptor have aroused a great interest supported by an exponential increased number of publications. However, recently the function of Gpr30 as an estrogen receptor has been strongly questioned in different publications rebutting the direct involvement of Gpr30 in estrogen signalling and proposing rather a subordinate role of Gpr30 to ERα (44, 45, 51).

Most studies on Gpr30 have been conducted *in vitro* without a strong *in vivo* models support. In order to understand the physiological function of Gpr30 *in vivo* we decided to characterize Gpr30-T181 Deltagen mice. Deltagen mice were generated by a "global" knockout strategy using a LacZ-neomycin replacement target vector. Since Deltagen mice did not show any obvious phenotype and protein expression analysis revealed high expression of Gpr30 in small arterial vessels and pancreas (60) we decided to challenge mutant mice with HFD, presumably enhancing a possible metabolic and a cardiovascular phenotype. Metabolic and hemodynamic tests *in vivo* were performed. In parallel to the HFD challenge, mice underwent an extensive primary screening, aimed at a deeper complete analysis of the mutant mice and a valuable starting point for further investigations. Moreover to confirm the results obtained in these mice and in order to exclude an incomplete phenotype potentially due to the adopted targeting strategy (81) we also performed baseline experiments in SHG17 Artemis mice, a Gpr30 KO mouse model generated through a recombinase-based approach (51).

3 Materials and Methods

3.1 Gpr30 mutant mouse models

3.1.1 Gpr30-T181 Deltagen mice

Gpr30-T181 mice were purchased by Deltagen (San Carlos, USA). Gpr30-T181 Deltagen mice were generated by gene targeting strategy. Embryonic stem (ES) cells derived from the 129/OlaHsd mouse substrain were used to generate chimeric mice. The third exon of Gpr30 mouse gene, coding for the open reading frame (ORF), was targeted by homologous recombination using a gene targeting construct containing a LacZ reporter gene and a neomycin resistance gene (LacZ-neo^r) (Fig. 3.1). ES cells from the 129/OlaHsd mouse substrain were transfected with the linearized construct. Selected ES cells containing the gene targeting construct were injected into C57BL/6 blastocyst and the blastocyst implanted into a CD-1 pseudo recipient. Male chimeras (producing C57BL/6 sperm and 129 sperm) were mated to C57BL/6 mice. Offspring that resulted from the outcross of the 129 sperm and the C57BL/6 ova were the F1 generation and had an agouti colour. Agouti pups were genotyped. F1 heterozygous males were in house backcrossed to C57BL/6 parental line, for at least 6 generations.

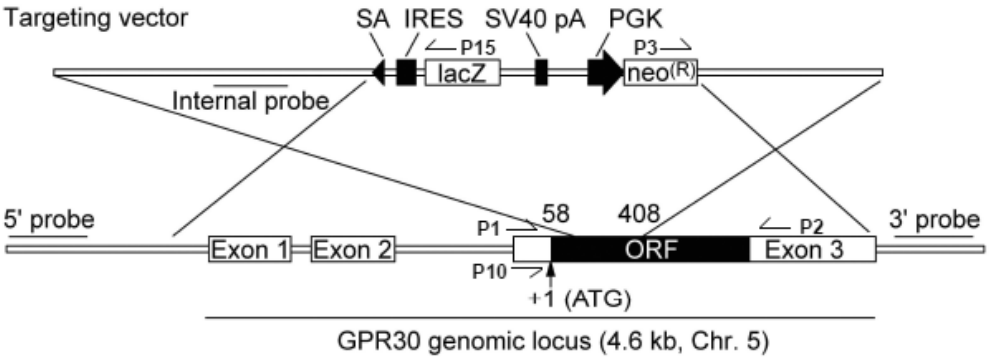

Figure 3.1: Targeting vector used to generate Gpr30-T181 Deltagen mice

The targeting vector is consisting in: a splice acceptor (SA) site, an internal ribosome entry site (IRES), a β-galactosidase gene sequence (LacZ), a polyadenylation site from SV40 virus (SV40 pa), and in a phosphoglycerate kinase (PGK) promoter. The PGK promoter drives the transcription of neomycin for a positive selection of ES cells undergoing homologous recombination. Gpr30 mouse gene is consisting of three exons; the third one contains the open reading frame (ORF): 349 bp of the ORF were deleted by the insertion of the targeting vector. The ATG position, a schematic representation of probes for southern blotting primers used in genotyping and Real-Time PCR are reported (P1, P2, P3, P10, P15). Adapted from Iseensee *et al.* (60).

3.1.2 SHG17 Artemis mice

SHG17 Artemis mice were provided by Bayer Schering Pharma (Berlin, Germany). Gpr30 KO mice were generated through a Cre-recombinase approach (45). The inactivation of Gpr30 was obtained deleting the exon 3 from the murine genome which encodes the complete ORF of the Gpr30 protein. The targeting construct was based on a genomic fragment containing the genomic sequence of exon 1, 2 and 3 and the surrounding introns of the murine Gpr30 gene. The fragment was modified in order to introduce two LoxP sites flanking the exon 3 and a cassette containing a PGK promoter driving the transcription of neomycin and thymidine kinase genes (PGK-tk-neo^r cassette) flanked by two Frt sites. After transfection in embryonic stem cells and selection with G418, one of the homologously recombined clones harbouring the targeted allele was used for the generation of chimeric mice by blastocyst injection. To eliminate exon 3 and the selection marker, mice heterozygous for the targeted allele were crossed with transgenic mice carrying a copy of Cre-recombinase gene. In order to eliminate the Cre recombinase transgene the resulting offspring heterozygous for the null allele was backcrossed with C57BL6 mice.

3.1.3 Genotyping of Gpr30-T181 Deltagen mice

3.1.3.1 Materials

Tail lysis buffer: NaAcetate 300 mM, Tris-HCl 10.0 mM, EDTA 5.0 mM, Triton X-100 1%, Proteinase K 750 µg/ml; pH 8.3.
dNTPs 10 mM (Fermentas, Burlington, Canada)
10 X Taq Buffer with Magnesium 15 mM (Eppendorf, Hamburg, Germany)
Taq DNA Polymerase 5 u/µl (Eppendorf, Hamburg, Germany)
Primers genes, sequences and relative abbreviations are reported in the table 3.1.

Table 3.1 Primers

Primer	Sequence	Gene/localization/orientation	Experiment
P1	GGTGGAGATCTACCTAGGTCCCGTG	Gpr30, exon 3; fw	Gpr30-T181 mice genotyping
P2	ACCTGTCGAAGCTCATCCAGGTGAG	Gpr30, exon 3; rev	Gpr30-T181 mice genotyping
P3	GGGGATCGATCCGTCCTGTAAGTCT	Neo: fw	Gpr30-T181 mice genotyping
P4	CCCGAATTCGTGCCATCTCAGGTAGGAGC	5´construct arm targeting vector Gpr30 T181-mice; fw	southern blotting: for 5´ probe
P5	CCCGAATTCCCAGAGCTGAGGTGCTTTCC	5´construct arm targeting vector Gpr30-T181mice; rev	southern blotting:for 5´ probe
P6	CCCGAATTCTTCTGCGTACTCTCCTATGTACC	3´construct arm targeting vector T181-mice; fw	southern blotting: for 3´ probe
P7	CCCGAATTCGCTCTGCCAAGTCCACTAAACC	3´construct arm targeting vector T181-mice; rev	southern blotting: for 3´ probe
P8	CCCGAATTCCACGTCTCTTTCCAACAGCTGC	LacZ-Neo^r-cassette Gpr30-T181 mice; fw	southern blotting: for internal probe
P9	CCCGAATTCAGTAGTCGCATCCATGGCTTCC	LacZ-Neo^r cassette Gpr30-T181 mice; rev	southern blotting: for internal probe
P10	TGTCCACCCTTCTGGTTTTC	Gpr30 exon 3; fw	Gpr30-T181 mice: mol. characterization:
P11	GGTAGATCTCCACCCCAACA	Gpr30 exon3; rev	Gpr30-T181 mice: mol. characterization:
P12	CTGCTTCTGCTTTGCTGATG	Gpr30 exon 3; fw	Gpr30-T181 mice: mol. characterization
P13	CGATGAGGGAGTAGCAGAGG	Gpr30 exon 3; rev	Gpr30-T181 mice: mol. characterization
P14	GTGCACATGCTTTACATGTGTTT	Lac Z; fw	Gpr30-T181 mice: mol. characterization
P15	GTGGCCATATTATCATCGTGTTT	LacZ; rev	Gpr30-T181 mice: mol. characterization
P16	TGTTCCTACCCCCAATGTGT	Gapdh; fw	Real Time: reference gene
P17	CCTGCTTCACCACCTTCTTG	Gapdh; rev	Real Time: reference gene
P18	TGTTGTTGGATATGCCCTTG	Hprt; fw	Real Time: reference gene
P19	TTGCGCTCATCTTAGGCTTT	Hprt; rev	Real Time: reference gene
P20	CCATCATCAATGGGTACAAGC	PO; fw	Real Time: reference gene
P21	CAGATGGATCAGCCAGGAAG	PO; rev	Real Time: reference gene
P22	ACCCACAGCTCTCTTGTGTGC	Shg17 mice targeting vector; fw	SHG1717 mice genotyping
P23	TCTGCGTACTCTCCTATGTACC	Shg17 mice targeting vector; fw	SHG1717 mice genotyping
P24	TCATTTTATCGCCTACTTGTTACC	Shg17 mice targeting vector; rev	SHG1717 mice genotyping
P25	GAGAACGCTCACACAAAGACC	Atp2a2; fw*	Thymus microarray validation
P26	CAATTCGTTGGAGCCCCAT	Atp2a2; rev*	Thymus microarray validation
P27	ACATGGTCTGGGACTTCTGG	Cat; fw	Thymus microarray validation
P28	CAAGTTTTTGATGCCCTGGT	Cat; rev	Thymus microarray validation
P29	TCTGCGTACTCTCCTATGTACC	Ccr5; fw	Thymus microarray validation
P30	TGTCATAGCTATAGGTCGGAACTG	Ccr5; rev	Thymus microarray validation
P31	ATTGACAGGATTGGAGCCCAGAGT	Nppa; fw**	Thymus microarray validation
P32	TGACACACCACAAGGGCTTAGGAT	Nppa; rev**	Thymus microarray validation

Primers list. fw: forward; rev: reverse; mol.: molecular; Gapdh: Glyceraldehyde-3-phosphate dehydrogenase; Hprt: hypoxanthine-guanine phosphoribosyltransferase; PO: ribosomal protein, large; Atp2a2: ATPase, Ca++ transporting, cardiac muscle, slow twitch 2; cat: catalase; Ccr5: chemokine (C-C motif) receptor 5; Nppa: natriretic peptide A.*: published in Primer Bank, http://pga.mgh.harvard.edu/primerbank/;. **: published in RT primer Data Base: http://medgen.ugent.be/rtprimerdb/index.php.

3.1.3.2 Method

Tail samples were collected in a 96-well format. Hundred µl tail lysis buffer were added to the biopsies. The samples were incubated over night at 55 °C and the day after centrifuged at 2000 rpm. In order to destroy proteinase K the supernatant was heated at 95 °C for 5 minutes. Supernatants were transferred in a new tube and subsequently diluted 1:10 in Tris 10 mM, pH 8.3. Two µl of the dilutions were used as template in genotyping PCR reaction (Table 3.2).
Inheritance of the targeting construct was monitored by three types of PCR genotyping assays (Table 3.2) using three primers (P1, P2, P3, Table 3.1). Primers P1 and P2 were drawn on the 5´ and 3´ regions of exon 3 respectively, flanking the targeting vector; primer P3 was drawn on the neomycin gene of the targeting vector (Fig. 3.1). The first type of reaction (multiplex, primers P1, P2 and P3) was designed to simultaneously detect the endogenous and targeted alleles and was used to genotype mice from both the F1 and F2 generations. The second type of reaction (targeted, primers P2 and P3) was designed to detect only the targeted allele and was used to genotype mice from the F1 generation. This step ensured that only heterozygous mutant mice (Gpr30-T181$^{+/-}$) proceeded to the breeding programs. The third type of reaction (endogenous, primers P1 and P2) was designed to detect the wildtype (Gpr30-T181$^{+/+}$) or endogenous allele and was only used to genotype mice from the F2 generation. This quality control step ensured that homozygous mutant mice (Gpr30-T181$^{-/-}$) were always accurately genotyped.

Table 3.2: Genotyping PCR reaction

Reagent		Amount (µl)	Final concentration
dH_2O		14.6	
10X Taq Buffer		2	1X
dNTPs		0.4	0.2 mM
Primer Mix* (5 µM each one)		0.8	0.2 µM
Taq DNA Polymerase		0.2	0.05 u/µl
Template		2	
Final volume		20	
Genotyping PCR reaction types			
Primer combination	Genome amplified fragment (bp)	Allele	Reaction
P1/P2/P3	433; 618	wildtype; targeted	multiplex
P2/P3	618	targeted	targeted
P1/P2	433	wildtype	endogenous

*for the multiplex PCR reaction primers P2 and P3 were used at the final concentration of 2.5 µM, whereas P1 primer at the final concentration of 5 µM

Thermic profile of the genotyping PCR reaction

1) 94 °C 3 min

2) 35 cycles:

94 °C 10 sec

60 °C 30 sec

68 °C 1.5 min

3) 68 °C 7 min

PCR products were separated on a 1.4% agarose gel for 50 min at 180 V (see also Results).

3.1.4 Southern Blotting*

3.1.4.1 Materials

Lyses buffer: Tris-Cl 10 mM, EDTA 100 mM, SDS 0.5%, pH 8.0

RNAse A 30 mg/ml (Sigma-Aldrich, St. Louis, USA)

Proteinase K 10 mg/ml (Boehringer Mannheim, Mannheim, Germany)

Buffered phenol (Roth, Karlsruhe, Germany)

Ammonium acetate10 M (Merck, Darmstadt, Germany)

Ethanol (Merck, Darmstadt, Germany)

TE: tris-EDTA solution

Nanodrop (Thermo Scientific, Wilmington, USA)

PCR2.1 TOPO cloning kit (Invitrogen, Carlsbad, USA)

PCR DIG Probe synthesis kit (Roche, Basel, Switzerland)

Restriction endonucleases enzymes:

EcoRI, BamHI, HindIII (New England Biolabs, Ipswich, USA)

TBE buffer: tris-borate-EDTA solution

DIG-labelled DNA marker (Roche, Basel, Switzerland)

Denaturation solution: NaOH 0.5 M, NaCl 1.5 M

Neutralization solution: Tris-HCl 0.5 M pH 7.5; NaCl 1.5 M

20X SSC: NaCl 3M, sodium citrate 300 mM, pH 7.0

Nylon membrane (Roche, Basel, Switzerland)

Transilluminator: (Stratagene, Cedar Creek, USA)

DIG Easy Hyb buffer (Roche, Basel, Switzerland)

Hybridisation oven: (Binder, Tuttlingen, Germany)

* Southern blotting was realized in collaboration with Jörg Isensee.

Low stringency buffer: 2X SSC, SDS 0.1%

High stringency buffer: 0.5X SSC, SDS 0.1 %

Washing buffer: maleic acid 0.1 M, NaCl 0.15 M, Tween 20 0.3 % (v/v), pH 7.0

Blocking solution: 10X blocking solution (Roche, Basel, Switzerland) diluted 1:10 in maleic acid buffer

Antibody solution: anti-digoxigenin-AP 75 mU/ml, 1:10000 in blocking solution

Detection buffer: Tris-HCl 0.1 M, NaCl 0.1 M, pH 9.5

CSPD

x-ray films: Amersham hyperfilm ECL (GE Healthcare, Buckinghamshire, UK)

3.1.4.2 Method

High molecular weight genomic DNA was isolated from liver and spleen using a phenol-based protocol according to Sambrook and Russel (177). Hundred mg of powdered tissue was suspended in 800 µl lyses buffer in a 2.0 ml tube. RNA was digested by adding 1 µl RNAse A for 1 h at 37 °C. The sample was gently mixed with 10 µl proteinase K and incubated at 50° overnight. After adding an equal amount of buffered phenol the solution was mixed for 10 min. The emulsion was separated by centrifugation at 5000 g for 15 min at room temperature. The viscous aqueous phase was carefully transferred into a new tube and 0.2 volumes of ammonium acetate 10 M and 2 volumes of ethanol were added. The precipitate was collected, washed twice with ethanol 70%, and stored in an open tube at room temperature until the ethanol was evaporated. Subsequently the DNA was dissolved in 200-500 µl Tris-HCl 10 mM at 4 °C for 12 hours. The obtained high molecular weight DNA was diluted 1:10 in TE and vigorously vortexed before quantification with a Nanodrop at 260 nm.

DIG-labeled probes were constructed in order to match outside and adjacent the 5´ and 3´ construct arms as well as the targeting vector (internal probe). The sequences were amplified from genomic DNA by PCR employing primers P4-P5 for the 5´ probe, P6-P7 for the 3´ probe, and P8-P9 for the internal probe. The probes sequences were subcloned in PCR2.1-TOPO vector. For DIG-labeling the PCR DIG Probe synthesis kit was used with purified plasmid DNA as template. Control reactions without DIG-dUTP were included.

About 10 µg genomic DNA was digested with 100 U of the restriction endonucleases EcoRI, Bam HI or Hind III in a total reaction volume of 50 µl at 37 °C overnight. Digested DNA samples (5 µg) were separated by gel electrophoresis in large gels (agarose 0.8% in TBE buffer) at 30 V overnight. Five µl of DIG-labelled DNA marker was used as molecular weight marker. The gel was briefly stained in ethidium bromide 0.3 µg/ml and examined under UV light.

DNA denaturation was obtained submerging the gel in HCl 250 mM for 10 min at room temperature and placing it twice in denaturation solution for 15 min. Following a quick rinse in double distilled water, the gel was submerged in a neutralization solution for 15 minutes and then equilibrated in 20X SSC for at least 10 min.

The DNA was transferred overnight onto a positively charged nylon membrane using a downward capillary transfer procedure. On the next day, the damp membrane was placed on a Whatman 3MM paper previously soaked in 2X SSC and exposed to UV light in a trans-illuminator. The blot was rinsed briefly in double distilled water, air dried and stored at 4 °C.

For hybridization the blots were placed in roller bottles containing 10 ml pre-warmed DIG Easy Hyb buffer and incubated for at least 30 minutes at 46.5 °C in a hybridization oven. To prepare the hybridization solution, 10 µl of DIG-labelled PCR product was diluted 1:5 in dH_2O, denatured at 95 °C for 5 min, chilled on ice, and added to 5 ml pre-warmed DIG Easy Hyb buffer. The pre-hybridization solution was replaced by the hybridization solution and blots were incubated at 46.5 °C overnight. On the next day they were washed twice for 5 min in low stringency buffer at room temperature transferred into high stringency buffer pre-warmed at 68 °C and incubated twice for 15 min at 68 °C with gentle shaking.

To visualize probe-targeted hybrids by chemiluminescence, the blots were washed twice for 2 minutes in washing buffer at room temperature, transferred into blocking solution for 30 min and incubated with antibody solution for 30 min while shaking. After washing twice for 15 minutes with washing buffer, the blots were equilibrated in detection buffer and placed on acetate sheets, covered with 1 ml diluted CSPD, sealed, and incubated for 10 min at 37 °C to enhance the luminescence reaction. Finally the x-ray films were exposed to the sealed blots for 30-60 min.

3.1.5 RNA extraction

3.1.5.1 Materials

PureLink™ Micro-to-Midi Total RNA Purification System (Invitrogen, Carlsbad, USA)
GIBCO ultraPURE distilled water DNAse, RNAse free (Invitrogen, Carlsbad, USA)
Dnase I, Amplification Grade 1 u/µl (Invitrogen, Carlsbad, USA)
GIBCO ultraPURE distilled water DNAse, RNAse free (Invitrogen, Carlsbad, USA)
Agilent 2100 Bioanalyzer (Agilent Technologies, Santa Clara, USA)
Agilent 2110 expert software (Agilent Technologies, Santa Clara, USA)
Agilent RNA6000 Nano Kit (Agilent Technologies, Santa Clara, USA)
RNA Nano Chips (Agilent Technologies, Santa Clara, USA)

3.1.5.2 Method

Using a rotor stator 10-60 mg of tissue sample was homogenized in 0.6 ml of RNA Lysis Solution containing guanidinium isothiocyanate. The sample was centrifuged at 2600 g for 5 minutes at room temperature. The supernatant was carefully transferred to a clean RNase-free tube. A volume of ethanol 70% was added to each volume of tissue homogenate. After mixing the sample was transferred to a RNA spin cartridge and centrifuged at 12000 g for 15 sec: the flow-through discarded. Ten µl of DNase I (1u/µl), properly resuspended in 70 µl of a DNase buffer, was added to the column for 15 minutes and subsequently removed through centrifugation at 12000 g for 15 sec. To remove impurities, the silica-based membrane in the spin cartridge binding RNA was properly washed, and RNA eluted using 30 µl of RNAse-free water.

For an electrophoretic analysis of the extracted RNA, 1 µl of the RNA sample was loaded in an Agilent Nano Chip in presence of 1 µl of RNA 6000 Nano marker. The RNA-chip was run in an Agilent 2100 Bioanalyzer and concentration and quality of the extracted RNA analysed through Agilent 2100 expert software. Indeed per each RNA sample analysed were reported and evaluated the RNA ratio (28S/18S) and a RNA integrity number (RIN).

3.1.6 Reverse transcription

3.1.6.1 Materials

High Capacity cDNA Archive Kit (Applied Biosystems, Foster City, USA)

3.1.6.2 Method

For the cDNA synthesis of RNA samples a reverse transcription reaction (RT+) along with a reverse transcription negative control (RT-) were assembled as reported in the Table 3.3. Samples were incubated at 25 °C for 10 min and at 37 °C for 120 min.

Table 3.3: Reverse transcription

Reagent	RT+ (µl)	RT- (µl)	Final Concentration
RNA 0.1 µg/ µl	10	10	0.05 µg/µl
RNAse -free H20	10	11	
10X RT Buffer	2	2	1X
dNTPs mix 100 mM	0.8	0.8	4 mM
10X Random Primers mix	2	2	1X
Multiscribe™ RT 50 u/µl	1	-	2.5 u/µl
Ribonuclease Inhibitor 20 u/µl	0.5	0.5	0.5 u/µl
Final volume	20	20	

3.1.7 Real Time PCR

3.1.7.1 Materials

Sybr-Green I Master Mix (Applied Biosystems, Foster City, USA)

Stratagene Mx3000P™ (Stratagene, Cedar Creek, USA)

Stratagene MxPro. Software (Stratagene, Cedar Creek, USA)

96 well Multiply-PCR plates (Sarstedt, Nümbrecht, Germany)

Primer 3 software (http://frodo.wi.mit.edu/)

3.1.7.2 Method

Real-Time PCR quantification of sequences within and flanking the Lacz-neo^r cassette was realized using the following couples of primers: P10-P11, P12-P13, P2-P3 and P10-P15 (Table 3.1). Quantification of the wildtype allele was realized using specific primers designed for Gpr30 (P1-P2) (Table 3.1).

Real-Time PCR reactions were performed in triplicate using SYBR-Green master mix. Real-Time was performed using per every cDNA sample the corresponding reverse transcription negative control (RT-). cDNA and RT- samples were diluted 1:50 in water in order to obtain approximately a final cDNA concentration of 1 ng/µl. The reactions were assembled as showed in Table 3.4.

Table 3.4: Real-Time PCR

Reagent	Amount (µl)	Final Concentration
SYBR Mix 2X	12.5	1X
H_2O	1.25	
Primer mix (5 pmol/µl each one)	1.25	0.25 pmol/µl
Template (1 ng/µl)	10	0.4 ng/µl
Final volume	25	

1) Relative quantification of gene expression

Normalisation and error propagation were calculated as in Vandesompele *et al.* (178).

3.1.8 SHG17 Artemis mice genotyping

3.1.8.1 Materials

See genotyping of Gpr30-T181 Deltagen mice.

3.1.8.2 Method

SHG17 Artemis mice genotyping was performed as described by Otto *et al.* (45). Genomic DNA was extracted from 1-2 mm long tail tips as above described (see Genotyping of Gpr30-T181 mice). Two PCR reaction using three primers P22, P23 and P24 (Table 3.1) were performed. The wildtype allele was amplified using primers 3´ to exon 3 (P22, P24) and mutant allele using primers flanking the inserted LoxP sites (P23, P24). Amplification of the wildtype allele resulted in a band of 398 bp, whereas amplification of the mutant allele resulted in a band of 560 bp.

Thermic profile of the genotyping PCR reaction

1) 94 °C 3 min

2) 35 cycles:

94 °C 45 sec

60 °C 1 min

72 °C 1 min

3) 72 °C 10 min

PCR products were separated on a 1.4% agarose gel for 50 min at 180 V (see also Results).

3.2 Primary screen

All animal procedures here reported were performed in accordance with German animal welfare law and with the permission of the District Government of Berlin.

Animals breeding were set up using, brother/sister mating (intercrosses) in the following ratio: 2 females: 1 male. 50 Gpr30-T181$^{+/-}$ females (N=6) were bred with 25 males Gpr30-T181$^{+/-}$ (N=6). A cohort of 80 animals was selected and the following mouse groups shipped to the Germany Mouse Clinic for a primary screen: 20 Gpr30-T181$^{-/-}$ females, 20 Gpr30-T181$^{+/+}$ females, 20 Gpr30-T181$^{-/-}$ males, 20 Gpr30-T181 $^{+/+}$ males. Breeding records were realized using both the "mating unit" system (each mating pair and its offspring were registered) and the animal/litter system (each litter and each individual animal were registered) (99). Animals were sent to the German Mouse Clinic at the age of 4 weeks.
The primary screen was performed on 8 weeks old animals, along two main pipelines and in the following areas: dismorphology, cardiovascular system, energy metabolism, clinical chemistry and haematology, eye, lung function, molecular phenotyping, behaviour, neurology, nociception, immunology and allergy, steroid metabolism, pathology (Fig. 3.2). All the experiments were performed in 10 weeks.

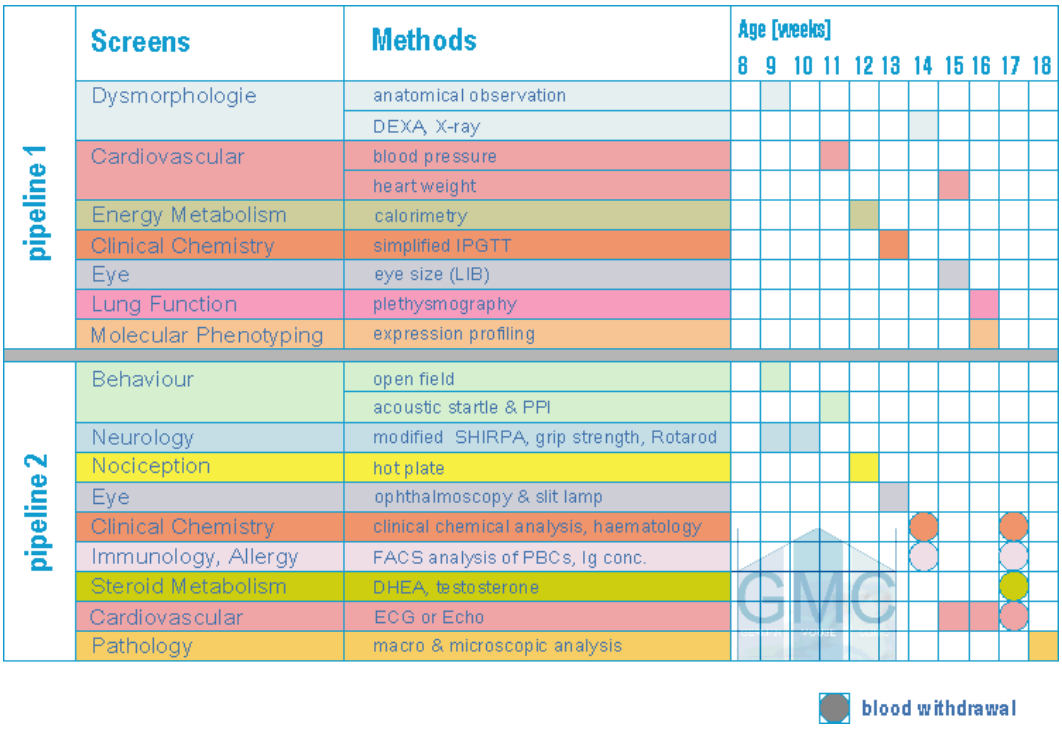

Figure 3.2: Workflow at the German Mouse Clinic

3.2.1 Microarray RNA analysis

3.2.1.1 Materials

RNeasy Midi kit (Qiagen, Hilden, Germany)

Hybridization buffer: 6X SSC, 0.5% SDS, 5X Denhardt's solution, 50% formamide

HS4800 Hybstation (Tecan, Männerdorf, Switzerland)

GenePix 4000A microarray scanner (Axon Instruments, Foster City, USA)

GenePix Pro 6.1 image processing software (Axon Instruments, Foster City, USA)

3.2.1.2 Method

1) Organ collection

Twelve male mice (6 Gpr30-T181$^{-/-}$ mice and 6 wildtype littermates) of the Gpr30 Deltagen mutant mouse line were provided to the molecular phenotyping screen. Brain, kidney and thymus organs were collected. To minimize the influence of circadian rhythm on gene expression, mice were killed between 9 am and 12 am by carbon dioxide asphyxiation.

2) Isolation of total RNA

Total RNA was isolated just before processing for expression profiling. For preparation of total RNA individual organs were thawed out in buffer containing chaotropic salt and homogenized using a Polytron homogenizer. Total RNA from individual samples was obtained according to manufacturer's protocol using RNeasy midi kits. The concentration was calculated from OD 260/280 measurement and 2 µg RNA aliquots were run on a formaldehyde agarose gel to check for RNA integrity. The RNA was stored at -80 °C in RNase free water.

3) Chip Hybridization

Two chip hybridizations were performed with RNA from all selected organs of each individual Gpr30-T181 mouse. Each chip hybridization experiment was performed against the identical pool of the same organ of reference RNA (reference RNA pool). For each individual Gpr30-T181 mouse the chip experiment included a color–flip experiment.

4) Reverse transcription and fluorescent labeling

For labeling 15 µg of total RNA were used for reverse transcription and indirectly labeled with Cy3 or Cy5 fluorescent dye according to a modified TIGR protocol (179). Labeled cDNA was dissolved in 50 µl hybridization buffer and mixed with 50 µl of reference cDNA solution (pool from 6 control animals) labeled with the second dye. This hybridization mixture was injected on a pre-hybridized microarray in a HS4800 Hybstation and incubated at 42 °C for 16 hours. After hybridization slides were washed with 3X SSC, 1X SSC, 0.5X SSC

and 0.1X SSC at room temperature. Slides were dried with nitrogen. Dried slides were scanned with a GenePix 4000A microarray scanner and the images were analysed using the GenePix Pro6.1 image processing software.

5) Normalization

To normalize the signal intensities of the two channels of the microarray experiment a moving average approach was used. The sum of the two signal intensities of each feature was calculated and these sums of all features were ranked. Following, the ratio of the moving averages (± 50 features) of both channels was calculated for each feature, leading to a signal intensity dependent on a normalization factor.

5) Detection of differentially expressed genes

For the identification of differentially expressed genes in the comparison of two conditions with microarrays (Gpr30-T181$^{-/-}$ vs. control mice) we used the Significance Analysis of Microarrays (SAM). The SAM statistic identifies significant changes in gene expression by performing a set of gene-specific t-tests. For each gene, a score is calculated on the basis of expression change relative to the standard deviation of repeated measurements for that gene. Genes with scores greater than a threshold delta were defined as significantly deregulated. Manual adjustment of this threshold delta allows the identification of smaller or larger gene cohorts. In addition, based on random permutations of all measurements, a false discovery rate was estimated.

6) Functional annotation and pathway analysis

For the detection of gene ontology (GO, www.geneontology.org) categories and KEGG pathways (Kyoto Encyclopedia of Genes and Genomes, www.kegg.com) with a significant overrepresentation of genes in a given group compared to the whole genome, the web-based DAVID tool was used (Database for Annotation Visualization and Integrated Discovery, National Institute of Allergy and Infectious Disease). Fisher's Exact test was applied to determine whether or not the proportion of those genes falling into each GO category or KEGG pathway differed significantly between the input data set and the whole genome. In order to create networks of biologically related genes Ingenuity Pathways Analysis was used (Ingenuity® Systems, www.ingenuity.com).

7) Gene expression validation through Real Time PCR

RNA extraction, reverse transcription and Real Time PCR were performed as above described. Four different couples of primers were used in order to perform Real Time PCR quantification of the following genes: ATPase, Ca^{++} transporting, cardiac muscle, slow twitch

2 (Atp2a2) also known as sarcoplasmic reticulum calcium-ATPase 2 (Serca2), catalase (Cat), chemokine (C-C motif) receptor 5 (Ccr5) and the natriuretic peptide A (Nppa), (Table 3.1). Relative quantification of gene expression was performed using the comparative Ct method (ΔΔCt) as described in (180). A de-regulation gene expression fold factor (2-ΔΔCt) was measured. Normalized Ct values of the gene of interest with the reference genes (house keeping genes) were compared using the Student's t-test, and the hypothesis of equality of means rejected with a p-value < 0.05.

3.3 Secondary screen

3.3.1 Groups

For the experiments were used male and female of both Gpr30 Deltagen and Artemis mutant mice, with sex-and age-matched control mice. Gpr30-T181 homozygous mutants (Gpr30-T181$^{-/-}$) and littermate control mice (Gpr30-T181$^{+/+}$) were fed with a high fat diet (HFD) or a control diet (CD); SHG17 homozygous mutant mice (SHG17$^{-/-}$) and littermate controls (SHG17$^{+/+}$) were fed with a standard diet.

Sex, diet, genotype, age and number of mice groups used for all the experiments are reported in Table 3.5.

Table 3.5: Animal groups

Deltagen Gpr30-T181 mice				
sex	diet	genotype	age (weeks)	number
female	CD	+/+	24	12
female	CD	-/-	24	9
male	CD	+/+	24	12
male	CD	-/-	24	10
female	HFD	+/+	24	12
female	HFD	-/-	24	9
male	HFD	+/+	24	11
male	HFD	-/-	24	11
Artemis SHG17 mice				
sex	diet	genotype	age (weeks)	number
female	standard	+/+	13	10
female	standard	-/-	13	10
male	standard	+/+	13	10
male	standard	-/-	13	10

3.3.2 Diets

3.3.2.1 Materials

Standard diet: complete diet for mice-maintenance meal V1534-300 (Ssniff, Soest, Germany)
High fat diet (HFD): rodent purified diet w/60% energy from fat, blue (TestDiet, Purina Mills LLC/PMI Nutrition International, Richmond, USA)
Control Diet (CD): rodent purified diet w/10% energy from fat, yellow (TestDiet, Purina Mills LLC/PMI Nutrition International, Richmond, USA)
The nutritional and energetic profiles of the last two diets are reported in the Tables 3.6 and 3.7 respectively:

Table 3.6: Rodents purified diets: nutritional profile

Components	Control diet		High fat diet	
	%	fat source: lard	%	fat source: lard
Protein	17.3		24.2	
Fat	4.3		34.7	
Fiber	4.7		5.5	
Carbohydrates	67.5		27.8	
Energy	Kcal/g		Kcal/g	
	3.78		5.21	

Table 3.7: Rodents purified diet: energetic profile

Components	Control diet		High fat diet	
	Kcal	%	Kcal	%
Protein	0.692	18.3	0.943	18.3
Fat	0.384	10.2	3.140	60.9
Carbohydrates	2.697	71.5	1.037	20.1

3.3.2.2 Method

Gpr30-T181 Deltagen mice were fed with HFD or CD for 25 weeks. Fresh food was used to replace old food twice per week. Mouse food intake was recorded twice per week between 10 a.m. and 12 a.m.

3.3.3 Body weight and body mass composition

3.3.3.1 Materials

Balance 1219 MP (Sartorius, Goettingen, Germany)
EchoMRI system (Echo Medical System, Houston, USA)

3.3.3.2 Method

Body weights were recorded twice per week between 10 a.m. and 12 a.m. Total body fat and lean mass of mice was assessed using an EchoMRI system. During the procedure, lasting 70 sec, mice were kept awake. For the measurements mice were put in an appropriate cylinder keeping them immobilized. Three different measurements per each mouse were recorded.

3.3.4 Intraperitoneal glucose tolerance test (IPGTT)

3.3.4.1 Materials

Precision Xtra Blood Glucose & Ketone Monitoring System glucometer (Abbott GmbH & Co.KJ, Wiesbaden, Germany)
Precision Xtra Blood Glucose Test Strips (Abbott GmbH & Co.KJ, Wiesbaden, Germany)
D-glucose, anhydrous (Sigma-Aldrich, St. Louis, USA)
Isotonic solution NaCl 0.9% (Fresenius Kabi, Bad Homburg, Germany)
Surgical Disposable Scalpel (Aesculap Ag & CO KG., Tuttlingen, Germany)

3.3.4.2 Method

The evening prior to the IPGTT mice were transferred into a clean cage only with water and fasted for 15 hours. The following morning mice were prepared for the glucose tolerance test: animals were weighed; the tail was nicked with a fresh razor blade by a horizontal cut of the very end, ~35 to 50 µl of blood was very gently massaged from the tail to a Precision Xtra glucometer test strip. Baseline blood glucose was measured by the glucose oxidase method using a Precision Xtra Blood Glucose & Ketone Monitoring System glucometer. When all mice were prepared the test was begun. A glucose solution (0.2 g/ml in 0.9% NaCl) was injected into the intraperitoneal cavity (1g glucose/Kg body weight). After 15, 30, 60, 90 and 120 minutes, blood glucose was sampled from the tail of each mouse by gently massaging a small drop of blood onto the glucose test strip. Glucose injections were timed so that the sample times were accurate for each animal. An IPGTT matrix example for a batch of 15 animals is reported in Table 3.8.

Area under the curve (AUC) values were calculated as reported by Nishikawa and colleagues (149).

Table 3.8: Intraperitoneal Glucose Tolerance Test Matrix

m	bw	g0	ig	t1	g1	t2	g2	t3	g3	t4	g4	t5	g5	t6	g6
1				0		15		30		60		90		120	
2				2		17		32		62		92		122	
3				4		19		34		64		94		124	
4				6		21		36		66		96		126	
5				8		23		38		68		98		128	
6				10		25		40		70		100		130	
7				12		27		42		72		102		132	
8				14		29		44		74		104		134	
9				16		31		46		76		106		136	
10				18		33		48		78		108		138	
11				20		35		50		80		110		140	
12				22		37		52		82		112		142	
13				24		39		54		84		114		144	
14				26		41		56		86		116		146	
15				28		43		58		88		118		148	

m: mouse identification number; bw: mouse body weight; g0: blood glucose in baseline; ig: injected glucose for the test (1g glucose/Kg body weight); tn scheduled time for injection (minutes); gn: measured blood glucose (mg/dl) at the time tn.

3.3.5 Echocardiography

3.3.5.1 Materials

Vevo 7700 (VisualSonics Inc., Toronto, Canada)

Vevo anaesthesia system (VisualSonics Inc., Toronto, Canada)

Isofluran Florene R (Abbott GmbH & Co.KJ, Wiesbaden, Germany)

Ultrasonic gel (Aquasonic 100, Fa. Parker, Fairfield, USA)

Electrodes gel (Signa Gel, Fa. Parker, Fairfield, USA)

Hair remover (Veet®, Reckitt Benckiser, Germany)

Surgical Tape Durapore™ (3M Health Care, Neuss, Germany)

Medical lamp (Petra Electric, Burgau, Germany)

3.3.5.2 Method

1) Animal preparation

Mice were anaesthetized using isoflurane (isoflurane 2%, oxygen 98%), and laid supine fixed to a platform for analysis through surgical tape stripes (Fig 3.3). Body temperature was monitored via a rectal thermometer and maintained at 36-38 °C using a heating pad and a medical lamp. All hair was removed from the chest using a chemical hair remover. Scanning was performed using an ultrasonic gel opportunely pre-warmed and spread on the mouse chest.

Figure 3.3: Echocardiography in mice, mouse preparation

Mice are fixed to a warmed plate using surgical tape, and a mask for anaesthesia (isoflurane).

2) Left ventricle: images acquiring

All the procedures used for echocardiography imaging and echocardiography calculations in the present study were performed as described and reported by Zhou and colleagues (2004) (173). A left parasternal transverse section of the left ventricle (LV) was obtained locating the transducer at the lower 1/3 of the mouse chest midline, orientating the direction of the transducer central axis in a posterior and slightly rightward direction so as to form approximately a 70° angle with the coronal plane. The orientation of imaging plane resulted rotated counter-clockwise from transverse plane approximately by 15° (Fig. 3.4, Fig. 3.5).

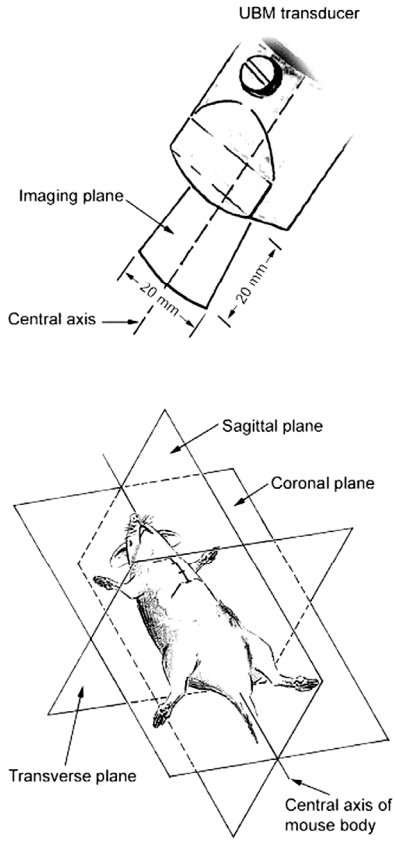

Figure 3.4: Echocardiography in mice, mouse orientation and its spatial relation with the transducer

In the upper panel it is shown the transducer and the related two-dimensional (2D) imaging planes. In the figure below the orthogonal planes of body mouse for investigation are schematically indicated, and the mouse chest midline subdivision in three parts reported. Taken from Zhou *et al.* (2004) (173).

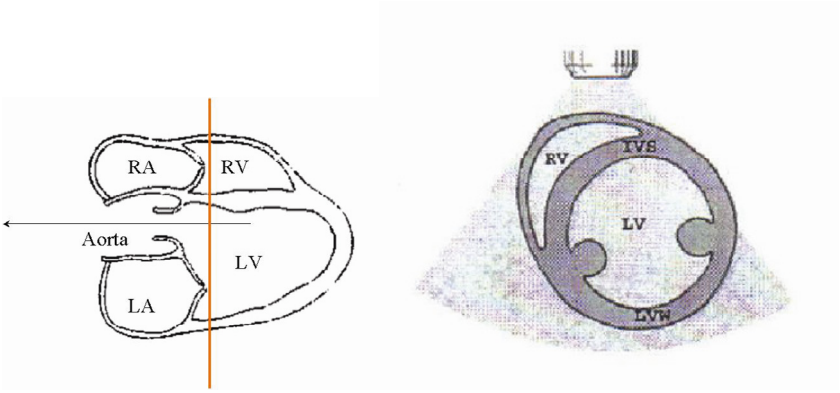

Figure 3.5: Echocardiography in mice, obtaining a left ventricle short axis view

Left: simplified heart schema in parasternal long axis view (heart sagittal section). The red line indicates schematically at which level the heart is transversally "cut" to obtain a left ventricle short axis view. Right: simplified 2D short axis view of the left ventricle as visualized by the operator in echocardiography (heart transversal section at papillar muscles level). Arrow: blood flow direction. RA: right atrium. RV: right ventricle. LV: left ventricle. LA: left atrium; IVS: internal ventricle septum; LVW: left ventricle wall.

3) Aorta: images acquiring

A right parasternal longitudinal section of the aortic arch with the descending tract in evidence was obtained locating the transducer at the middle 1/3 of the mouse chest midline, and orientating the direction of the transducer central axis leftward and posterior so as to form approximately a 40° angle with the coronal plane. The orientation of imaging plane resulted parallel to the central axis of mouse body (Fig. 3.6). A right parasternal longitudinal section of the aorta was obtained locating the transducer at the lower 1/3 of the mouse chest midline, orientating the direction of the transducer central axis leftward and posterior so as to form roughly a 70° angle with the coronal plane. The orientation of imaging plane resulted parallel to the central axis of mouse body. A right parasternal transverse section of the ascending aortic tract was obtained locating the transducer at the lower 1/3 third of the mouse chest midline, and orientating the direction of the transducer central axis posterior, slightly superior and leftward so as to form approximately a 70° angle with the coronal plane. The orientation of imaging plane resulted rotated counter clockwise from transverse plane approximately by 30°.

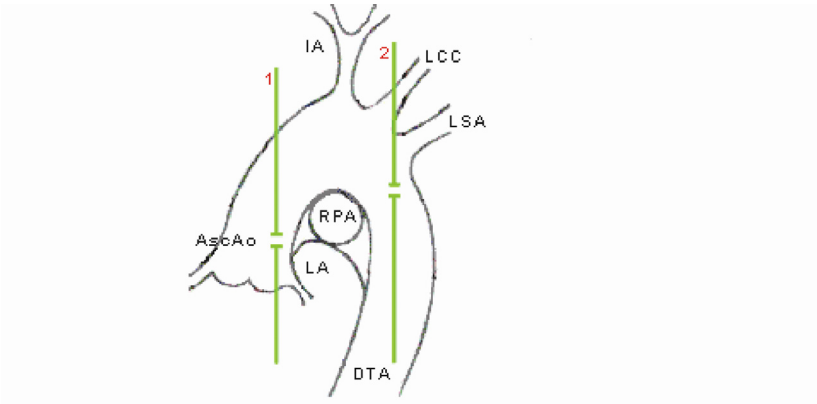

Figure 3.6: Echocardiography in mice, simplified schema of the mouse aortic arch

The green lines evidence the descending and the ascending aortic tracts. AscAo: ascending aorta. LA: left atrium; RPA: right pulmonary artery; IA: inanimate artery; LCC: left common carotid; LSA: Left subclavian; DTA: descending thoracic aorta.

4) Left ventricular parameters, formulas and calculations

A left ventricle short axis view was obtained to measure in M-Mode the following parameters left ventricular internal diameter in diastole (LVIDd) and left ventricular internal diameter in systole (LVIDs) (Fig. 3.7). Left ventricular volume in diastole (LV Vold), left ventricular volume in systole (LV Vols), ejection fraction (EF) and fractional shortening (FS) were calculated using the following formulas:

LV Vold= [7/ (2,4xLVIDd)] x $LVIDd^3$

LV Vols= [7/ (2,4xLVIDs)] x $LVIDs^3$

EF= 100 x [(LV Vold-LV Vols)/LVIDd]

FS= 100 x [(LVIDd-LVIDs)/LV Vold]

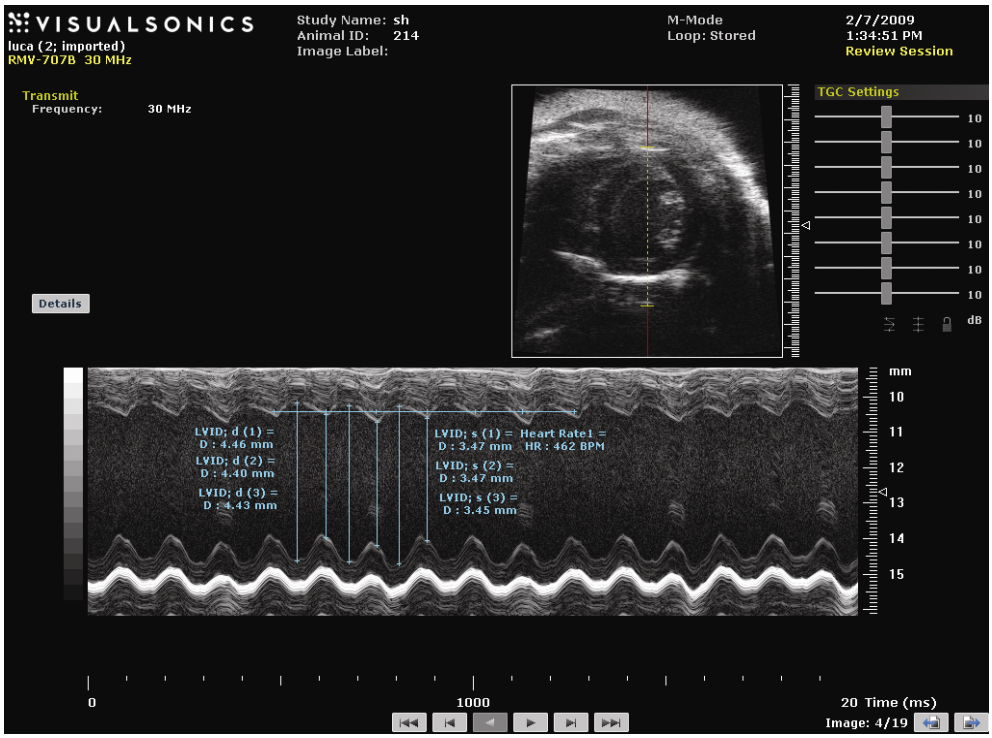

Figure 3.7: Echocardiography in mice

Left ventricle short axis view (upper panel) and measurements of LVIDd (3), LVIDs (3) and HR in M-Mode (lower panel) are shown. LVIDd: left ventricle diameter in diastole (mm); LVIDs: left ventricle diameter in systole (mm). HR: heart rate (beats per minute, BPM).

5) Aorta parameters

Right parasternal longitudinal sections of the ascending aortic tract and aortic arch were obtained to measure the end-diastolic diameter (EDD) of the aorta in B-Mode and M-Mode, respectively (Fig. 3.8 and 3.9). In particular a cine loop was recorded and a cine frame opportunely selected in order to operate EDD measurements in B-Mode.

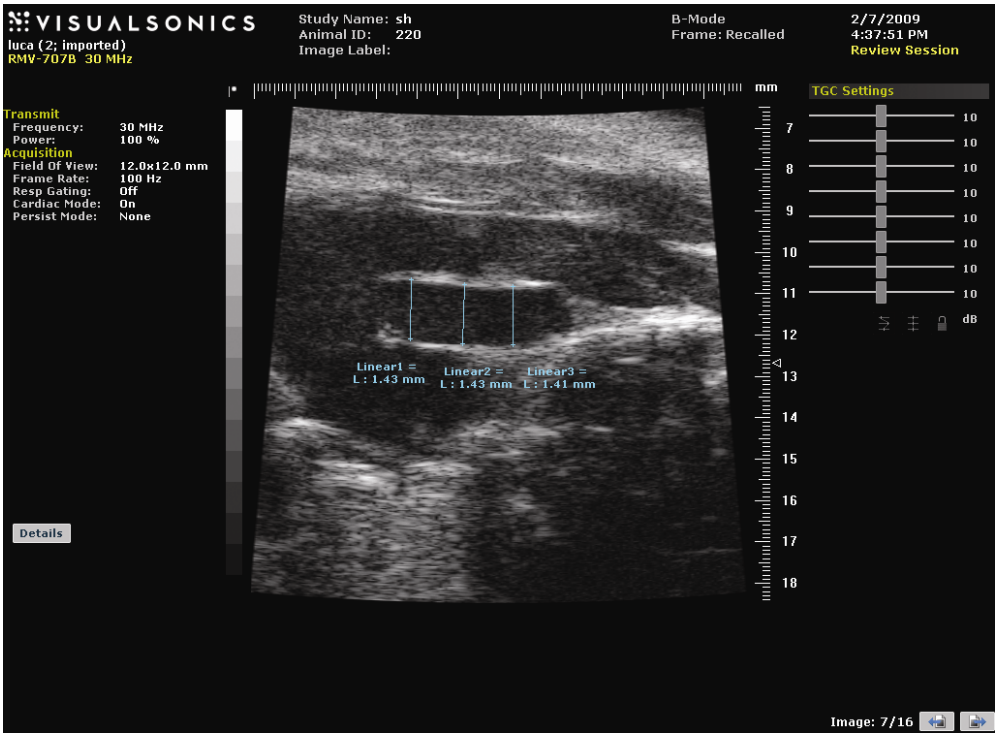

Figure 3.8: Echocardiography in mice

A right parasternal longitudinal section of the ascending aortic tract in a frame selected from a cine-loop and relative measurements of the aorta EDD in three different points are shown. EDD: end-diastolic diameter (mm).

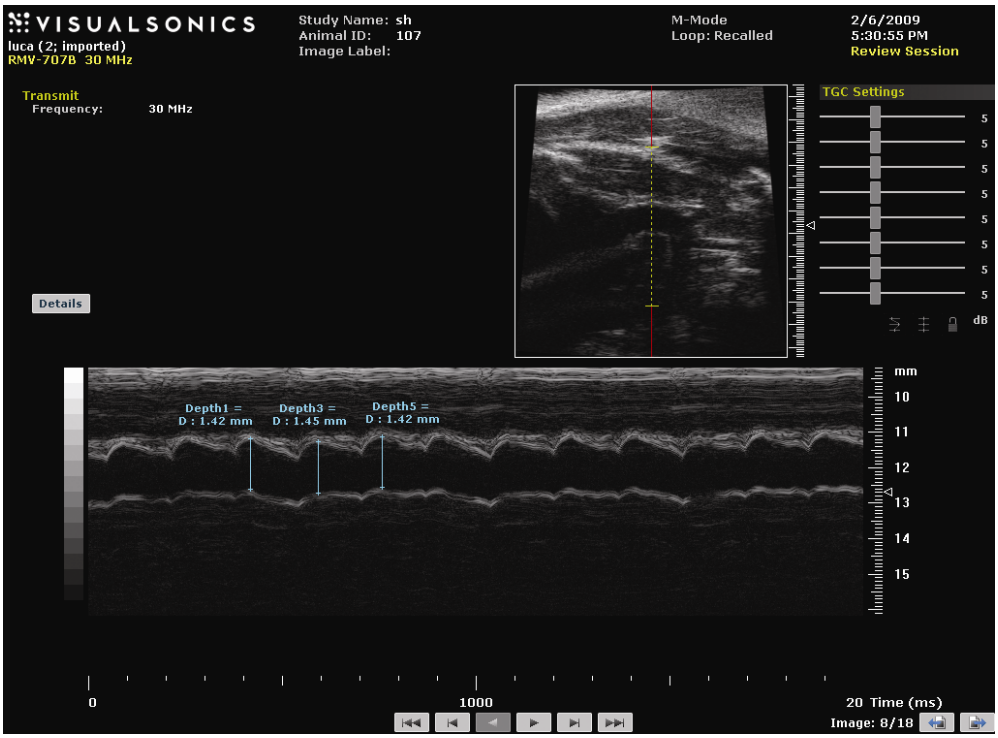

Figure 3.9: Echocardiography in mice

A right parasternal longitudinal section of the aortic arch (upper panel) and measurements of the aorta EDD (3) in M-Mode (lower panel) are shown. EDD: end-diastolic diameter (mm).

A right parasternal longitudinal section of descending aortic tract and an aorta short axis view were obtained in order to measure the blood flow velocity in the descending ($AoVel_{desc}$) and ascending ($AoVel_{asc}$) tracts of the aorta in Doppler-Mode, respectively (Fig 3.10 and Fig 3.11).

6) Data collection

Between 10 and 15 pictures per mouse study were collected. Per each study 6 measurements obtained from two selected pictures of LVIDd, LVIDs, EDD (B-Mode, M-Mode), $AoVel_{desc}$ and $AoVel_{asc}$ were recorded and the average calculated. Aortic blood flow velocity (AoVel) was expressed as an average of $AoVel_{desc}$ and $AoVel_{asc}$ values.

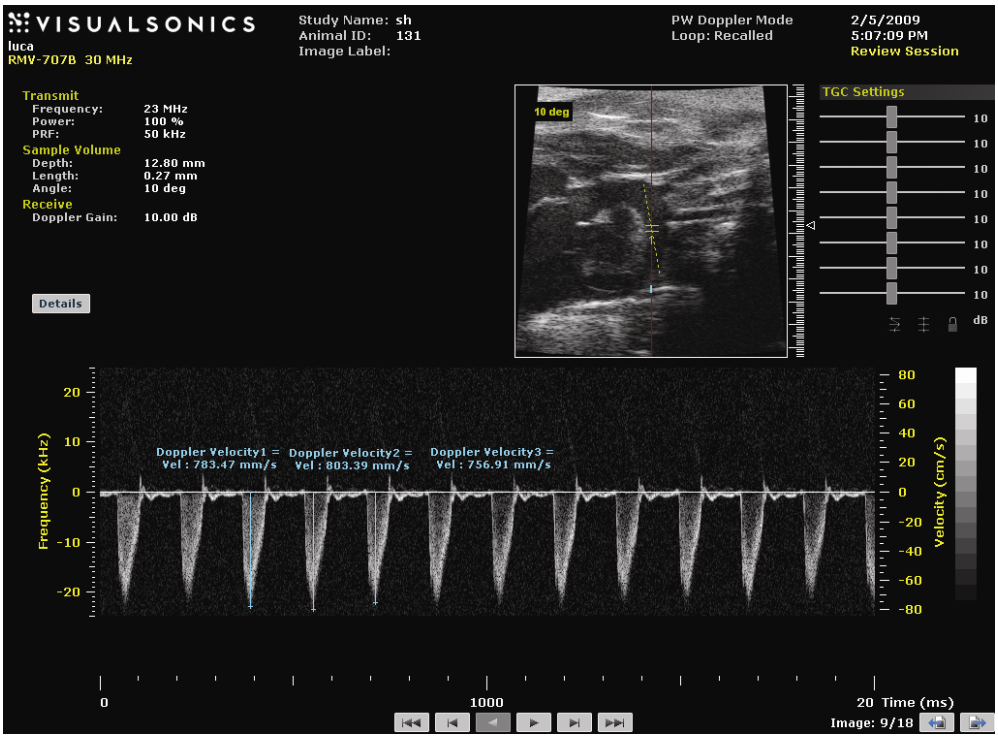

Figure 3.10: Echocardiography in mice

A right parasternal longitudinal section of aortic arch (upper panel) and blood flow velocity (cm/sec) measurements in Doppler (3) of the descending aortic tract (lower panel) are shown.

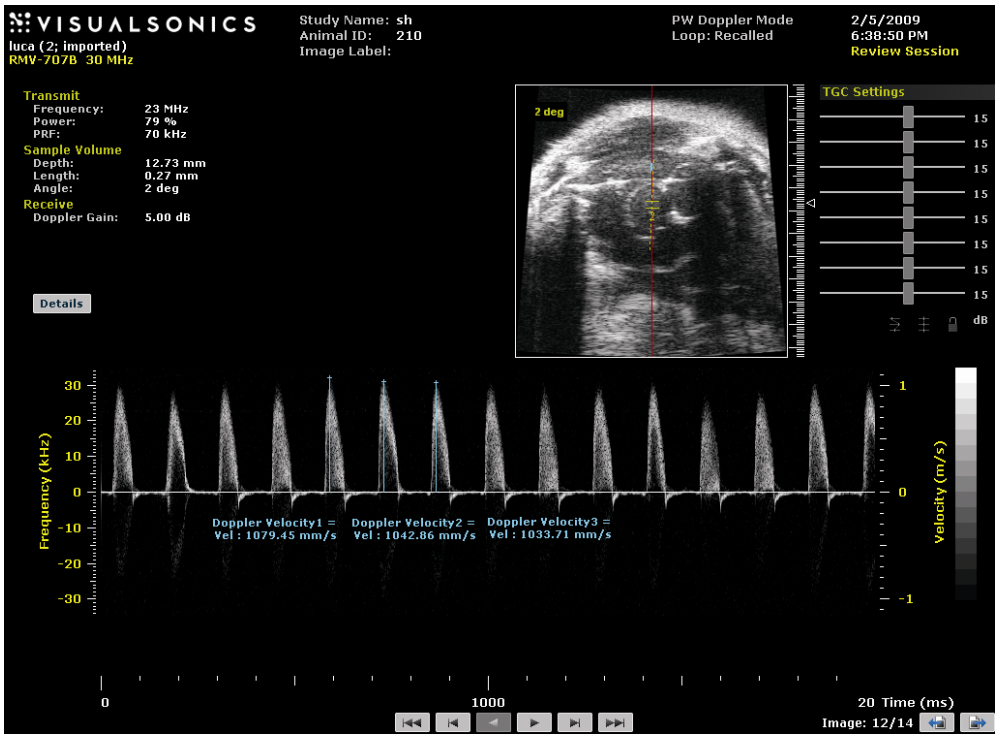

Figure 3.11: Echocardiography in mice

A right parasternal transversal section of the ascending aortic tract (short axis view of the aorta, upper panel) and blood flow velocity (cm/sec) measurements in Doppler (3) of the ascending aortic tract (lower panel) are shown.

3.3.6 Electrocardiogram (ECG)

3.3.6.1 Materials:

Vevo anaesthesia system (VisualSonics Inc., Toronto, Canada)
PowerLab record unit: PowerLab System ML840, Animal Bio Amp ML136, needle electrodes 29 gauge MLA1204 (AD instruments, Lexington, Australia)
PowerLab analysis unit: Chart software v 5.4 for Windows (AD instruments, Lexington, Australia)

3.3.6.2 Method

An Animal Bio Amplifier ML136 was connected to an ECG Lead Switch Box (PowerLab System ML840) to enable ECG recording using three needle electrodes (3 Leads ECG, positive negative and earth) carefully inserted subcutaneously in the mouse limbs and secured with tape. The ECG tracings were filtered using a high pass setting of 0.3 Hz and low pass setting of 1 kHz. During the procedure the mouse was anesthetized with isoflurane (isoflurane 2%, oxygen 98%) via facemask, following induction in a chamber containing 5% isoflurane. Per each mouse the signal was acquired for 1 minute. The ECG records were analysed using the Chart 5.4 software. During offline analysis 1 minute recording was analysed for heart rate calculated as the reciprocal of the average of R-R peaks distances between valid beats (Fig. 3.12, Fig. 3.13).

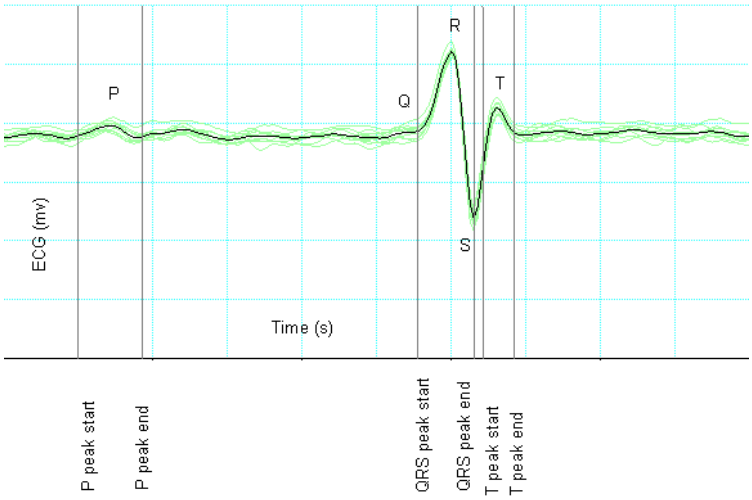

Figure 3.12: ECG in mice

Calculated signal-averaged ECG (10, green lines) over 10-15 seconds of recording showing the wave composition of an ECG signal (P, QRS and T peaks are reported in the picture).

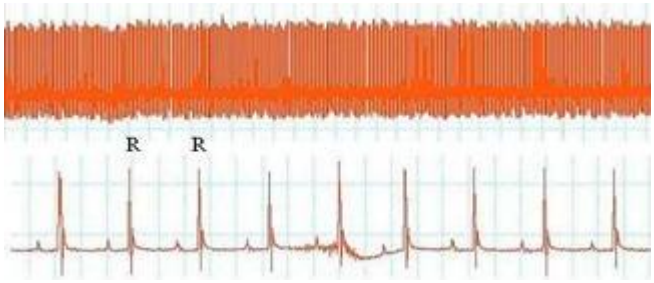

Figure 3.13: ECG recording over 1 minute: example of one R-R peaks distance

3.3.7 Blood chemistry

3.3.7.1 Materials

Isofluran Florene R (Abbott GmbH & Co.KJ, Wiesbaden, Germany)
End-to-end capillaries (Sarstedt AG & Co., Nümbrecht, Germany)
Litium-Heparin tubes 20 µl, K2EDTA (Synlab, Berlin, Germany)
Olympus AU 400 (at Synlab laboratories, Berlin, Germany)

3.3.7.2 Method

1) Retro-orbital puncture
Mouse blood samples were obtained using a retro-orbital puncture under isoflurane anaesthesia. Blood was drained using a sterile and heparinized end-to-end capillary in sterile tubes provided with Li-Heparin. Blood samples were immediately stored at 4 °C and subsequently centrifuged at 4000 rpm for 10 min. Plasma supernatant was carefully transferred in new tubes and stored at –20 °C.
2) Blood analysis
Analysis of samples was realized at Synlab in Berlin (www.synlab.vet/de). The following parameters were checked:
alanine aminotransferase (ALAT), albumin (Alb), α –amylase (Amy), alkaline phosphatase (AP), aspartate transaminase (ASAT), bilirubin (Bil), calcium (Ca), cholesterol (Ch), creatinine (Cr), creatine kinase (CK), fructosamine (Fru), γ-glutamyl transferase (GTT), glucose (Glu), high-density lipoprotein-cholesterol (HDL-cholesterol), inorganic phosphate (IP), iron (Fe), lactate dehydrogenase (LDH), lipase (Lip), low-density lipoprotein-cholesterol (LDL), triglycerides (TG), urea.

3.3.8 Mouse housing

Our animal facility at the Center for Cardiovascular Research-Charité houses mice in plastic cages with filter-paper-covered plastic microisolator tops. A maximum of five mice per cage providing good animal care has been kept. Food and water were available *ad libitum*. A circadian light cycle of 12 hours light/12 hours dark was maintained in the housing room. Temperature and humidity were controlled.

3.4 Statistical analysis

3.4.1 Materials

Spss 12.0 software (Spss Inc., Chicago, Usa)

3.4.2 Method

Statistical analysis was performed using the Spss 12.0 software. Experimental groups were compared using the statistical procedure analysis of the variance (ANOVA). In particular means were compared using the ANOVA one-way procedure. Levene test was chosen for evaluating homogeneity of the variance test. Post-hoc analysis for multiple comparisons was realized using Tukey´s test or Tamhane test; significance level fixed at 5% and null hypothesis rejected with a p value < 0.05.

4 Results

4.1 Gpr30 mutant mouse models

In order to understand the *in vivo* function of Gpr30, two different Gpr30 mouse models were used for an extensive phenotypical analysis: Gpr30-T181 Deltagen mice (60) and SHG17 Artemis mice (45). Deltagen mice were generated through a homologous recombination approach in 129/Sv ES cells. A LacZ-neo^r cassette was used to disrupt the ORF in the Gpr30 exon 3. SHG17 mice were generated through a Cre-recombinase approach and the inactivation of Gpr30 was obtained deleting the entire Gpr30 exon 3 from the murine genome.

4.2 Molecular characterization of Gpr30-T181 Deltagen mice

4.2.1 Genotyping

Mutant ES cells (129/Sv) containing the targeting gene construct were injected into C57BL/6 blastocysts and these implanted into a CD-1 pseudo pregnant recipient. Male chimeras were then mated to C57BL/6 wildtype females. The offspring represents the F1 generation and shows an agouti coat colour the higher the contribution of the transgenic cells (129/Sv) was. For the germ line transmission evaluation, agouti pups were genotyped and heterozygous mutants selected and backcrossed to C57BL/6 for at least 6 generations.

Briefly genotyping was performed using tail biopsies from 4 weeks old animals digested and analysed by PCR. PCR analysis was performed using a combined PCR approach with two independent reactions. In the first reaction (M) three primers and in the second one (T) two primers were used to amplify specific bands corresponding to the mutant (618 bp) and wildtype allele (433 bp), respectively. Heterozygous animal alleles were characterized by the presence of both bands, i.e. 433 and 618 bp (Fig. 4.1).

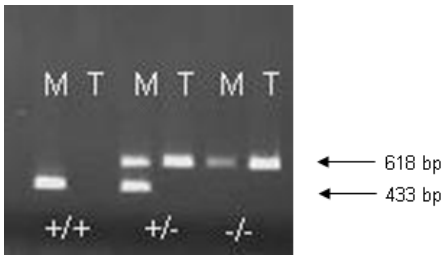

Figure 4.1: Gpr30-T181 Deltagen mouse genotyping

Three different samples of wildtype (+/+), heterozygous (+/-) and homozygous (-/-) mutant mice were analysed by PCR using two reactions (M and T) to detect the mutant (618 bp) and the wildtype (433 bp) alleles. PCR products were run on 1.4% of agarose gel. Arrows indicate the mutant and the wildtype bands, respectively.

4.2.2 Southern blotting

In order to verify the correct and single integration of the LacZ-neo^r cassette into the mouse genome, a Southern blotting analysis was performed (Materials and Methods Fig. 3.1; Fig. 4.2). Genomic DNA from liver of wildtype, heterozygous and homozygous Gpr30-T181 Deltagen mice was used. Two probes hybridizing outside and adjacent the 5´ and 3´ arms (5´ and 3´probes respectively) and a probe hybridizing to the targeting vector (internal probe) were used. The integration of the 5´ construct arm was confirmed by detecting a 10.5 kb EcoRI-fragment from the wildtype allele and an 8.8 kb targeted fragment. Integration of the 3´ construct arm was confirmed by the 3´ external probe detecting fragments of 6.1 and 6.8 kb corresponding to the wildtype allele, and two fragments of 6.8 kb and 10.7 kb corresponding to the targeted allele. Single vector integration was verified using an internal probe which detected two fragments of 6.1 and 6.9 kb corresponding to the wildtype allele as well as two fragments of 2.0 and 2.5 kb corresponding to the targeted allele. As shown in Fig. 3.2 all the detected fragments had the expected size, confirming a single successful event of homologous recombination.

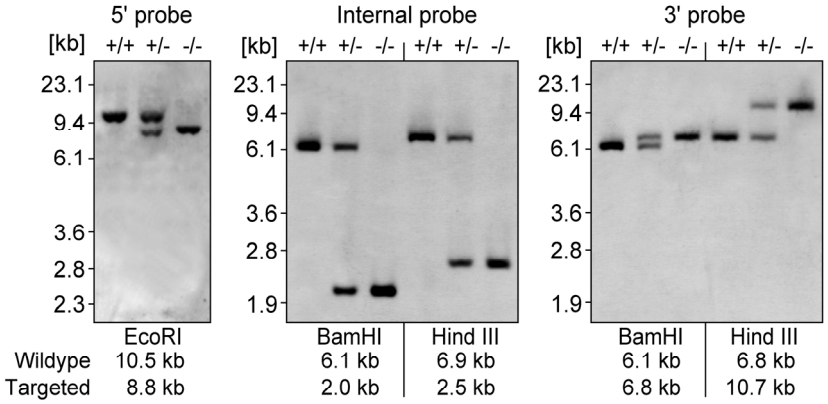

Figure 4.2: Southern blotting

Analysis of genomic DNA from liver of wildtype (+/+), heterozygous (+/-) and homozygous (-/-) Gpr30-T181 Deltagen mice. The blots show the hybridization products for the three different probes (5´, internal and 3´probes), and the corresponding enzymatic digestions (EcoRI, BamHI, Hind III).

4.2.3 Real Time PCR

Then we evaluated the correct splicing and proper expression of the targeted locus. Therefore brain cDNA samples from male and female wildtype, heterozygous and homozygous Gpr30-T181 Deltagen mice were used for the quantification analysis of sequences flanking and within the targeting vector. Primers within the 5´ region of exon 3 and within the LacZ cassette (Materials and Methods Fig. 3.1) were used to evaluate proper splicing within the targeted Gpr30 locus as well as LacZ expression levels. Highest relative expression levels of the amplicon obtained using primers within the 5´ region of exon 3 and the 3´ of the LacZ cassette were found in homozygous Gpr30-T181 mice. Consistently with these results intermediate values were found in heterozygous Gpr30-T181 mice (Fig. 4.3 a). The results showed that the cassette spliced to the 5´ region of exon 3. Using a couple of primers designed in the neo^r cassette and in the 3´ region of exon 3, a fusion transcript of the neo^r gene and part of exon 3 was also detected (Fig. 4.3 b). Our results point to a correct splicing of the mutated exon 3 and to a transcription product of the neo^r gene and the 3´ region of this exon. Note that the highest expression levels of this mutant transcript occur in homozygous mutant mice (Fig. 4.3 b).

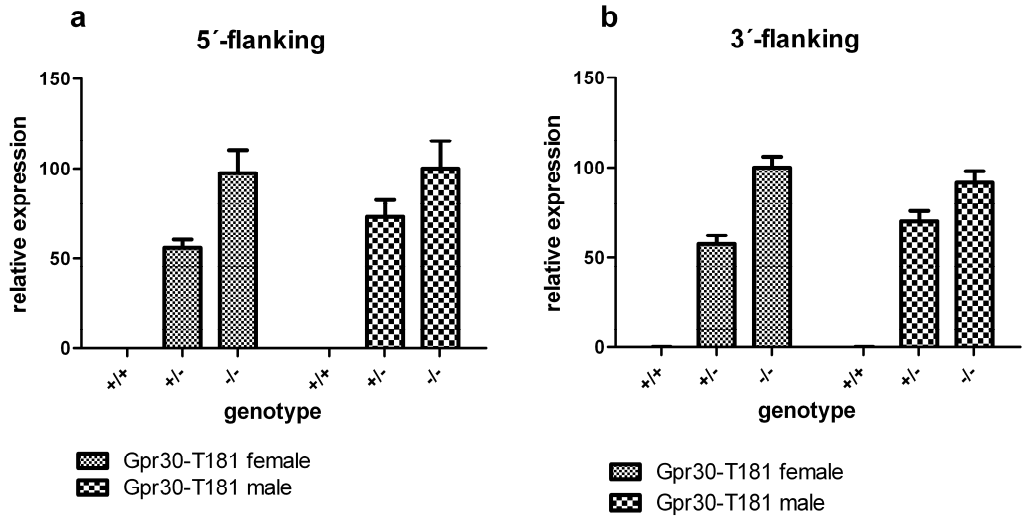

Figure 4.3: Real Time PCR quantification of the fusion transcripts

Real Time PCR quatification of the fusion transcripts was performed using brain cDNAs from wildtype (+/+), heterozygous (+/-) and homozygous (-/-) male and female Gpr30-T181 Deltagen mice. a) relative expression levels of a fusion transcript using primers within the 5´ region of exon 3 and the LacZ cassette. b) relative expression levels of a fusion transcript using primers within the 3´ region of exon 3.

To simplify the analysis of potential phenotype alterations, we first examined Gpr30 gene expression levels in different tissues and organs. Therefore a relative quantification of Gpr30 mRNA levels was performed using different tissue cDNAs from male and female Gpr30-T181 heterozygous mice. Heterozygous Gpr30-T181 mice were used because in a preliminary analysis we could show that LacZ expression exactly reflected Gpr30 expression (60). Therefore the experiments were done using only one set of mice allowing a smaller number of animals to be sacrificed. The highest expression levels of Gpr30 were found in brain vessels and the lowest in the liver (Fig. 4.4). In addition, no differences between sexes were detected.

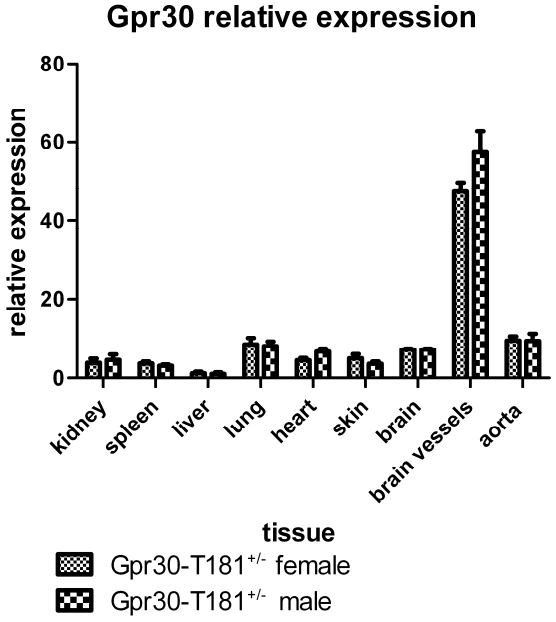

Figure 4.4: Gpr30 mRNA relative expression

Gpr30 mRNA relative expression levels were measured using Real Time on different tissue cDNAs from a heterozygous Gpr30-T181 male mouse and a heterozygous Gpr30-T181 female mouse respectively. Gpr30 highest relative expression was found in brain vessels and the lowest in the liver.

4.3 SHG17 Artemis mice genotyping

SHG17 Artemis mice were obtained through a Cre-recombinase lox P approach. Gpr30 inactivation was achieved by deleting the complete exon 3 containing the ORF of the Gpr30 gene. SHG17 mice were generated on a pure C57BL/6 genetic background and genotyping was performed as described by Otto and colleagues (45). The wildtype allele was amplified using primers 3´ to exon 3 and the mutant allele using primers flanking the inserted LoxP sites. Amplification of the wildtype allele resulted in a band of 398 bp, whereas amplification of the mutant allele resulted in a band of 560 bp.

Briefly, genotyping PCR analysis was performed using a combined strategy of two reactions (M and T) and three primers. For wildtype animals only the band of 398 bp was obtained, whereas for the heterozygous an additional fragment of 560 bp was observed (Fig. 4.5).

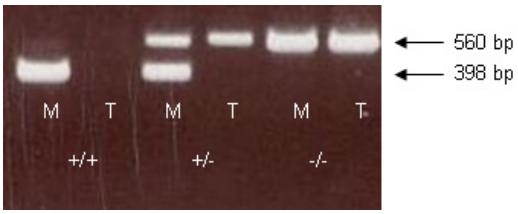

Figure 4.5: SHG17 Artemis mice genotyping

Three different samples of wildtype (+/+), heterozygous (+/-) and homozygous (-/-) mutant mice were analysed by PCR using two reactions (M and T) to detect the mutant (560 bp) and the wildtype (398 bp) alleles. PCR products were run on 1.4% of agarose gel. Arrows indicate the mutant and the wildtype bands, respectively.

4.4 Gpr30-T181 Deltagen mice phenotypic assessment

In order to assess the physiological function of Gpr30 *in vivo*, Gpr30-T181 Deltagen mice underwent an extensive phenotypic analysis at two different levels: 1) a primary screen performed at the German Mouse Clinic, providing a comprehensive phenotype analysis of the mice; 2) a secondary screen consisting of the diet-induced obesity (DIO) model based on the use of a defined high fat diet (HFD).

4.4.1 Primary screen

Gpr30-T181 Deltagen mice underwent a primary screen consisting of a wide phenotype analysis in many different fields of mouse genetics, physiology and pathology (Materials and Methods Fig. 3.2). The analysis was performed on a cohort of 80 animals: 40 homozygous mutant mice (20 males and 20 females) and 40 age-sex-matched wildtype littermates as controls.

The most relevant result was observed in the immunological analysis. A flow cytometric analysis of several T cell lines in blood samples of both Gpr30-T181$^{-/-}$ male and female mice was performed. Gpr30-T181$^{-/-}$ male and female mice showed lower levels of T cells and a lower proportion of CD62L expressing cells within the T cell cluster compared to control mice (Table 4.1). In particular, the fraction of CD4^{+} cells was reduced by 24.8% and by 30.2% in females and males Gpr30-T181$^{-/-}$ respectively. The number of CD8^{+} cells was also lower by 20.6% in Gpr30-T181$^{-/-}$ females and by 28.2% in Gpr30-T181$^{-/-}$ males. CD62L expressing T cell levels represent the naïve T cell compartment, newly produced in the thymus. These cells were reduced by 59% and 44.9% in female and male Gpr30-T181$^{-/-}$ mice, respectively. These results were confirmed in a second independent experiment, suggesting a potential immunological susceptibility in Gpr30-T181$^{-/-}$ mice.

Table 4.1: Immunology screen of Gpr30-T181 Deltagen mice

females						
parameter	1st bleeding			2nd bleeding		
	-/-	+/+	p value	-/-	+/+	p value
CD3+	21.5 ± 0.9	26.6 ± 1.6	< 0.05	18.7± 0.9	24.0± 1.7	< 0.05
CD3e+/CD4+	9.7 ± 0.5	12.9 ± 1.1	< 0.05	8.5 ± 1.0	11.6 ± 0.	< 0.05
CD3e+/CD8a+	8.5 ± 0.4	10.7 ± 0.6	< 0.05	7.4 ± 0.4	9.9 ± 0.7	< 0.05
CD3e+/CD4+/CD25+	6.4 ± 0.5	4.9 ± 0.4	< 0.05	7.5 ± 0.6	5.6 ± 0.5	< 0.05
CD3e+/gd+	0.38 ± 0.02	0.046 ± 0.03	n.s	0.35 ± 0.02	0.4 ± 0.02	n.s
CD4+/CD62L+	16.8 ± 4.8	40.1 ± 6.4	<0.01	25.6 ± 5.2	58.9 ± 6.0	<0.001
CD4+/CD44+	70.4 ± 0.8	73.1 ± 1.5	n.s	72.9 ± 0.8	75.4 ± 0.9	n.s
CD8a+/CD62L+	19.0 ± 5.6	47.4 ± 7.2	<0.01	29.8 ± 5.6	66.3 ± 6.8	<0.001
CD8a+/CD44+	58.1 ± 0.9	58.8 ± 1.2	n.s	64.1 ± 0.8	62.4 ± 0.9	n.s
CD11b+/Gr1+	7.6 ± 0.9	6.3 ± 0.4	n.s	16.4 ± 2.1	12.6 ± 0.6	n.s
CD11b+/nonGra/nonNK	6.2 ± 1.0	5.9 ± 0.4	n.s	4.03 ± 0.6	3.0 ± 0.5	n.s
NK+CD5+	0.3 ± 0.01	0.3 ± 0.02	n.s	0.3 ± 0.02	0.4 ± 0.02	n.s
NK+CD5-	3.6 ± 0.03	3.8 ± 0.2	n.s	3.4 ± 0.7	3.7 ± 0.3	n.s
CD19+	58.19 ± 1.7	54.3 ± 2.1	n.s	53.7 ± 2.2	50.3 ± 1.9	n.s
CD19+/IgD+	92.8 ± 0.03	92.6 ± 0.04	n.s	92.8 ± 0.8	90.7 ± 0.9	n.s
CD19+/CD5+	2.5 ± 0.1	2.6 ± 0.2	n.s	1.9 ± 0.1	2.5 ± 0.2	<0.01
CD19+/MHCII+/B220+	81.8 ± 1.2	85.2 ± 0.9	<0.05	84.1 ± 1.0	82.8 ± 1.0	n.s
CD11b+/NK+	45.4 ± 1.8	51.8 ± 2.4	<0.05	39.6 ± 1.9	44.4 ± 2.4	n.s
males						
parameter	1st bleeding			2nd bleeding		
	-/-	+/+	p value	-/-	+/+	p value
CD3+	13.6 ± 1.3	18.7 ± 1.0	<0.01	12.3 ± 1.0	17.2 ± 1.0	<0.01
CD3e+/CD4+	6.0 ± 0.6	8.6 ± 0.6	<0.01	5.1 ± 0.5	7.4 ± 0.6	<0.01
CD3e+/CD8a+	5.6 ± 0.5	7.8 ± 0.5	<0.01	5.9 ± 0.5	8.1 ± 0.4	<0.01
CD3e+/CD4+/CD25+	7.1 ± 0.5	5.9 ± 0.5	n.s	8.3 ± 0.5	6.2 ± 0.06	<0.05
CD3e+/gd+	0.27 ± 0.03	0.3 ± 0.02	n.s	0.25 ± 0.03	0.3 ± 0.02	n.s
CD4+/CD62L+	22.6 ± 7.1	43.4 ± 7.1	n.s	16.8 ± 2.8	42.6 ± 7.9	<0.01
CD4++/CD44+	70.5 ± 1.0	72.0 ± 0.9	n.s	69.3 ± 1.2	70.5 ± 0.9	n.s
CD8a+/CD62L+	28.2 ± 7.1	48.6 ± 7.2	n.s	24.2 ± 3.4	50.1 ± 8.1	<0.05
CD8a+/CD44+	65.4 ± 1.8	63.8 ± 1.9	n.s	66.2 ± 0.8	64.3 ± 1.3	n.s
CD11b+/Gr1+	9.6 ± 1.8	8.0 ± 0.9	n.s	16.4 ± 1.1	14.7 ± 1.0	n.s
CD11b+/nonGra/nonNK	6.3 ± 0.7	6.0 ± 0.6	n.s	3.3 ± 0.1	3.4 ± 0.2	n.s
NK+CD5+	0.3 ± 0.03	0.3 ± 0.01	n.s	0.3 ± 0.02	0.3 ± 0.03	n.s
NK+CD5-	3.3 ± 0.2	3.2 ± 0.2	n.s	4.2 ± 0.3	3.7 ± 0.3	n.s
CD19+	66.8 ± 2.4	63.6 ± 1.9	n.s	60.3 ± 1.9	57.4 ± 1.5	n.s
CD19+/IgD+	92.7 ± 0.3	93.5 ± 0.2	<0.05	92.1 ± 0.5	92.2 ± 0.4	n.s
CD19+/CD5+	1.9 ± 0.1	2.4 ± 0.1	<0,05	1.4 ± 0.1	1.9 ± 0.1	<0.05
CD19+/MHCII+/B220+	85.1 ± 0.7	85.7 ± 0.8	n.s	81.4 ± 1.2	81.2 ± 1.2	n.s
CD11b+/NK+	29.7 ± 3.1	32.8 ± 2.4	n.s	48.0 ± 3.5	45.4 ± 2.6	n.s

Immunology screen of Gpr30-T181 Deltagen mice. Main lineages: CD3+ T cells, CD4+ T cells, CD8+ T cells, γδT cells, T regulatory cells (CD4+ CD25+), B cells (CD19+, responsive B220+), B1 B cells (/CD5+), mature B cells (/IgD+), granulocytes (CD11b+Gr1+), NK cells (DX5+CD3-), NK T cells (DX5+CD3+). Subpopulations are identified by bi-variate gating with the following markers: Tcells/non T cells: CD25, CD62L, Ly-6C, CD44, CD45RB, CD103. CD19+ cells: IgD, B220, CD11b, CD5, Gr1. CD19-cells: Gr1, B220, CD5, CD11b. +/+: Gpr30-T181 wildtype mice; -/-: Gpr30-T181 homozygous mutant mice. Statistical analysis: means comparison by t-test. The most relevant results are evidenced in red.

Slight differences between Gpr30-T181$^{-/-}$ mice and control mice were also observed in the behavioural and clinical chemistry screens.

Behavioural analysis of spontaneous activity in a novel environment measured by the Open Field Test (OFT) revealed subtle behavioural alterations in Gpr30-T181 mice$^{-/-}$. Briefly, the OFT was conducted in a transparent and infrared light permeable acrylic test arena (45.5 x 45.5 x 39.5 cm). For data analysis the arena was divided in two areas: the periphery defined as a corridor of 8 cm width along the walls and the remaining part representing the centre. The following parameters were measured: distance travelled, resting and permanence time as well as speed of movement in the centre of the arena or in the periphery. During a 20 min observation period Gpr30-T181$^{-/-}$ mice compared to control mice moved significantly less during the first 5 minutes, with a lower speed and later to the centre of the arena (Table 4.2).

Table 4.2: Behavioural observations of Gpr30-T181 Deltagen mice

parameter	control		Gpr30-T181 mutant		p value in two-way ANOVA		
	males	females	males	females	sex	genotype	interaction
trav.distance (cm)	5967.6 ± 442.59	6667.95 ± 372.69	5576.38 ± 162.02	5548 ± 206.87	ns	< 0.05	ns
centre-mean velocity (cm/s)	23.77 ± 0.92	29.07 ± 1.56	22.77 ± 1.21	24.11 ± 1.16	ns	< 0.05	ns
latency (s)	6.41 ± 1.62	4.64 ± 0.96	11.2 ± 2.28	7.55 ± 2.05	ns	< 0.05	ns

Behavioural observations of Gpr30-T181 Deltagen mice. The travelled distance indicates the total distance travelled by the mice during the Open Field Test. Centre-mean velocity indicates the velocity of mice in entering the centre of the test arena. Latency indicates the time spent to enter the centre of the arena. A genotype effect was observed in all three parameters. Trav: travelled. Statistical analysis: Two-way Anova. Values are expressed ± standard deviation.

In the clinical chemistry analysis, several parameters were measured and among these, alkaline phosphatase (AP) activity resulted significantly lower in Gpr30-T181$^{-/-}$ female mice than in the respective controls (Fig.4.6). Males showed a similar trend. In a second analysis AP levels resulted slightly, but not significantly lower in Gpr30-T181$^{-/-}$ female mice compared to control mice. Moreover changes in AP levels were also observed in mutant male mice in response to HFD (secondary screen), suggesting a potential link between Gpr30 and AP activity.

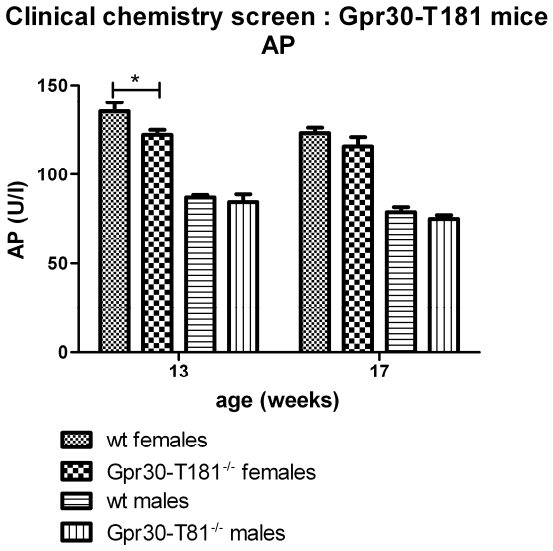

Figure 4.6: Primary screen of Gpr30-T181 Deltagen mice

Clinical chemistry revealed in a first experiment slightly but significantly higher values of alkaline phosphatase (AP) in littermate control female mice compared to homozygous mutant mice. In a second analysis no differences were reported between groups. Male mice 13 or 17 weeks old did not show any significant difference. Statistical analysis: Two-way ANOVA and means comparisons by t-test, * p-value < 0.05.

In order to understand the molecular basis of the phenotypic alterations detected in the immunological behavioural and clinical chemistry screens and taking into account also Gpr30 gene expression pattern, microarray analysis was performed on three different organs: thymus, brain and kidney. Briefly, tissue RNA was isolated from Gpr30-T181$^{-/-}$ male mice and control mice, the latter constituting the RNA reference pool. For each RNA sample chip hybridazations were performed in duplicate. Normalization of the two channels (2 probes per array) was obtained through the calculation of a moving average with a fixed length window (± 50). Significance Analysis of Microarrays (SAM) did not identify differentially expressed gene in brain or kidney. However, SAM identified 20 significantly regulated genes in the thymus of Gpr30-T181$^{-/-}$ mice compared to wildtype controls. All the genes resulted to be down-regulated. Some of these genes are reported in the Table 4.3, as well as Gene Ontology classification, significance level (q value) and fold change.

Table 4.3: Gene ontology annotation of deregulated genes in the thymus of Gpr30-T181$^{-/-}$ Deltagen mice

Gene symbol	Molecular function	Biological process	Cellular component	q-value (%)	Fold change
Nppa	hormone activity	regulation of blood pressure; regulation of blood vessel size	extracellular region; cytoplasm	0.00	-9.09
Wnt7a	signal transducer activity; receptor binding	signal transduction; Wnt receptor signaling pathway	extracellular region; proteinaceous extracellular matrix; extracellular space	19.25	-8.33
Tnnt2	actin binding; tropomyosin binding; troponin C binding; troponin I binding	regulation of heart contraction; muscle filament sliding; negative and positive regulation of ATPase activity; response to calcium ion	troponin complex	24.75	-8.33
Ccr5	actin binding; phosphoinositide phospholipase C activity; G-protein coupled receptor activity; protein binding; coreceptor activity; C-C chemokine receptor activity	chemotaxis; inflammatory response; immune response; cellular defense response; G-protein coupled receptor protein signaling pathway; elevation of cytosolic calcium ion concentration	cytoplasm; endosome; plasma membrane; integral to plasma membrane; external side of plasma membrane	24.75	-4.00
Serca2	nucleotide binding; magnesium ion binding; calcium-transporting ATPase activity; calcium ion binding; ATP binding; hydrolase activity	regulation of the force of heart contraction; ATP biosynthetic process; cation transport; cellular calcium ion homeostasis; ER-nuclear signaling pathway	membrane fraction; microsome; integral to plasma membrane; membrane; sarcoplasmic reticulum membrane	32.08	-6.25
Cat	aminoacylase activity; catalase activity; growth factor activity; heme binding; protein homodimerization activity; metal ion binding; NADP or NADPH binding	response to reactive oxygen species; triglyceride metabolic process; cholesterol metabolic process; cell proliferation; aerobic respiration	mitochondrion; peroxisome; peroxisomal membrane	39.51	-6.67
Hspa1a	protein stabilization	folding of the newly translated proteins, ubiquitine-proteasome pathway	cytosol	51.67	-16.67
Myl4	motor activity; actin monomer binding; calcium ion binding; structural constituent of muscle; myosin II heavy chain binding	regulation of the force of heart contraction; muscle organ development; positive regulation of ATPase activity; cardiac muscle contraction	muscle myosin complex; myosin complex; A band	51.67	-4.35
Slc35e1		transport	membrane; integral to membrane	51.67	-9.09
Usp26	ubiquitin thiolesterase activity; peptidase activity; cysteine-type peptidase activity	ubiquitin-dependent protein catabolic process	nucleus	51.67	-7.14
Atp13a4	nucleotide binding; magnesium ion binding; ATP binding; ATPase activity	ATP biosynthetic process; cation transport	membrane; integral to membrane	51.97	-4.17
Itfg1	protein binding		extracellular region; membrane	53.52	-10.00

Gene ontology annotation. SAM: Significance Analysis of Microarrays; Nppa: natriuretic peptide precursor A; Wnt7a: wingless-type MMTV integration site family, member 7A; Tnnt2: troponin T type 2; Ccr5: chemokine (C-C motif) receptor 5; Serca2: sarcoplasmic reticulm Ca(2+)-ATPase2; Cat: catalase; Hspa1a: heat shock 70kDa protein 1A; Myl4: myosin, light chain 4´; Slc35e1: solute carrier family 35, member E1; Usp26: ubiquitin specific peptidase 26; Atp13a4: ATPase type 13A4; Itfg1: integrin alpha FG-GAP repeat containing ; q value: significance; fold change: regulation factor.

SAM analysis identified Nppa, Serca2, Ccr5, and Cat genes to be down-regulated in the thymus of Gpr30-T181$^{-/-}$ males. Some of these genes are known to be involved in T cell development such as the Nppa gene (181). Their involvement might contribute to substantiate the hypothesis of a lower rate of T cells in the thymus of mutant mice. Therefore, in order to validate microarray results, Nppa, Serca2, Ccr5, and Cat mRNA levels were measured in thymus cDNA of male homozygous mutants and wildtype control mice using Real-Time PCR. Real-Time results are reported in Table 4.4. In agreement with microarray analysis, a pronounced trend of down-regulation for Nppa, Ccr5, Atpa2a and Cat gene expression was found in Gpr30-T181$^{-/-}$ mice compared to wildtype control mice. Nppa, Ccr5, Atpa2a and Cat genes resulted 14, 5, 7 and 6 times down-regulated in mutant mice, respectively. Note, that the small number of animals used (4 wildtypes and 5 mutants), might explain p values not expressing significant differences.

Table 4.4: Validation of microarray data

GOI/ Biological replicate		Normalized Ct biological replicate Gpr30-T181 $^{+/+}$	Normalized Ct biological replicate Gpr30-T181 $^{-/-}$	ΔΔCt	Fold-expression	p value
Nppa	1	31.55	31.91	3.74	0.07	0.19
	2*	34.89	30.08			
	3	27.40	31.94			
	4	24.82	31.79			
	5		32.60			
Ccr5	1	30.46	33.79	2.26	0.21	0.11
	2*	34.04	29.73			
	3	27.55	31.70			
	4	30.09	31.60			
	5		31.32			
Serca2	1	27.67	30.07	2.79	0.14	0.12
	2*	30.97	26.27			
	3	23.64	28.34			
	4	26.04	29.73			
	5		28.48			
Cat	1	26.85	29.27	2.61	0.16	0.14
	2*	30.13	25.45			
	3	22.76	27.27			
	4	25.33	28.00			
	5		27.98			

Validation of microarray data. GOI: gene of interest. Nppa: natriuretic peptide precursor A; Ccr5: chemokine (C-C motif) receptor 5; Serca2: sarcoplasmic reticulum Ca(2+)-ATPase 2; Cat: catalase. ΔΔCt was calculated as: average of normalized Gpr30-T181$^{-/-}$ Ct values- average of normalized Gpr30-T181$^{+/+}$ Ct values. Reference genes used for normalization of Ct values were: Gapdh: Glyceraldehyde-3-phosphate dehydrogenase; Hprt: hypoxanthine-guanine phosphoribosyltransferase; PO: ribosomal protein, large. Fold-expression= $2^{-\Delta\Delta Ct}$. p value calculated in a t-test used to compare Ct value means obtained in Gpr30-T81$^{+/+}$ versus Gpr30-T181$^{-/-}$ mice. *: Ct value of the biological replicate 2, among Gpr30-T81$^{+/+}$ mice, was identified as an outlier (mouse weight 20.4 g vs. mouse weight average 29.2 ± 1.57 g) and excluded in the fold calculation.

4.4.2 Secondary screen

In order to unravel a potential metabolic and cardiovascular role of Gpr30, Deltagen mice were challenged in a diet induced obesity model (DIO model) by a defined high fat diet (HFD). Wildtype and homozygous mutant, male and female mice, were fed for 25 weeks with a defined high fat diet (HFD) along with age-and sex matched littermates fed with a control diet (CD) (Fig.4.7). Mice were analysed for body weight and body mass composition (by nuclear magnetic resonance), glucose metabolism (by intraperitoneal glucose tolerance test), left ventricular function (by echocardiography) and blood chemical parameters (by blood chemistry). Experiments were performed at three different time-points: before starting HFD (1st time-point or baseline experiments, mice age 6 months); after 4 weeks of HFD (2nd time-point, mice age 8 months); and after 20 weeks of HFD (3rd time-point, mice age 12 months).

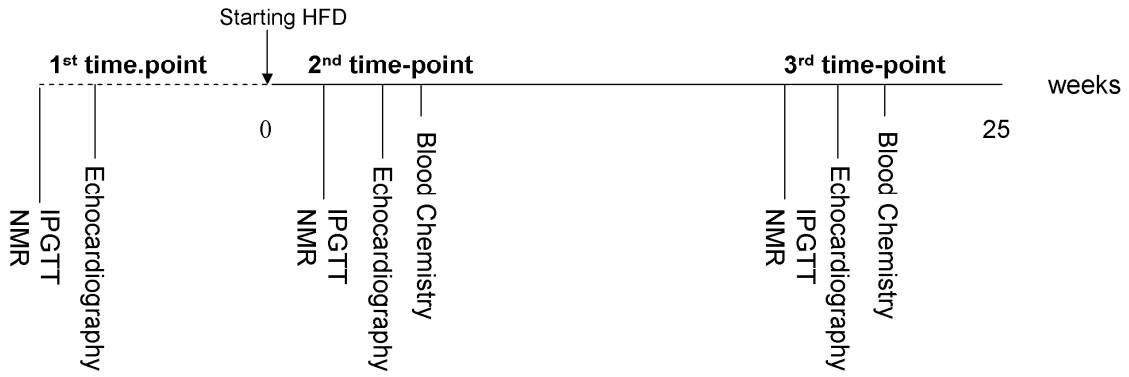

Figure 4.7: HFD workflow

Mice were fed with HFD or CD for 25 weeks. Experiments were performed at three different time-points. NMR: nuclear magnetic resonance; IPGTT: intra-peritoneal glucose tolerance test. HFD: high fat diet, (60% Kcal from fat); CD: control diet (14% Kcal from fat); 1st time-point: before starting HFD (mice age 6 months); 2nd time-point: 4 weeks of HFD (mice age 8 months); 3rd time-point: 20 weeks of HFD (mice age 12 months).

4.4.2.1 Body weight and body mass composition

In order to assess the endocrine function of Gpr30-T181 Deltagen mice in response to HFD, animals underwent different metabolic measurements. Body weight was regularly recorded twice per week, lean and fat mass accumulation assessed by NMR and glucose clearance analysed by IPGTT.

During the experiment, mice on HFD gained progressively weight compared to groups on CD. Moreover no differences in both sexes were reported between Gpr30-T181$^{-/-}$ and control mice (Fig. 4.8).

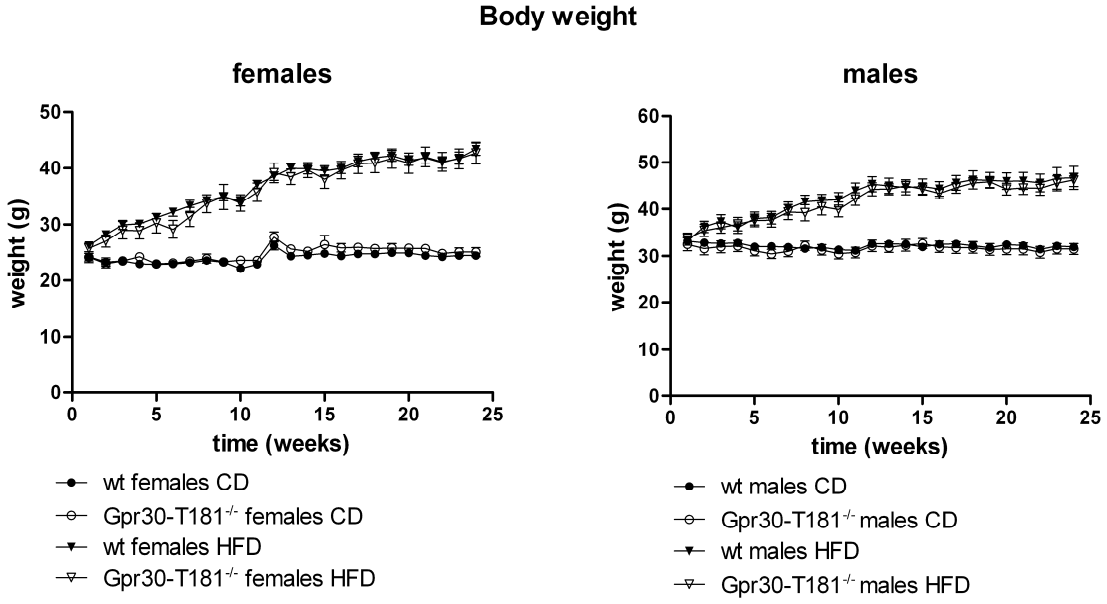

Figure 4.8: Gpr30-T181 Deltagen mice, body weight (BW)

BW was recorded twice per week for 25 weeks. Mice on HFD gain progressively more weight. However, genotype did not make any difference in weight gaining. CD: control diet. HFD: high fat diet. wt: control littermates.

Body mass composition assessed by NMR did not show any genotypic difference between groups assigned to HFD or CD. However, as expected a stronger increase of fat mass was reported in animals fed with HFD compared to littermate controls (Fig. 4.9).

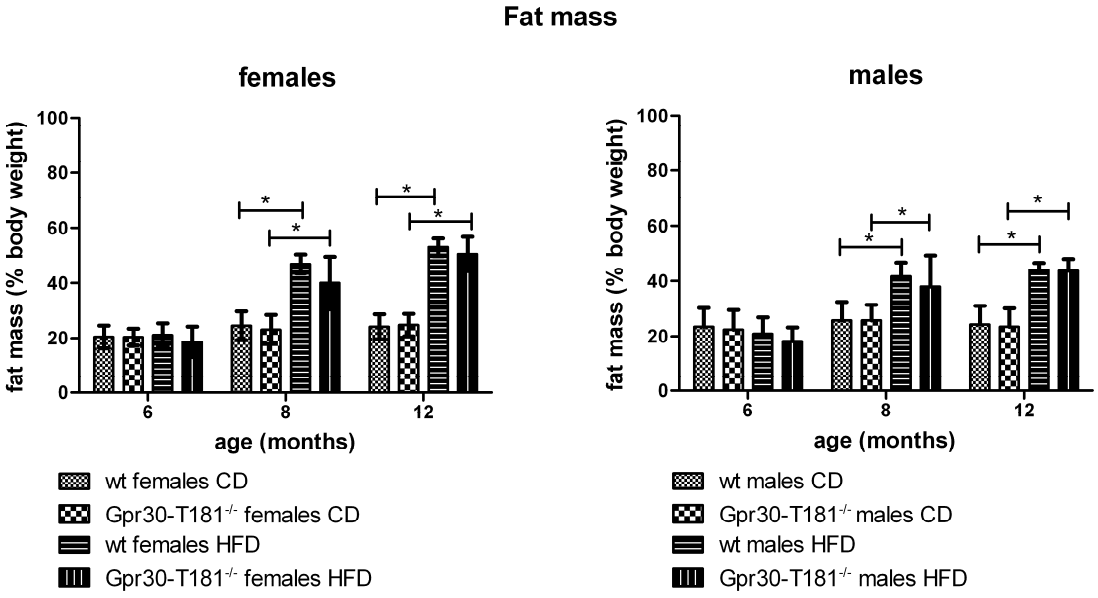

Figure 4.9: Gpr30-T181 mice, nuclear magnetic resonance (NMR)

Animals on HFD accumulated progressively more fat. As expected a significant difference in both sexes was found between mice on HFD and mice on CD. However, genotype did not make any difference. CD: control diet. HFD: high fat diet. *: Statistical analysis: One-way ANOVA followed by post-hoc analysis for multiple comparisons, * p value < 0.05. wt: control littermates.

4.4.2.2 Intraperitoneal Glucose Tolerance test (IPGTT)

In order to detect potential differences in glucose clearance efficiency between homozygous mutant and control mice the IPGTT was performed. Mice on HFD (2nd and 3rd time-points) showed wider peaks of glucose clearance compared to mice on CD, reflecting the tendency, following HFD, to develop a less efficiency in glucose clearance (Fig. 4.10). Moreover for a statistical analysis, area under the curve (AUC) values were calculated. No statistically significant differences were found between homozygous mutant and control mice (Fig. 4.11).

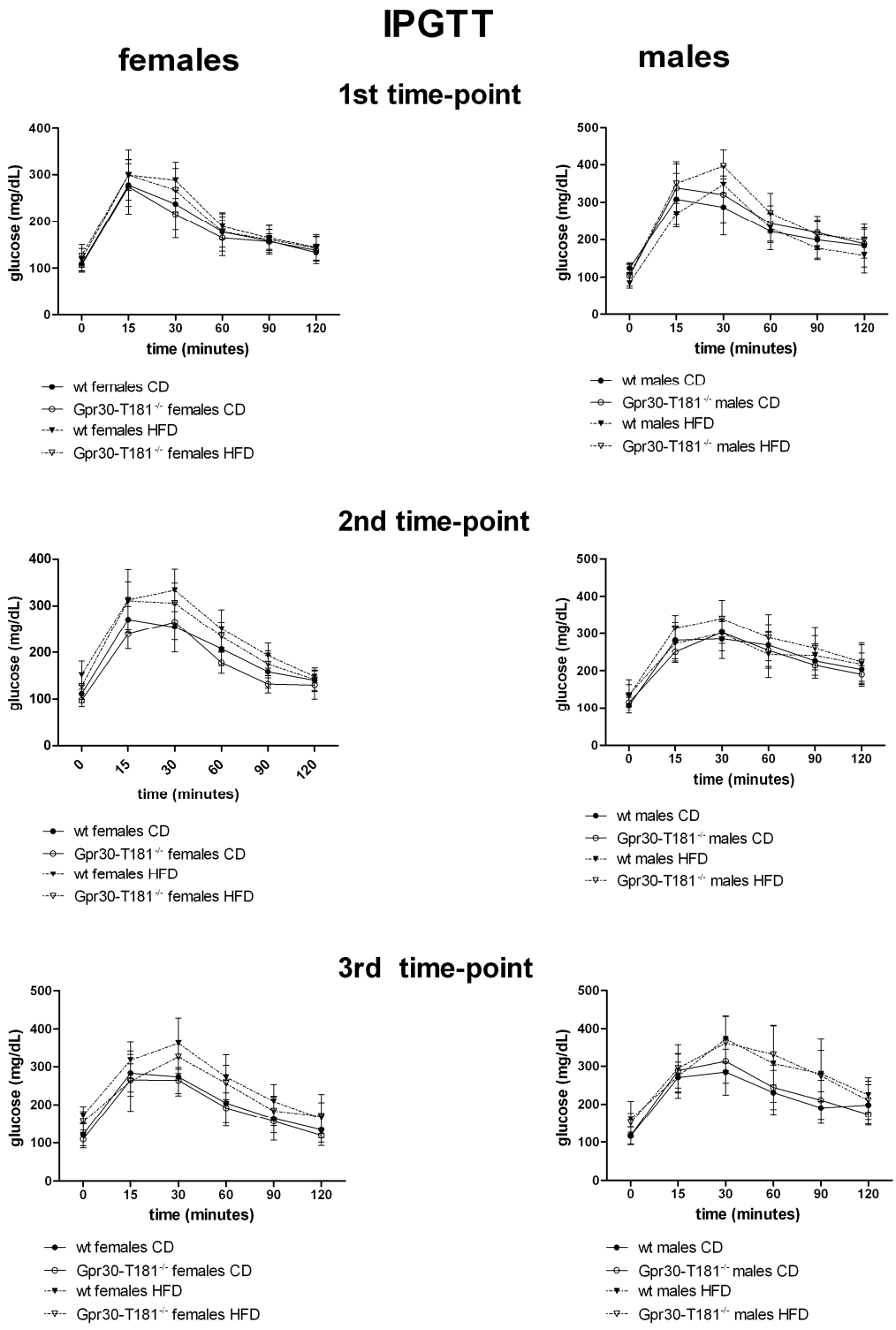

Figure 4.10: Gpr30-T181 mice, intraperitoneal-glucose tolerance test (IPGTT)

IPGTT measurements were performed at three different time-points. Mice on HFD showed metabolic curves (dashed lines) with a wider profile, reflecting a slower efficiency in metabolizing glucose. In particular, this trend is evident in both sexes and genotypes after 20 weeks of HFD (3rd time-point). wt: control littermates.

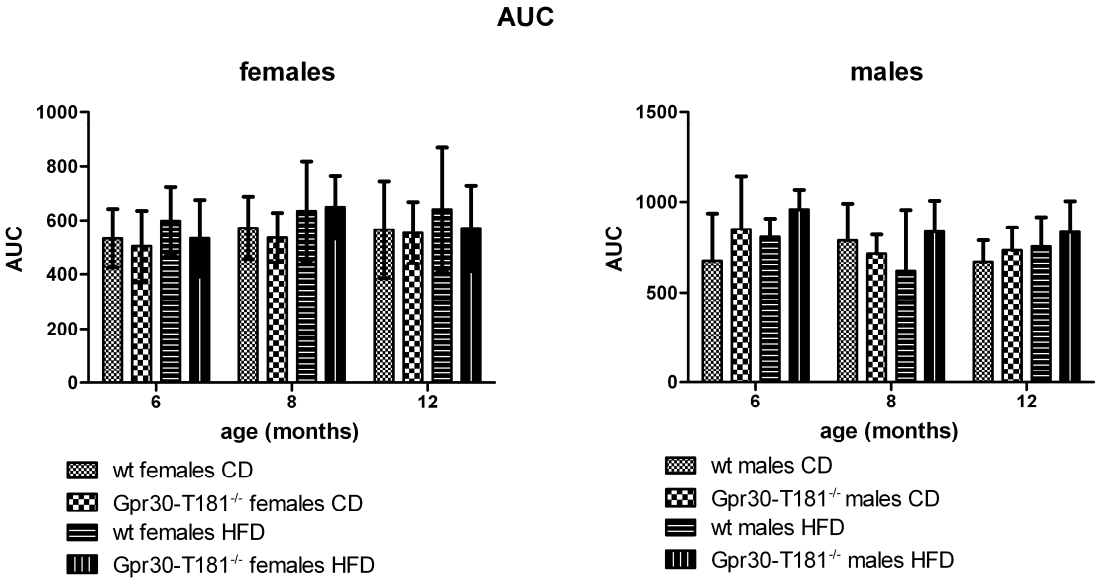

Figure 4.11: Gpr30-T181 Deltagen mice intraperitoneal glucose tolerance test (IPGTT), area under the curve (AUC)

In order to compare glucose clearance efficiency between the different groups, AUC values were calculated from curves in Fig. 3.10. No statistically differences were found between homozygous mutant and control mice on HFD or CD. Statistical analysis: One-way ANOVA followed by post-hoc analysis for multiple comparisons. wt: control littermates.

4.4.2.3 Echocardiography

Left ventricular function and potential changes induced by HFD on the heart were assessed using echocardiography. In order to analyse left ventricular systolic function, ejection fraction (EF), fractional shortening (FS) and left ventricular internal diameter in diastole (LVIDd) and in systole (LVIDs) were measured. Left ventricular diastolic function was examined measuring aortic blood flow velocity (AoVel).

The only significant difference between homozygous and mutant mice was found in baseline measurements. Six months old Gpr30-T181$^{-/-}$ female mice showed a slight but significant decrease of AoVel when compared to control female mice (Fig. 4.12, Table 4.5), suggesting a potential impaired cardiac output. However, the same difference was not found in female mutant mice at 8 and 12 months of age. Statistical analysis did not reveal other significant genotype-dependent differences (Table 4.5 and Table 4.6.).

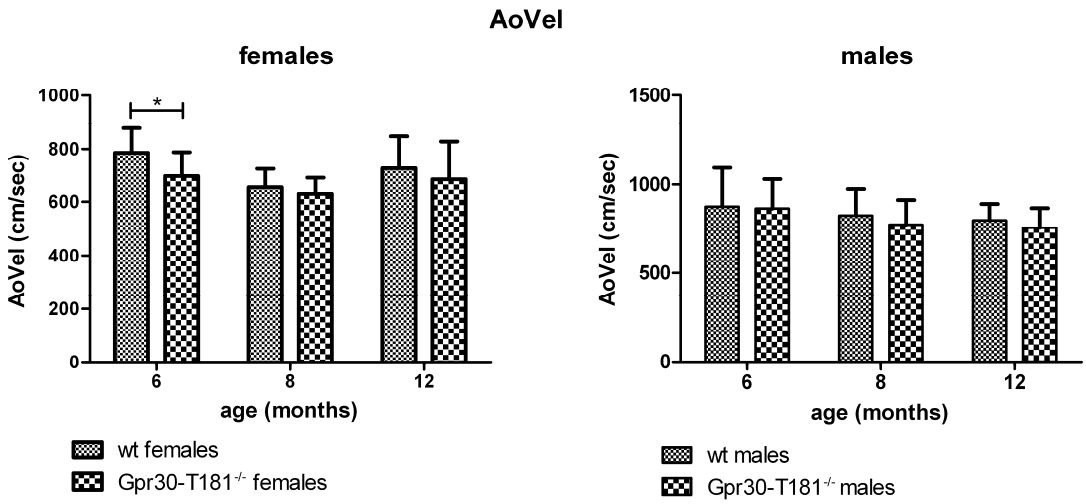

Figure 4.12: Gpr30-T181 Deltagen mice, echocardiography

The analysis revealed a slight but significant decrease of AoVel in 6 months old Gpr30-T181$^{-/-}$ female mice compared to control mice, suggesting a potential impaired cardiac output. However this difference was not found at 8 and 12 months of age. On the right, AoVel values in male mice are shown: no statistically significant differences were found among groups. Statistical analysis: t-test. *: p value < 0.05. wt: control littermates.

Table 4.5: Echocardiography of Gpr30-T181 Deltagen female mice

groups	time-point		parameters							
			EF	FS	LVIDd	LVIDs	AoVel	HR	EDD(M)	EDD(B)
+/+ ♀	baseline	mean	50.53	25.76	4.12	3.06	785.83	445.36	1.66	1.51
		± s.d	8.90	5.63	0.23	0.37	90.44	47.93	0.16	0.07
-/- ♀	baseline	mean	46.92	23.50	4.2	3.22	698.40	433.28	1.65	1.52
		± s.d	8.61	5.13	0.35	0.41	89.39	53.97	0.60	1.52
t-test p value			n.s	n.s	n.s	n.s	.03	n.s	n.s	n.s
+/+ ♀ CD	2nd	mean	43.51	21.46	4.38	3.44	675.63	398.33	n.a	n.a
		± s.d	5.77	3.39	0.17	0.24	98.11	29.24	n.a	n.a
-/- ♀ CD	2nd	mean	42.79	21.26	4.20	3.32	629.84	399.16	n.a	n.a
		± s.d	12.09	7.24	0.23	0.44	93.19	41.89	n.a	n.a
+/+ ♀ HFD	2nd	mean	46.40	23.02	4.24	3.38	713.88	447.72	n.a	n.a
		± s.d	4.13	2.40	0.24	0.41	105.98	35.91	n.a	n.a
-/- ♀ HFD	2nd	mean	51.63	26.71	4.13	3.04	782.43	439.50	n.a	n.a
		± s.d	10.93	7.41	0.15	0.39	174.24	50.91	n.a	n.a
ANOVA p value			.030	.036	n.s	n.s	.003	.012		
+/+ ♀ CD	3rd	mean	49.06	24.95	4.23	3.17	727.80	470.66	n.a	n.a
		± s.d	9.33	5.88	0.22	0.33	148.86	52.58	n.a	n.a
-/- ♀ CD	3rd	mean	44.61	22.01	4.07	3.17	687.69	481.06	n.a	n.a
		± s.d	7.70	4.70	0.24	0.24	172.26	48.41	n.a	n.a
+/+ ♀ HFD	3rd	mean	51.63	26.71	4.13	3.04	782.43	439.50	n.a	n.a
		± s.d	10.93	7.41	0.15	0.39	174.24	50.91	n.a	n.a
-/- ♀ HFD	3rd	mean	45.73	23.80	4.36	3.35	707.94	446.50	n.a	n.a
		± s.d	6.41	3.73	0.20	0.27	154.49	48.83	n.a	n.a
ANOVA p value			n.s	n.s	n.s	n.s	n.s	n.s		

Echocardiography of Gpr30-T181 Deltagen female mice. +/+ ♀ CD: wildtype female mice on control diet; -/- ♀ CD: Gpr30-T181$^{-/-}$ female mice on control diet ; +/+ ♀ HFD: wildtype female mice on high fat diet; -/- ♀ HFD: Gpr30-T181$^{-/-}$ female mice on high fat diet. EF: ejection fraction (%); FS: fractional shortening (%); LVIDd: left ventricular internal diameter in diastole (mm); LVIDs: left ventricular internal diameter in systole (mm); AoVel: aorta blood flow velocity (cm/s). HR: heart rate (beats/min). EDD (M): end-diastolic diameter calculated in M-mode. EDD (B): end-diastolic diameter calculated in B-mode. Statistical analysis: t-test and One-way ANOVA

followed by post-hoc test for multiple comparisons. Hypothesis of equality of the means rejected with a p value < 0.05. Note that the in one-way ANOVA analysis, only statistically significant differences found in post-hoc tests between mutant and control mice groups, on CD, or on HFD, respectively, were considered relevant. s.d: standard deviation. n.s: not significant (p value > 0.05); n.a: not available. Values significantly different are reported in red.

Table 4.6: Echocardiography of Gpr30-T181 Deltagen male mice

groups	time-point		parameters					
			EF	FS	LVIDd	LVIds	AoVel	HR
+/+ ♂	baseline	mean	51.55	26.74	4.50	3.30	873.55	422.15
		± s.d	11.45	7.78	0.40	0.49	221.22	42.96
-/- ♂	baseline	mean	50.34	25.67	4.47	3.33	862.25	423.92
		± s.d	7.35	4.50	0.31	0.37	168.22	51.53
t-test p value			n.s	n.s	n.s	n.s	n.s	n.s
+/+ ♂ CD	2nd	mean	45.67	22.86	4.61	3.68	826.89	416.33
		± s.d	7.15	4.27	0.29	0.47	171.92	46.24
-/- ♂ CD	2nd	mean	43.69	22.90	4.67	3.60	780.53	401.70
		± s.d	7.51	2.95	0.30	0.30	161.31	54.64
+/+ ♂ HFD	2nd	mean	53.05	27.82	4.38	3.18	808.81	455.14
		± s.d	13.45	8.82	0.33	0.54	217.95	64.48
-/- ♂ HFD	2nd	mean	44.56	22.20	4.63	3.60	838.50	426.22
		± s.d	5.33	3.09	0.58	0.46	295.29	58.48
ANOVA p value			n.s	n.s	n.s	n.s	n.s	n.s
+/+ ♂ CD	3rd	mean	45.28	22.59	4.55	3.53	798.37	466.22
		± s.d	7.01	4.05	0.41	0.42	119.35	31.95
-/- ♂ CD	3rd	mean	43.02	21.36	4.55	3.58	756.54	456.11
		± s.d	8.64	4.97	0.53	0.55	115.21	44.66
+/+ ♂ HFD	3rd	mean	51.90	26.70	4.45	3.27	866.83	467.00
		± s.d	6.05	3.75	0.34	0.39	178.98	57.40
-/- ♂ HFD	3rd	mean	47.02	23.46	4.33	3.30	806.79	463.78
		± s.d	3.40	1.93	0.56	0.51	224.90	59.31
ANOVA p value			.0018	.014	n.s	n.s	n.s	n.s

Echocardiography of Gpr30-T181 Deltagen male mice. +/+ ♂ CD: wildtype male mice on control diet; -/- ♂ CD: Gpr30-T181$^{-/-}$ male mice on control diet; +/+ ♂ HFD: wildtype male mice on high fat diet; -/- ♂ HFD: Gpr30-T181$^{-/-}$ male mice on high fat diet. EF: ejection fraction (%); FS: fractional shortening (%); LVIDd: left ventricular internal diameter in diastole (mm); LVIDs: left ventricular internal diameter in systole (mm); AoVel: aorta blood flow velocity (cm/s). HR: heart rate (beats/min). Statistical analysis: t-test and One-way ANOVA followed by post-hoc test for multiple comparisons. Hypothesis of equality of the means rejected with a p value < 0.05. Note that in the one-way ANOVA analysis, only statistically significant differences found in post-hoc tests between mutant and control mice groups, on CD, or on HFD, respectively, were considered relevant. s.d: standard deviation. n.s: not significant (p value > 0.05).

4.4.2.4 Blood chemistry

In order to detect potential alterations induced by HFD in Gpr30-T181 Deltagen mice, blood chemistry analysis was performed and several parameters were checked (Table 4.7 and Table 4.8).

Table 4.7: Blood chemistry of Gpr30-T181 Deltagen female mice

group	time-point		parameters											
			ALAT	Alb	Amy	AP	ASAT	Bil	Ca	Ch	CK	Cre	Fe	Fru
+/+ ♀ CD	2nd	mean	0.51	57.57	45.73	1.82	1.54	5.79	1.85	2.15	2.16	10.52	22.18	248.00
		± s.d	0.17	3.30	5.81	0.40	0.38	0.82	0.17	0.43	0.95	1.85	8.76	23.08
-/- ♀ CD	2nd	mean	0.45	57.00	46.77	1.52	1.47	5.79	1.89	1.89	1.76	9.93	20.19	241.38
		± s.d	0.18	1.65	6.00	0.16	0.33	0.58	0.19	0.29	0.97	1.44	4.41	26.28
+/+ ♀ HFD	2nd	mean	1.50	57.69	55.58	1.32	2.48	4.68	2.08	3.98	2.57	8.89	28.07	243.42
		± s.d	0.27	2.79	4.75	0.14	0.48	0.86	0.17	0.66	0.95	0.96	3.10	19.66
-/- ♀ HFD	2nd	mean	1.17	57.53	56.75	1.19	1.92	4.68	1.92	3.61	1.62	9.45	35.23	235.50
		± s.d	0.44	2.71	7.90	0.25	0.39	0.52	0.24	0.56	0.89	0.97	6.81	11.34
ANOVA p value			.000	n.s	.000	.000	.000	.001	.031	.000	n.s	.032	.000	n.s
+/+ ♀ CD	3rd	mean	0.30	28.37	19.33	0.85	0.91	1.70	0.95	0.96	0.61	6.60	7.21	138.55
		± s.d	0.16	2.08	1.98	0.34	0.40	0.26	0.10	0.22	0.31	0.95	2.65	18.11
-/- ♀ CD	3rd	mean	0.31	28.56	20.45	0.60	0.81	1.75	1.03	0.87	0.62	6.74	8.19	142.38
		± s.d	0.24	1.82	2.81	0.13	0.44	0.33	0.09	0.18	0.35	0.74	2.10	12.85
+/+ ♀ HFD	3rd	mean	1.08	29.93	24.67	0.54	1.50	1.69	1.13	1.97	1.22	6.29	12.88	125.33
		± s.d	0.27	0.77	3.77	0.11	0.28	0.18	0.03	0.29	0.25	0.59	2.61	5.39
-/- ♀ HFD	3rd	mean	1.09	28.28	27.58	0.50	1.50	1.66	1.02	1.60	0.68	6.00	13.06	114.80
		± s.d	0.34	1.39	6.81	0.11	0.37	0.19	0.10	0.18	0.30	0.87	5.36	10.55
ANOVA p value			.000	n.s	.000	.008	.001	n.s	.001	.000	.000	n.s	.000	.002
group	time-point		parameters											
			GGT	GLDH	Glu	HDL	IP	LDH	LDL	Lip	TG	Urea		
+/+ ♀ CD	2nd	mean	0.04	187.08	11.14	1.56	1.89	5.60	0.44	0.59	0.48	7.37		
		± s.d	0.02	86.09	2.36	0.38	0.26	2.37	0.05	0.25	0.11	1.32		
-/- ♀ CD	2nd	mean	0.05	175.00	10.56	1.40	1.86	4.82	0.42	0.60	0.47	7.36		
		± s.d	0.02	70.71	1.49	0.24	0.22	1.80	0.07	0.17	0.09	1.07		
+/+ ♀ HFD	2nd	mean	0.05	406.00	11.55	3.17	1.79	8.14	0.64	0.67	0.73	8.68		
		± s.d	0.02	120.85	1.94	0.57	0.22	3.34	0.08	0.17	0.12	0.89		
-/- ♀ HFD	2nd	mean	0.03	322.50	11.64	2.87	1.84	6.31	0.58	0.55	0.81	8.51		
		± s.d	0.01	121.16	1.98	0.50	0.33	3.27	0.09	0.10	0.25	1.17		
ANOVA p value			n.s	.000	n.s	.000	n.s	.061	.000	n.s	.000	.035		
+/+ ♀ CD	3rd	mean	0.03	80.00	5.07	1.35	0.86	1.96	0.41	0.46	0.25	2.86		
		± s.d	0.02	70.74	0.69	0.33	0.11	0.71	0.07	0.10	0.03	0.38		
-/- ♀ CD	3rd	mean	0.02	87.25	5.49	1.26	0.93	1.91	0.39	0.48	0.24	3.00		
		± s.d	0.01	95.17	0.43	0.28	0.12	1.11	0.07	0.09	0.01	0.25		
+/+ ♀ HFD	3rd	mean	0.03	337.00	5.21	3.14	0.92	2.97	0.62	0.71	0.40	3.54		
		± s.d	0.01	103.03	0.62	0.42	0.11	0.65	0.12	0.10	0.05	0.62		
-/- ♀ HFD	3rd	mean	nd	287.00	4.99	2.58	0.93	3.66	0.51	0.97	0.42	3.19		
		± s.d	nd	151.87	0.70	0.34	0.11	0.52	0.07	0.23	0.13	0.64		
ANOVA pvalue			n.s	.000	n.s	.000	n.s	.000	.000	.000	.000	.022		

Blood chemistry of Gpr30-T181 Deltagen female mice. +/+ ♀ CD: wildtype female mice on control diet; -/- ♀ CD: Gpr30-T181$^{-/-}$ female mice on control diet ; +/+ ♀ HFD: wildtype female mice on high fat diet; -/- ♀ HFD: Gpr30-T181$^{-/-}$ female mice on high fat diet; ALAT: alanine aminotransferase (µKat/l); Alb: albumin (g/l); Amy: α –amylase (µKat/l); AP: alkaline phosphatase (µKat/l); ASAT: aspartate transaminase (µKat/l); Bil: bilirubin (µmol/l); Ca: calcium (mmol/l); Ch: cholesterol (mmol/l); Cre: creatinine (µmol/l); CK: creatine kinase (µKat/l); Fru: fructosamine (µmol/l); GTT: γ-glutamyl transferase (µKat/l); Glu: glucose (mmol/l); GLDH: glutamate dehydrogenase; HDL: high-density lipoprotein-cholesterol (mmol/l); IP: inorganic phosphate (mmol/l); Fe: iron (µmol/l); LDH: lactate dehydrogenase (µKat/l); Lip: lipase (µKat/l); LDL: low-density lipoprotein-cholesterol (mmol/l); TG: triglycerides (mmol/l); urea: urea (mmol/l). Statistical analysis: One-way ANOVA followed by

post-hoc test for multiple comparisons. Hypothesis of equality of the means rejected with a p value < 0.05. Note that only statistically significant differences found in post-hoc tests between mutant and control mice groups, on CD, or on HFD, respectively, were considered relevant (in red). p values in post-hoc test: ASAT, <0.035; Ch, < 0.029; CK, < 0.015; HDL, < 0.034. s.d: standard deviation. n.s: not significant (p value > 0.05). nd: not detected.

Table 4.8: Blood chemistry of Gpr30-T181 Deltagen male mice

group	time-point		parameters										
			ALAT	Alb	Amy	AP	ASAT	Bil	Ca	Ch	CK	Cre	Fe	Fru
+/+ ♂ CD	2nd	mean	0.70	55.20	57.43	0.98	1.24	5.21	1.95	3.58	2.57	9.53	29.47	243.17
		± s.d	0.52	3.56	9.09	0.16	0.52	0.97	0.23	0.93	1.05	0.79	5.75	19.06
-/- ♂ CD	2nd	mean	0.70	57.22	56.74	1.06	1.20	6.06	2.01	3.84	2.84	9.74	30.50	250.20
		± s.d	0.44	3.76	6.92	0.18	0.36	1.28	0.24	0.69	0.92	0.71	8.47	14.98
+/+ ♂ HFD	2nd	mean	1.20	60.49	79.43	0.89	1.43	3.37	2.20	5.65	1.89	9.26	33.74	231.13
		± s.d	0.51	5.01	8.10	0.17	0.36	0.38	0.31	0.55	0.54	1.68	8.44	21.08
-/- ♂ HFD	2nd	mean	1.23	58.08	76.54	0.85	1.39	3.25	2.03	5.31	1.70	9.84	31.28	221.38
		± s.d	0.72	2.32	10.30	0.12	0.37	0.60	0.34	0.66	0.85	2.11	6.37	14.17
ANOVA p value			.059	.033	.000	.027	.587	.000	.275	.000	.028	n.s	n.s	.007
+/+ ♂ CD	3rd	mean	0.34	57.98	51.31	1.03	0.93	3.71	2.09	3.65	2.37	11.03	18.30	264.60
		± s.d	0.12	4.15	7.31	0.15	0.31	0.69	0.20	0.52	2.51	2.11	6.34	31.96
-/- ♂ CD	3rd	mean	0.54	57.13	43.29	1.03	1.08	3.96	2.08	3.32	2.57	10.34	20.50	278.25
		± s.d	0.33	3.12	9.33	0.23	0.42	0.68	0.29	0.58	1.64	1.14	9.41	19.11
+/+ ♂ HFD	3rd	mean	2.49	61.15	65.60	1.49	1.98	3.25	2.22	5.52	3.20	12.20	25.55	258.80
		± s.d	0.72	0.94	9.84	0.27	0.36	0.30	0.11	0.68	2.04	2.32	6.39	20.13
-/- ♂ HFD	3rd	mean	1.88	60.48	64.96	1.00	1.78	3.33	2.08	5.61	1.97	12.00	22.67	251.33
		± s.d	0.50	2.09	5.17	0.27	0.57	0.39	0.23	0.89	1.46	1.65	8.29	19.13
ANOVA p value			.000	.021	.000	.000	.000	.042	n.s	.000	n.s	n.s	n.s	n.s
group	time-point		parameters										
			GGT	GLDH	Glu	HDL	IP	LDH	LDL	Lip	TG	Urea		
+/+ ♂ CD	2nd	mean	0.08	278.18	10.48	2.71	1.78	6.51	0.52	0.70	0.83	7.64		
		± s.d	0.03	155.81	2.90	0.73	0.23	5.44	0.14	0.19	0.22	1.12		
-/- ♂ CD	2nd	mean	0.09	294.00	11.59	2.94	2.03	4.96	0.53	0.67	0.70	7.50		
		± s.d	0.01	174.88	2.91	0.51	0.26	1.75	0.12	0.12	0.11	0.74		
+/+ ♂ HFD	2nd	mean	0.08	407.14	14.16	4.50	1.97	6.26	0.76	0.78	1.18	9.34		
		± s.d	0.00	208.14	1.89	0.45	0.42	2.83	0.14	0.25	0.36	1.44		
-/- ♂ HFD	2nd	mean	nd	423.75	12.69	4.16	2.05	6.64	0.62	0.72	0.94	9.91		
		± s.d	nd	248.02	1.16	0.46	0.31	3.30	0.11	0.16	0.27	0.95		
ANOVA p value			.075	n.s	.016	.000	n.s	n.s	.001	n.s	.002	.000		
+/+ ♂ CD	3rd	mean	0.06	240.60	10.12	2.94	1.91	3.52	0.52	1.10	0.77	7.03		
		± s.d	0.04	160.68	2.13	0.43	0.34	1.44	0.14	0.34	0.12	1.00		
-/- ♂ CD	3rd	mean	0.04	222.80	10.34	2.62	1.88	3.59	0.53	1.00	0.74	7.00		
		± s.d	0.02	150.79	2.42	0.50	0.25	0.94	0.11	0.23	0.19	0.94		
+/+ ♂ HFD	3rd	mean	0.06	751.86	9.84	4.39	2.23	7.24	0.76	0.82	0.85	7.69		
		± s.d	0.02	325.52	1.37	0.54	0.20	1.63	0.15	0.21	0.26	0.49		
-/- ♂ HFD	3rd	mean	0.07	655.14	10.12	4.49	1.87	5.66	0.76	1.06	0.93	7.84		
		± s.d	0.02	235.93	0.99	0.66	0.28	1.10	0.20	0.36	0.18	0.71		
ANOVA pvalue			n.s	.000	n.s	.000	.035	.000	.001	n.s	n.s	.069		

Blood chemistry of Gpr30-T181 Deltagen male mice. +/+ ♂ CD: wildtype male mice on control diet; -/- ♂ CD: Gpr30-T181$^{-/-}$ male mice on control diet ; +/+ ♂ HFD: wildtype male mice on high fat diet; -/- ♂ HFD: Gpr30-T181$^{-/-}$ male mice on high fat diet; ALAT: alanine aminotransferase (µKat/l); Alb: albumin (g/l); Amy: α – amylase (µKat/l); AP: alkaline phosphatase (µKat/l), ASAT: aspartate transaminase (µKat/l); Bil: bilirubin (µmol/l); Ca: calcium (mmol/l); Ch: cholesterol (mmol/l); Cre: creatinine (µmol/l); CK: creatine kinase (µKat/l); Fru: fructosamine (µmol/l); GTT: γ-glutamyl transferase (µKat/l); Glu: glucose (mmol/l); GLDH: glutamate dehydrogenase; HDL: high-density lipoprotein-cholesterol (mmol/l); IP: inorganic phosphate (mmol/l); Fe: iron (µmol/l); LDH: lactate dehydrogenase (µKat/l); Lip: lipase (µKat/l); LDL: low-density lipoprotein-cholesterol (mmol/l); TG: triglycerides (mmol/l); urea: urea (mmol/l). Statistical analysis: One-way ANOVA followed by post-hoc test for multiple comparisons. Hypothesis of equality of the means rejected with a p value < 0.05. Note that only statistically significant differences found in post-hoc tests between mutant and control mice groups, on

CD, or on HFD, respectively, were considered relevant (in red). p values in post-hoc test: AP, < 0.01. s.d: standard deviation. n.s: not significant (p value > 0.005); nd: not detected.

After 20 weeks of HFD, total cholesterol (Ch), high density lipoprotein (HDL) and creatine kinase (CK) plasma levels were significantly higher in control female mice compared to homozygous mutant mice (Fig. 4.13, 4.14 and 4.15). Such a variation in HDL and total cholesterol might indicate an imbalance of lipid metabolism, whereas unchanged values of CK might suggest a well preserved muscular metabolism in female mutants despite HFD. Indeed, after 20 weeks of HFD, alkaline phosphatase (AP) plasma levels were found significantly higher in control male mice compared to homozygous mutant mice (Fig. 4.16). An increase of AP levels may indicate liver or bone disorders induced by HFD, an effect maybe attenuated in mutant males.

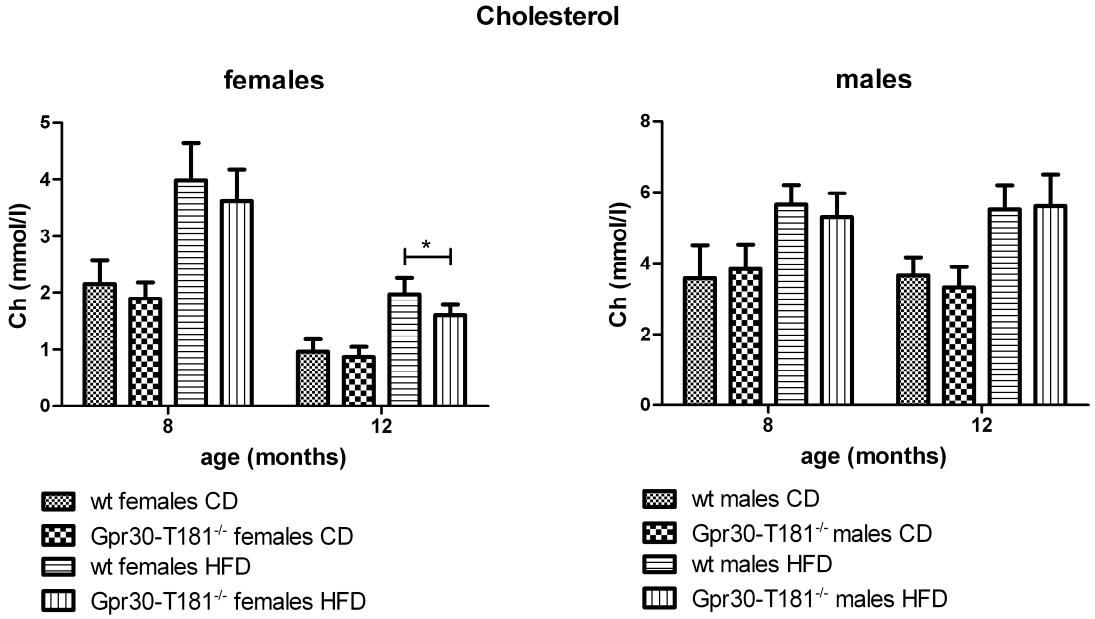

Figure 4.13: Blood chemistry of Gpr30-T181 Deltagen mice: cholesterol (Ch) levels

After 20 weeks of HFD total Ch levels in homozygous mutant females (12 months old) were significantly lower than in control mice, probably reflecting diminished levels of the HDL component also registered in mutant females (see Fig. 3.14). This finding might suggest a slight impairment in lipid metabolism. On the right Ch values in males are shown: no genotype-dependent differences were observed at any time-point. Statistical analysis: One-way ANOVA followed by post-hoc analysis for multiple comparisons, * p value < 0.05. wt: control littermates.

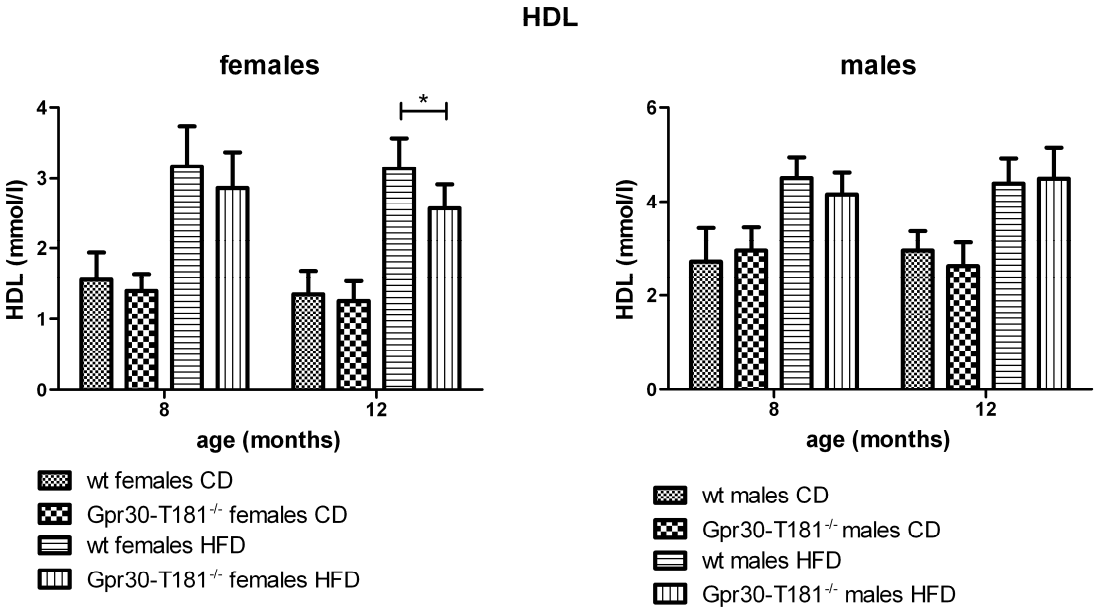

Figure 4.14: Blood chemistry of Gpr30-T181 Deltagen mice: high density lipoprotein (HDL) levels

After 20 weeks of HFD HDL levels in homozygous mutant females (12 months old) were significantly lower than in control mice. This finding might suggest a slight impairment in reverse cholesterol transport. On the right HDL levels in males are shown: no genotype-dependent differences were observed at any time-point. Statistical analysis: One-way Anova followed by post-hoc analysis, *: p value < 0.05. wt: control littermates.

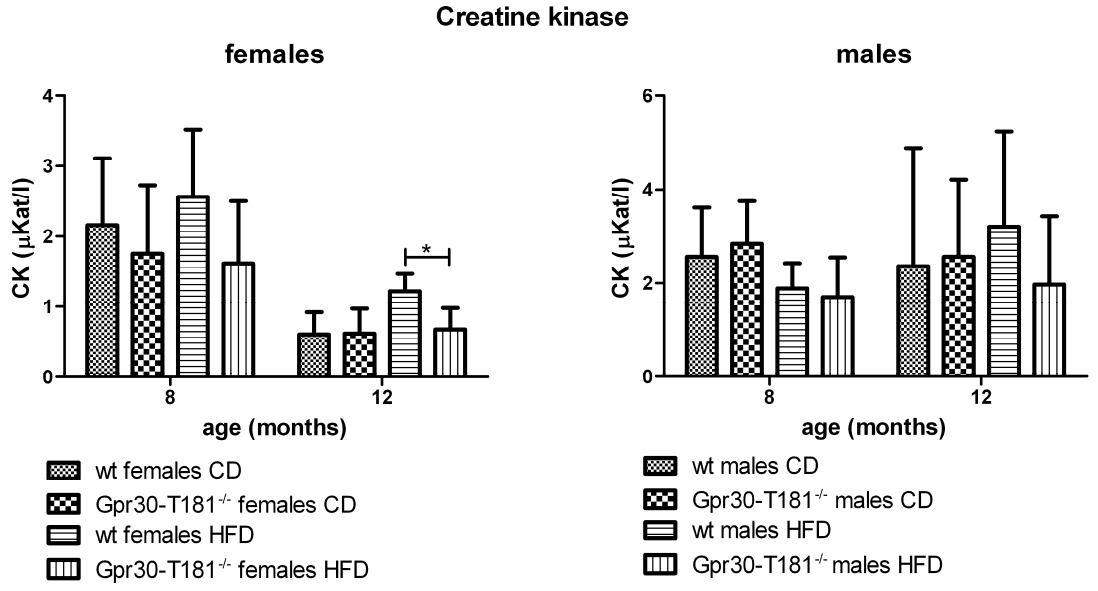

Figure 4.15: Blood chemistry of Gpr30-T181 Deltagen mice: creatine kinase (CK) levels

After 20 weeks of HFD CK levels in homozygous mutant females (12 months old) were significantly lower than in control mice, a result probably indicating an unaltered muscular metabolism in mutant females. On the right CK male levels are shown: no genotype-dependent differences were observed at any time-point. Statistical analysis: One-way Anova followed by post-hoc analysis for multiple comparisons, *: p value < 0.05. wt: control littermates.

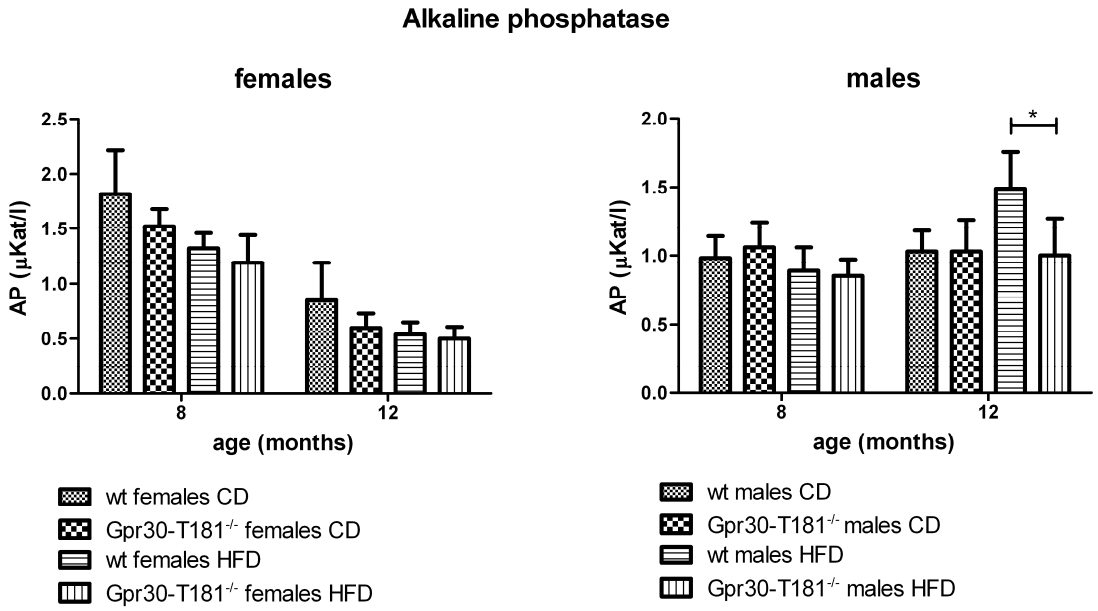

Figure 4.16: Blood chemistry of Gpr30-T181 Deltagen mice: alkaline phosphatase (AP) levels

After 20 weeks of HFD AP levels in homozygous mutant males (12 months old) were significantly lower than in control mice (right panel). This finding might suggest a better adaptation of male homozygous mutant mice in terms of liver or bone disorders induced by HFD. On the left AP levels in females are shown: no genotype-dependent differences were observed at any time-point. Statistical analysis: One-way Anova followed by post-hoc analysis for multiple comparisons, *: p value < 0.01. wt: control littermates.

4.5 SHG17 Artemis mice phenotypic assessment

SHG17 Artemis mice were generated by a Cre-recombinase approach leading to the complete deletion of the exon 3 of Gpr30 gene. Moreover these mice do not retain at genomic level any targeting cassette such as LacZ or neomycin, and they can be considered full Gpr30 KO mice. Therefore, and in order to exclude a potential influence of the LacZ-neo^r cassette on the phenotype achieved in Deltagen, Artemis mice were analysed in baseline for thymus gene expression, body weight, body mass composition, glucose metabolism, and left ventricular function.

4.5.1 Thymus gene expression

Statistical analysis of microarray (SAM) revealed in the thymus of Deltagen male homozygous mutant mice several genes to be down-regulate and this effect could be validated by Real-Time PCR. Nppa, Serca2, Ccr5 and Cat gene expression analysis by Real-Time PCR, was also performed in the thymus of male Artemis mice. In these mice gene expression was clearly unchanged, being the fold of gene deregulation always close to 1 (Table 4.9). The different results obtained in Deltagen and Artemis mice showed for the two mutant mice a divergent phenotype, likely reflecting the two different strategies used to generate them. Therefore, the presence of the LacZ-neo^r cassette in Deltagen mice might have determined the immunological phenotype observed in this Gpr30 mouse model.

Table 4.9: Validation of microarray data

GOI/ Biological replicate		Normalized Ct biological replicate SHG17$^{+/+}$	Normalized Ct biological replicate SHG17$^{-/-}$	ΔΔCt	Fold-expression	p value
Nppa	1	34.57	28.09	-0.08	1.06	0.96
	2	31.43	32.72			
	3	32.61	31.96			
	4	33.34	33.32			
	5	30.55	36.02			
Cccr5	1	28.84	26.39	0.20	0.87	0.84
	2	27.20	27.67			
	3	27.10	26.98			
	4	27.98	28.26			
	5	28.58	31.39			
Atp2a2	1	27.28	25.22	0.23	0.85	0.76
	2	26.21	26.46			
	3	25.99	25.91			
	4	26.42	27.21			
	5	27.02	29.29			
Cat	1	26.90	24.47	0.01	0.99	0.99
	2	25.26	25.55			
	3	25.24	24.76			
	4	25.78	26.53			
	5	26.72	28.65			

Validation of microarray data. GOI: gene of interest. Nppa: natriuretic peptide precursor A; Ccr5: chemokine (C-C motif) receptor 5, Serca2: sarcoplasmic reticulum Ca(2+)-ATPase 2, Cat: catalase. ΔΔCt was calculated as: average of normalized SHG17$^{-/-}$ Ct values- average of normalized SHG17$^{+/+}$ Ct values. Reference genes used for normalization of Ct values were: Gapdh: Glyceraldehyde-3-phosphate dehydrogenase; Hprt: hypoxanthine-guanine phosphoribosyltransferase; PO: ribosomal protein, large; Fold-expression= $2^{-\Delta\Delta Ct}$. p value calculated in a t-test used to compare Ct value means obtained in SHG17$^{+/+}$ versus SHg17$^{-/-}$ mice.

4.5.2 Body weight and body mass composition

Body weight of 13, 16, 19, 21 and 22 weeks old SHG17 Artemis mice was measured. No genotype-dependent differences were found among groups (Fig. 4.17).

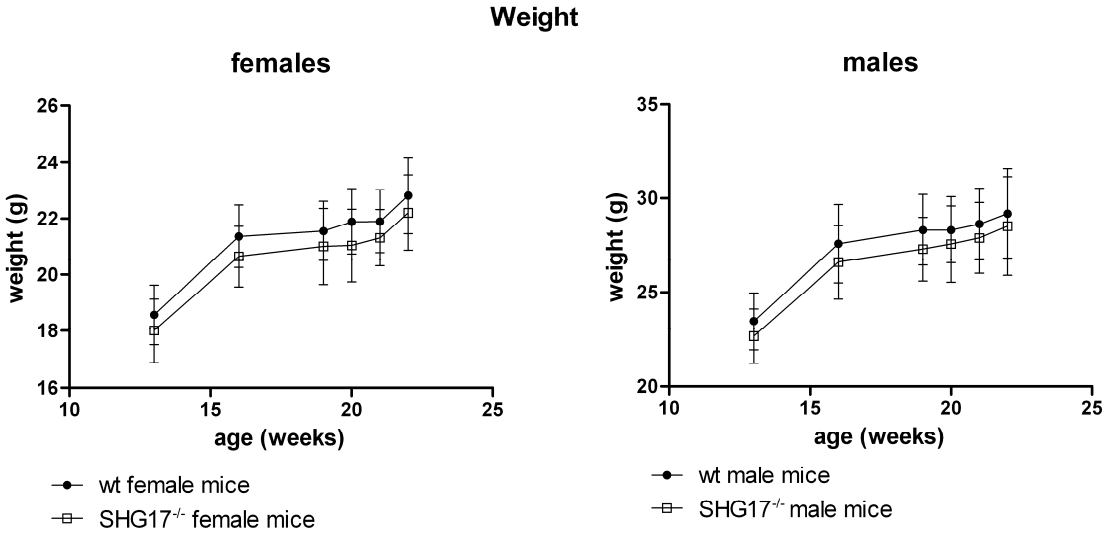

Figure 4.17: SHG17 Artemis mice, body weight (BW)

BW of mice between 13 and 22 weeks old was measured. No genotype-dependent differences were found among female or male groups.

Body mass composition was assessed by NMR and results are reported in Fig. 4.18. No relevant differences were observed between control mice and SHG17$^{-/-}$ mice among male or female groups. Fat mass in SHG17$^{-/-}$ female mice was slightly but significantly higher than in SHG17$^{-/-}$ male mice [(13.11 ± 2.11)% body weight vs. (10.53 ± 1.66)% body weight] evidencing a sexual dimorphism in body mass composition only for this Gpr30 KO mouse model.

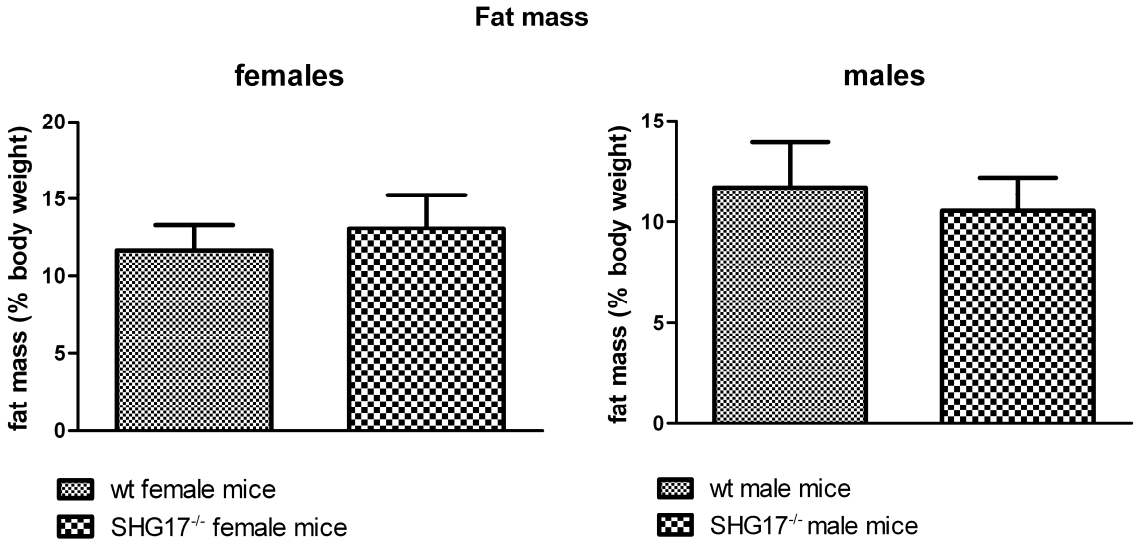

Figure 4.18: SHG17 Artemis mice, nuclear magnetic resonance (NMR)

Fat mass composition did not differ between SHG17 mice and relative control groups. However SHG17$^{-/-}$ female fat mass was significantly higher than in SHG17$^{-/-}$ male mice, evidencing a sexual dimorphism for this mutant mouse model (13.11 ± 2.11 vs. 10.53 ± 1.66; p-value <0.05). Statistical analysis: t-test.

4.5.3 Intraperitoneal glucose tolerance test

Intraperitoneal glucose tolerance test was performed on 17 weeks old SHG17 Artemis mice. The experiment did not evidence any difference between groups in terms of glucose clearance as reported in Fig 4.19.

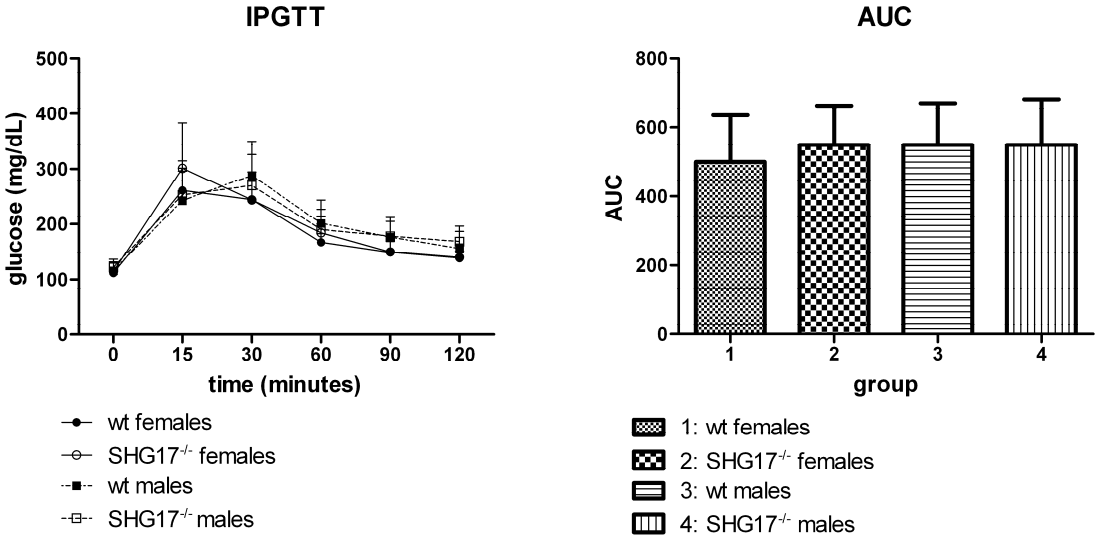

Figure 4.19: SHG17 Artemis mice, IPGTT

On the left IPGTT curves of SHG17 Artemis mice; on the right calculation of the area under the curves (AUC). IPGTT was performed using 17 weeks old mice. No differences were found among groups. Statistical analyisis: One-way ANOVA followed by post-hoc analysis for multiple comparisons.

Altogether our results pointed to exclude in both Deltagen and Artemis mutant mice a metabolic phenotype in terms of body weight regulation, fat mass deposition and glucose clearance.

4.5.4 Echocardiography

In order to assess the left ventricular function of SHG17 Artemis mice, 14 weeks old animals underwent echocardiographic analysis. In particular control male mice showed a significantly higher heart rate (HR) value compared to SHG17$^{-/-}$ male mice (Table 4.10). The same trend was observed between female groups, even tough the reported difference was not statistically significant. In order to confirm this result, a second method was adopted and ECG analysis performed. However in this case no differences in HR were reported among groups (Table 4.10). Artemis mice as well as Deltagen mice did not show any cardiac abnormality, at least for the parameters evaluated in this study.

Table 4.10: Echocardiography of SHG17 mice

groups	time-point		parameter						
			EF	FS	LVIDd	LVIDs	AoVel	HR	HR(ECG)
+/+ ♀	baseline	mean	51.37	26.21	4.17	3.08	855.59	432.00	474.58
		± s.d	9.04	5.54	0.14	0.26	170.35	35.56	45.78
-/- ♀	baseline	mean	45.97	22.77	4.15	3.20	838.35	415.10	463.53
		± s.d	6.36	3.79	0.24	0.21	151.78	41.59	28.32
t-test p value			ns	ns	ns	ns	ns	ns	ns
+/+ ♂	baseline	mean	45.92	22.91	4.50	3.46	936.01	438.33	452.92
		± s.d	6.20	3.63	0.24	0.22	152.01	33.12	36.31
-/- ♂	baseline	mean	49.94	25.05	4.53	3.40	1008.42	412.89	450.12
		± s.d	3.91	2.39	0.23	0.23	298.15	29.22	35.17
t-test p value			ns	ns	ns	ns	ns	.048	ns

Echocardiography of SHG17 Artemis mice. +/+ ♀: wildtype control female mice; -/- ♀: SHG17$^{-/-}$ female mice; +/+ ♂: wildtype control male mice; -/- ♂: SHG17$^{-/-}$ female mice. EF: ejection fraction (%); FS: fractional shortening (%); LVIDd: left ventricle internal diameter (mm); LVIDs: left ventricle internal diameter systole (mm); HR: heart rate (beats/min) recorded in echocardiography. HR (ECG): heart rate (beats/min) recorded in electrocardiogram (ECG). Statistical analysis: t-test. s.d: standard deviation. n.s: not significant (p value > 0.05). Values significantly different are reported in red.

5 Discussion

The Gpr30 receptor aroused in the last years a strong interest for two main reasons: 1) as GPCR, it represents a potential pharmacological target (28); 2) as estrogen receptor, it offers new perspectives for understanding estrogen biology (176, 182). However the role of estrogen as Gpr30 ligand remains one of the most controversial aspects and it is still under debate. Several studies have provided evidence against the involvement of estrogen in Gpr30 signalling (44). Moreover the *in vivo* function of Gpr30 is still unknown. In order to gain new insights into Gpr30 physiological function, the main goal of the present thesis was an extensive phenotypic study of two Gpr30 mutant mouse models: Gpr30-T181 Deltagen and SHG17 Artemis mice.

5.1 Gpr30 mutant mouse models

Deltagen mice were obtained through an insertion of a LacZ-neo^r cassette into the third Gpr30 exon, leading to the disruption of the ORF. Artemis mice, conversely, were obtained through a Cre/LoxP recombinase system leading to the deletion of the entire Gpr30 exon 3. Deltagen mice had the relevant advantage to incorporate the LacZ gene reporter that allowed us to establish a precise gene pattern expression for Gpr30 (60). However this model showed two drawbacks: 1) the insertion of the LacZ-neo^r cassette may lead to phenotypes not related to Gpr30 ablation (183); 2) a fusion transcript including the neomycin gene and part of exon 3. Concerning the first aspect it has to be mentioned that the phenotype of several GPCR KO that still keep the targeting vector at the genomic level was already successfully established (111). Moreover the expression of a truncated protein and the hypothesis of a "leaky" KO mouse has most likely to be excluded for two reasons: 1) the presence of stop codons in all the three possible reading frames at the 3´ end of the LacZ-neo^r cassette; 2) the nonsense reading frame of the remaining part of exon 3 spliced to the neomycin gene. Unfortunately, the absence of Gpr30 in Deltagen mice was not shown in western blot yet (60). Therefore to refer to these mice as mutants rather than KO mice may represent a more appropriate terminology.

Artemis mice do not maintain the selection marker and were generated on a pure C57BL/6 background. They could be considered in every respect Gpr30 KO mice (184) representing an invaluable term of paragon for results obtained in Deltagen mice.

5.2 Primary screen

Deltagen mice underwent an extensive primary screen in many different fields of mouse physiology. The most relevant findings were achieved in the immunological and in the behavioural screen.

5.2.1 Immunological screen

A flow cytometric analysis of Deltagen mice revealed statistically significant lower frequencies of T cells compared to wildtype control mice, along with a lower proportion of CD62L expressing cells within the T cell cluster, representing the naïve T cell compartment newly produced in the thymus (185). This finding was in agreement with Wang and colleagues results (62), who showed that apoptosis rate in T cell receptor $\beta^{-/low}$ double positive thymocytes was doubled in Gpr30 KO mice in comparison to controls. A lower rate of T cells produced in the thymus may actually explain the reduced number of circulating T cells in Deltagen mice. To analyse the molecular basis of this observation, we decided to determine the gene expression profile of Deltagen mice thymus in comparison to wildtype littermates. Significance Analysis of Microarrays (SAM) revealed 20 down-regulated genes. Up-regulated genes were not found. The small number of down-regulated genes unfortunately did not allow us to perform a pathway analysis (DAVID or Ingenuity Pathway analysis). Nevertheless, some of them might contribute to explain the reduced number of T cells reported.

Four genes drew our attention: the natriuretic precursor-peptide A (Nppa), the chemokine (C-C motif) receptor 5 (Ccr5), the sarcoplasmic reticulum calcium-ATPase 2 (Serca2 or Atp2a2), and the catalase (Cat). These genes are involved in T cell maturation and proliferation. Their decrease in the thymus of Deltagen mice might be associated with an enhanced mechanism of T cells apoptosis, likely leading to a reduced number of leukocytes circulating in the blood of these mice. Therefore, and in order to substantiate our hypothesis and in order to validate thymus microarray results, mRNA levels of these genes were measured by Real-time PCR. A pronounced trend of down-regulation consistent with microarray results was found.
Nppa, known also as atrial natriuretic peptide (ANP), is a member of the natriuretic peptide family and is normally expressed in high concentrations in the atrium (186). It acts through the natriuretic peptide receptor A (NPR-A), a guanylyl cyclase-linked receptor, that uses cyclic GMP as intracellular messenger (187). Nppa is able to induce diuresis and natriuresis as well as vessel vasodilatation, being involved in the regulation of volume-pressure homeostasis. ANP and the natriuretic peptide B (NPB) are markedly increased in patients

with myocardial infarction as well as in those with congestive heart failure (187). However, Nppa has been also proposed as endogenous thymus development regulator (188). It was actually shown to be produced in the thymus and its receptors have been found in thymocytes (189, 190). In fetal thymic organ cultures (FTOC) conducted in the presence of ANP, the peptide was able to modulate thymocyte differentiation (188). Moreover newborn animals showed much higher levels of ANP in the thymus than adults (181) evidencing its involvement in thymus maturation. Therefore the reduced expression of ANP in the thymus of Deltagen mice might have interfered with T cell maturation. However, a precise link between ANP levels expression and a reduced number of T cells in Deltagen mice was not yet established, and further experiments are needed to clarify this aspect.

Ccr5 is a member of the beta chemokine receptor family, predicted to be a seven transmembrane protein similar to G protein-coupled receptors. It is expressed by T cells and macrophages, and it is known to be an important co-receptor for macrophage-tropic viruses, including HIV, to enter host cells (191). Defective alleles of this gene have been associated with HIV resistance (192). CCR5 is important in immune cell cross talk. Interaction with the natural ligand macrophage inflammatory protein (MIP)-1β promotes and controls the recruitment of cells to sites of inflammation, the immune synapse formation, T cells interactions within lymph nodes and the activation and differentiation of T cells (193). Moreover Ccr5 was shown to be able to induce a calcium-dependent intracellular signalling cascade triggered by the mycobacterial heat shock protein 70; a process, promoting downstream dendritic cell association and immune synapse formation between dendritic and T cells (193). On this regard it is interesting to note that SAM analysis and Real-Time PCR revealed the Serca2 gene, an intracellular calcium pump, to be down-regulated in the thymus of Deltagen mice. It is known that calcium plays an important role in life and death of T cells; elevation of intracellular free calcium is one of the key triggering signals for T cell activation by antigen (194). Serca pumps are calcium intracellular pumps that specifically maintain low levels of cytosolic calcium concentrations by actively transporting it from the cytosol into the sarco/endoplasmic reticulum lumen (195). Therefore one might speculate that decreased levels of Serca2 associated to decreased levels of Ccr5, might have induced an increase of intracellular calcium, and that such an increase might have enhanced for instance a calcium-induced T lymphocyte apoptosis pathway (196).

Catalase is an enzyme responsible within cells for converting H_20_2 into H_20 and O_2 playing in the cells a pivotal detoxifying function. H_20_2 as ROS may lead to irreversible cellular damages. Catalase overexpression or catalase enzyme addition to cell culture medium, have

been shown to protect cells against apoptosis and oxidative stress (197, 198). Tome and colleagues showed that overexpression of catalase in a thymoma cell line (WEHI7.2), prevented apoptosis following glucocorticoid stimulation (dexamethasone) (199). Catalase down-regulation in the thymus of Deltagen mice might represent a further T- cell apoptosis promoting factor.
Additional experiments are required to establish a clear link between these genes and the reduced frequency of lymphocytes in Deltagen mice. As a first step, Real-Time PCR may be performed on a larger number of thymi samples in order to measure statistically significant differences in gene expression levels between mutant and control mice. Moreover, a western blot analysis may aid to verify decreased protein expression levels.

Altogether the results achieved so far pointed to a role of Gpr30 in mediating T cell maturation. Lack of Gpr30 may be associated to an increase of T cell apoptosis. Wang and colleagues already proposed an immunological function for Gpr30 (62). However for this interpretation some controversial aspects have to be taken into consideration. Concerning the results of Wang and co-workers it has to be mentioned that 1) the α-ERKO mice used in this study still expressed a splice variant of ERα; 2) the ovarian cycle phase and therefore the estrogen levels of Gpr30 KO female mice used in G1 experiments, were not assessed (184). These factors might have contributed to observe effects not necessary related to the Gpr30 lack. Moreover experiments aimed at confirming the phenotype found, did not show the same results in Artemis mice. Real-Time experiments performed on thymi of these revealed a different gene expression profile: the expression of Nppa, Ccr5, Serca2 and Cat genes was unchanged. In addition we did not find in Artemis mice a decrease in circulating leukocytes as was previously observed in Deltagen mice (184). The molecular basis of the different phenotypes might indeed be related to the presence of the selection marker in Deltagen mice (184). Altogether these observations prompted us to reconsider the immunological function of Gpr30 (60, 184).

5.2.2 Behavioural screen

In an Open Field Test (OFT) Deltagen mice compared to wildtype control mice moved less and slower, and entered later the centre of the field. This behavioural pattern of Gpr30-T181 mice suggested a subtle increase in anxiety-related behaviour in reaction to novelty. The phenotype might be related to the expression of Gpr30 in the dentate gyrus of the hippocampus (60), a brain region involved in the neuronal circuite mediating anxiety (200). Moreover the results would be in agreement with the study of Dennis and colleagues, showing G1 and estrogen able to reproduce the effects of the antidepressant drug desipramine (57). However in this study the effects of specific ERα and ERβ agonists and antagonists where not shown. Whether Gpr30 was the only responsible for antidepressant estrogen effects has to still be clarified. Since only small differences were observed between Deltagen mutant and control mice, a secondary behavioural screen may be required. In addition in Deltagen mice the contribution of a cardiovascular phenotype to the observed anxiety-related behaviour could then be evaluated. Indeed, the results obtained in the OFT may reflect an increased sensitivity towards the fatigue in Deltagen mice.

5.3 Secondary screen

Gene expression studies revealed Gpr30 to be mainly expressed in the microvasculature endothelium (a sensitive target of pathologies connected to diabetes), as well as in the pancreas and in the stomach (45). Deltagen preliminary data indicated higher values of LDL in female mutant mice, suggesting a potential metabolic imbalance characterized by a sexual dimorphism. Therefore, we decided to challenge these mice with a defined HFD, as a potential enhancer of a metabolic and/or cardiovascular phenotype. In order to exclude a phenotype effect due to the presence of the selection marker in Deltagen mice, baseline experiments were also performed on Artemis mice, devoid of any targeting vector cassette.

5.3.1 Metabolic screen

Deltagen mice fed with a HFD did not show any difference in terms of body weight when compared to wildtype littermate control mice. These results were in contrast with those reported in other studies. Martensson and colleagues showed an age-dependent reduction in body weight (-9.6% at 19 weeks) associated with a proportional reduction in skeletal growth in Gpr30 KO female mice (61). In our hands body weight and body mass composition (NMR) of Deltagen mice did not show any genotypic difference even in response to HFD. A direct comparison of body composition and body weight between Artemis and the mice used by Martensson and colleagues at the same age (13-22 weeks) did not reveal any difference. Martensson and co-workers also reported reduced glucose sensitivity and increased plasma glucose levels in 6 months old KO female mice. We were not able to observe any change in glucose clearance in Deltagen mice at 6, 8 or 12 months old of age. Plasma glucose levels of Deltagen 8 and 12 months old mice did not differ from control mice. Genotype-dependent differences were not observed even under HFD conditions. Similar results were found for Artemis mice in baseline. The differences between the two studies might be explained taking into account experimental procedures and different Gpr30 KO mouse models used. In the Martensson and colleagues study AUC values of glucose metabolism were not provided, and differences were only calculated point by point in the glucose clearance curves. Nevertheless an assumption of glucose reduced sensitivity in Gpr30 KO mice was claimed. It has to be mentioned that it remains unclear whether in all experimental settings littermates were used. Additional caveats of this study might be a mixed genetic background of the mice and a rather limited molecular analysis of the targeting vector insertion (184).

Using another Gpr30 KO mouse model (62) Haas and colleagues found increased body weight and visceral adiposity in both male and female, 10-11 months old Gpr30 KO mice (68). Like Deltagen mice, the mice generated by Wang and collegaues maintain the selection marker and are on a mixed genetic background. In contrast to our study, a single integration of the targeting vector was not accurately verified, and homozygous intercrosses were used to generate experimental mice. Therefore the results reported by Haas and colleagues might not be necessary related to Gpr30 ablation.

For a comprehensive discussion of our results, the limits of the HFD model used in this thesis may be mentioned. Even though a clear trend of a decreased efficiency in glucose clearance was observed in HFD animals, a rigorous statistical analysis revealed no significant differences between control and HFD groups. C57BL/6 mice are known to be prone to develop obesity and glucose resistance (150) but it has to be noticed that the energy source used in a DIO model (animal or vegetal fat), as well as strain and age of the mice may lead to different results in terms of body weight gaining and glucose metabolism. Lard, the diet energy source used in our study, induces more moderate effects on glucose plasma levels and glucose clearance, compared for instance to diets based on butterfat (201). Moreover C57BL/6 middle-aged animals (around 1 year old) were shown to respond to HFD in terms of body weight and glucose tolerance, in a minor extension when compared to young animals (4 weeks old) (149). Therefore we could not exclude the unexpected and rather moderate effects of HFD due to the use of lard as energy source and of middle aged animals. However results obtained in baseline on both Gpr30 mutants, Deltagen and Artemis mice still encourage us to exclude a role of Gpr30 in body weight regulation and glucose clearance.

5.3.2 Cardiovascular screen

So far there was no study reporting a left ventricular analysis by echocardiography in Gpr30 mutant mice *in vivo*. Our data revealed a slight, but significant decrease of the AoVel (-8%) in 6 months old Deltagen female mice. This difference was obtained when comparing 18 homozygous mutants with 24 littermate control mice. AoVel can be actually used as a surrogate of cardiac output, and a comparison among groups can be done providing the same the aortic diameter in the different groups (Table 4.5) (202). A decreased cardiac output might be associated to an increased resistance of systemic vascular bed. This finding was consistent with the results of Haas and colleagues. These authors hypothesized a role for Gpr30 in regulating vascular tone showing the ability of Gpr30 to lower blood pressure upon estrogen stimulation (68). Therefore Gpr30 may act as a vasodilator, increasing vessel diameter and

decreasing vascular bed resistance. Conversely the lack of Gpr30 might be associated with a reduced vasodilatation and with an increase of vascular bed resistance, reflected by lower values of AoVel. However, comparing 9 homozygous mutants with 12 littermate control mice, we did not observe any AoVel difference between 8 and 12 months old female and control mice. A different age and a smaller number of mice might explain these results.

Several observations led to critically reconsider these conclusions. Echocardiography was performed also on Artemis mice. No differences were found in terms of AoVel between wildtype and littermate controls. The observation of a decreased heart rate in Artemis male mice was not confirmed using ECG. Moreover Deltagen mice were shown to be normotensive (120) (no data are available for Artemis mice yet). Altogether, the data obtained for Deltagen and Artemis mice seem to exclude a cardiovascular phenotype, at least concerning the systolic and diastolic parameters measured in this study.

Moreover and as opposed to the data reported by Park and colleagues (160), HFD did not induce any changes in cardiac function in mutant mice. Indeed, we could not detect any decline in fractional shortening (FS) induced by HFD. Age and genetic background of the mice may account for the different results obtained (Park *et al*. used 2 months old C57BL/6 mice). However our results seem to support previous reports that question the efficacy of HFD in causing relevant cardiac abnormalities in rodents (157).

5.3.3 Clinical chemistry

The most relevant results concerning clinical chemistry of Deltagen mice were observed after 20 weeks of HFD (3^{rd} time-point). In particular, cholesterol and HDL plasma levels of homozygous mutant females were found significantly lower than in littermate controls. Cholesterol and HDL were found decreased by 19% and 18%, respectively.

The process that regulates plasma HDL levels both in human and mice it is not fully understood yet. Mice normally have higher levels of HDL than LDL, in contrast to humans where the predominant form is represented by LDL (161). Most of the plasma cholesterol is transported on three major lipoprotein classes: very low density lipoproteins (VLDL)-cholesterol, LDL-cholesterol and HDL-cholesterol. The total plasma cholesterol detected in the clinical chemistry analysis is the sum of all the cholesterol carried by these three

lipoproteins (203). VLDL levels were not measured in this study, but triglycerides provide an indirect evaluation of VLDL amount.

HDL is believed to play a key role in the so called reverse cholesterol transport, a pathway aimed at removing cholesterol from the extra-hepatic tissues back to the liver for biliary excretion, or to steroidogenic organs such as the adrenals, the ovary and the testes (204). Nascent HDL particles are made in the liver and the intestine. They are secreted as particles containing mainly phospholipids and apolipoprotein-AI. In mice, HDL maturation is a process depending on the progressive accumulation of apoliporotein-E, leading in its turn to an increased affinity of hepatic receptors to HDL (205). A decrease of total cholesterol plasma levels recorded in homozygous mutant female mice might be interpreted, at first sight, as a good adaptation of Deltagen mice to HFD. However, the reduction of the HDL component might conversely reflect a slight imbalance of the cholesterol reverse transport and its beneficial effects in protecting from atherosclerosis (203).

Under equal dietary and cholesterol efflux and uptake conditions (120) and in presence of diminished HDL levels, a compensatory increase of LDL and/or VLDL levels would have been expected. However, LDL levels in homozygous mutant females were the same as in control mice. A direct measurement of VLDL levels was not performed. Therefore, a linear interpretation of the data was not possible. Still an altered reverse cholesterol transport in Deltagen mice would be consistent with Gpr30 expression in blood vessels. As a consequence of a reduced HDL clearance, LDL receptor and hepatic LDL receptor-like proteins may be reduced. Therefore, additional studies on these proteins at mRNA and protein levels, may aid to clarify and confirm the observed phenotype.
Notably only homozygous mutant female mice developed this slight decrease in plasma HDL levels. This sexual dimorphism in lipid profile might underline a mechanism related to sexual hormones such as estrogen. Indeed, estrogens were reported to be associated with lower cholesterol and LDL levels (206).

After 20 weeks of HFD, CK levels were increased in female wildtype mice by almost 50% in comparison to control mice. Remarkably, this effect could not be observed in homozygous mutant female mice. CK is an enzyme catalyzing the following reaction: $MgADP^{-} + CrP^{2-} + H^{+} \leftrightarrow Cr + MgATP^{2-}$ (where Mg: magnesium, ADP: adenosine diphosphate, CrP^{2-}: creatine phosphate, H^{+}: proton, Cr: creatine, ATP^{2-}: adenosine triphosphate) (207). CK can be present

in four different isoforms playing a key role in energy transfer and cellular buffering. CK isoforms are most found in cells and tissues with a high demand in metabolic energy such as the brain, the heart or the skeletal muscle. Plasma levels are representing the total of the different isoforms. In particular, high plasma CK levels are normally associated with muscle damage. Then, CK is released into the blood stream, leading to harmful effects on the kidney (161). Interestingly, creatine and urea levels, two parameters for kidney function, were comparable between groups fed with HFD, providing evidence for a similar kidney function in both mutant and control mice.

HFD was already shown to lead to an increase of CK plasma levels in rats (208). Moreover obesity is associated with an increase in the percentage of fast twitch, oxidative-glycolitic muscle fibers (type IIb fibers) that use glucose as an energy substrate, and to a reduction of slow-twitch oxidative muscle fibers with a high content of mitochondria (type I fibers) (209, 210). Therefore, an increase of CK under HFD conditions may reflect an increase of glycolytic enzyme activity in the muscle associated with a predominant energy buffering effect of the enzyme (conversion of Cr in CrP^{2-}). Deltagen female mice seemed not to show such a response after 20 weeks of HFD, resembling CK plasma levels observed in mice on CD. Studies on adenylate kinase (AK) and nucleoside diphosphokinase (NDPK), tightly connected to CK activity in maintaining an optimal muscle performance, may help to confirm and better understand these results (211). Interestingly, reduction of plasma CK in HFD conditions was observed in rats treated with L-carnitine (208). L-carnitine is a molecule essential for the transport of long-chain fatty acids from the cytosol to mitochondria, able to stimulate β-oxidation. GPCRs are known to play an important role in fatty acids oxidation, acting for instance on cyclic AMP (212), a second messenger already associated with Gpr30 signalling (36). Altogether, Gpr30 might be involved in the metabolism of smooth muscle cells in the brain, where we already reported highest Gpr30 expression (60).

After 20 weeks of HFD, homozygous mutant males showed stable plasma levels of alkaline phosphatase (AP). Conversely, control males showed increased AP plasma levels by almost 50% under the same conditions. This effect could not he observed in Deltagen female mice, although a slight difference between mutant and control females was already reported at the primary screen. An increase of plasma AP activity may be related to bone metabolism disorders or to liver disease, being these organs the main source of ALP activity (161). Although the increase of ALAT, ASAT and GLDH plasma levels in mice fed with HFD

might suggest the onset of liver disorders in both groups, lower levels of AP in Deltagen male mice, might suggest a better preserved hepatic function in response to HFD in mutant males. Moreover AP activity has also been associated with afferent vessels of the brain (213) and employed as a marker for blood-brain barrier (BBB) maturation (214). Interestingly, the highest expression levels of Gpr30 were found in brain vessels (60). Whether brain AP is also a component of the total AP detected in the blood chemistry analysis is unknown, but a potential link between AP vessel brain activity and Gpr30 might be considered.

A challenging aspect concerning the parameters measured in blood chemistry in mice is the high variability found among different strains, and even among animals of the same strain (215). Deltagen mice were generated on a mixed genetic background (6^{th} generation C57BL/6 backcrosses), and an effect on blood chemistry results can not be ruled out (184). However, a solid backcross breeding approach, aimed at re-establishing a pure C57BL/6 background, and the use of littermate controls in every experiment, likely reduced such an effect. Further experiments on Artemis mice may substantiate our findings.

5.4 An estrogen receptor can do more

The *in vivo* results achieved so far using Deltagen and Artemis mice may contribute to face the main controversy concerning Gpr30, namely whether it functions or not as an estrogen receptor. Estrogen is known to play a pivotal role in metabolism. Several studies show that estrogens and estrogen analogues decrease weight, fat store and food intake in mice and rats (129, 216, 217). It has been shown that α-ERKO and ArKO mice become obese and insulin resistant (125, 127, 129) and that glucose and insulin resistance is more severe under HFD conditions in α-ERKO mice (218). However, a metabolic phenotype in terms of body weight regulation, fat mass and glucose clearance, comparable to ERKO and ArKO mice could be excluded in both, Gpr30-deficient, Deltagen and Artemis mice.

Remarkably, some of the parameters measured, such as HDL, were altered only in homozygous mutant females under HFD. Our findings might suggest an involvement of estrogen in regulating lipid metabolism in females under HFD conditions through Gpr30. However, estrogen-mediated signalling by Gpr30 was not analysed in the present study and sex differences are not necessarily estrogen-dependent.

It has been reported that α-ERKO mice show an abnormal mating behaviour and many other anomalies in reproductive organs, partially common to β-ERKO mice (219). Mating or

fertility disturbances were not observed in either Deltagen or Artemis mice (45, 51). Several processes associated with estrogen regulation, such as bone and cartilage development, as well as nociception and energy metabolism were analysed in the primary screen. Remarkably, no differences were found between homozygous mutant and control mice.

In an overall interpretation of the data obtained in the context of the current literature, one may hypothesize a similar function for different estrogen receptors. This seems an incorrect or even misleading assumption. However, both α- and β-ERKO mice develop significant anomalies in metabolism, fertility and reproduction, being estrogen the lowest common denominator between them. This does not seem to be the case in Gpr30-deficient, Deltagen and Artemis mice. Indeed, the results obtained in this study are consistent with several reports showing that Gpr30 may not required for the normal estrogen response in some of the well-known estrogen regulated processes (220).

5.5 Conclusions and outlook

In order to better understand Gpr30 function *in vivo* we conducted a wide phenotypic study on two Gpr30 mutant mice: Gpr30-T181 Deltagen and SHG17 Artemis mice. Deltagen mice provided the crucial advantage of expressing a reporter gene (LacZ) that allowed us an extensive analysis of Gpr30 expression in any organ or tissue at any time point (60). Artemis mice, being generated on a pure C57BL/6 background and devoid of any selection marker, constituted the second Gpr30 mouse model, being essential for substantiating the results obtained with the Deltagen mice. A summary of experiments and results are shown in Table 5.1.

Table 5.1: Results summary

	Gpr30 mouse model			
Experiments performed in baseline	Deltagen		Artemis	
	♀	♂	♀	♂
BW	ns	ns	ns	ns
NMR	ns	ns	ns	ns
GTT	ns	ns	ns	ns
Echo	decresed AoVel in mutant mice	ns	ns	ns
Clinical Chem.	decreased AP levels in mutant mice (primary screen)	ns	na	na
Immunology	lower frequencies of T cells	lower frequencies of T cells	unchanged levels of T cells	na
Molecular Phen.	na	20 down-regulated genes in thymus RNA microarray experiments; confirm of a down-regulation trend for Nppa, Ccr5, Serca2, Cat genes in Real-Time PCR	na	absence of a down-regulation trend of Nppa, Ccr5, Serca2, Cat genes in Real-Time PCR
	Gpr30 mouse model			
Experiments performed during HFD protocol	Deltagen		Artemis	
	♀	♂	♀	♂
BW	ns	ns	na	na
NMR	ns	ns	na	na
GTT	ns	ns	na	na
Echo	ns	ns	na	na
Clinical Chem.	decreased levels of plasma Ch, HDL and CK in mutant mice on HFD	decreased levels of plasma AP in mutant mice on HFD	na	na

Results summary: ♀: female homozygous mutant mice; ♂: male homozygous mutant mice; ns: no significant differences found between deficient Gpr30 mice and littermate control mice; na: not available; BW: body weight; NMR: nuclear magnetic resonance; GTT: glucose tolerance test; Echo: echocardiography; Clinical chem.: clinical chemistry; Molecular phen.: molecular phenotyping; AP: alkaline phosphatase; Ch: cholesterol; HDL: high density lipoprotein; CK: creatine kinase; Nppa: natriuretic precursor peptide A; Ccr5: chemokine (motif C-C) receptor 5; Serca2: sarcoplasmic reticulum calcium ATPase 2, Cat: catalase.

Both, Deltagen homozygous male and female mutants, showed lower frequencies of circulating T cells, suggesting an immunological role of Gpr30 in regulating T cell maturation. Gene expression analysis of the thymus allowed us to identify which genes might be involved in determining this phenotype. We focussed on Nppa, Ccr5, Serca2 and Cat genes, all being down-regulated in mutant mice in comparison to controls. An enhanced calcium-dependent T cell apoptosis, leading to lower levels of circulating T cells might be involved. Deltagen mice may therefore constitute a mouse model for immunological susceptibility. A further cytometric and gene expression analysis using Artemis mice, however did not reveal the same results. The likelihood that the insertion of the LacZ-neo^r cassette might have led to the reduction of circulating T cells in Deltagen mice can not be excluded.

For the first time a hemodynamic study on both Deltagen and Artemis mice was performed. A decreased value of aortic blood velocity in Deltagen females and a lower heart rate in Artemis male mice were found, suggesting in both cases a potential impairment of diastolic function. However, blood pressure measurements by the tail-cuff method were performed in the primary screen (120) and no significant differences were found between Deltagen and control mice. Indeed, an impaired cardiac function could not be substantiated in further experiments, in which both Deltagen and Artemis mice did not show any relevant heart abnormalities, at least for the parameters measured. On the other hand, the predominant expression of Gpr30 in the vasculature of the brain and the kidney, suggest a role of Gpr30 in vessel diameter regulation and may therefore deserve further attention. To this end alternative and direct blood pressure measurements, such as catheterization and radio-telemetry, may offer a more exhaustive analysis for future experiments (221).

Some studies have claimed a metabolic function of Gpr30 (61, 68). However the metabolic screen conducted in Deltagen and Artemis mice allowed us to exclude a relationship between the lack of Gpr30 and body weight regulation, fat mass storage and efficiency in glucose clearance. Discrepancies between our and other studies might be explained by taking into account the different Gpr30 mouse models used and the different experimental approaches taken (184). Deltagen mice fed with HFD showed a different profile compared to controls, probably indicating a role of Gpr30 in regulating lipid and muscle metabolism. Decreased levels of cholesterol and HDL in homozygous mutant females fed with HFD, may suggest a possible impairment of the reverse cholesterol pathway in these mice. This phenotype may be

confirmed and further analysed on an ApoE-KO background, a well established model in atherosclerosis research (222). Moreover, stable levels of creatine kinase in mutant mice fed with a HFD suggest a potential involvement of Gpr30 in regulating muscle metabolism. The lack of Gpr30 might therefore contribute to preserving an optimal muscular metabolism, despite alterations induced by a HFD. Similarly, lower levels of alkaline phosphatase found in male mutants might underline a better response of the liver against alterations induced by HFD. Consequently, in further experiments one may expect reduced levels of liver steatosis in mutant in comparison to control mice, which may confirm a preserved liver function in Gpr30-deficient mice under HFD conditions.

The results obtained in this study were also discussed in the frame of the question, whether Gpr30 may function or not as an estrogen receptor. We showed that Gpr30 may not be required for the normal estrogen response in different estrogen-regulated physiological processes (e.g. metabolism, mating behaviour, bone development and nociception). Our findings support previous publications rebutting the role of Gpr30 as a new estrogen receptor (44, 184), but disagree with the conclusions reported in earlier prominent publications in which Gpr30 was claimed to be an estrogen receptor and even renamed into G protein estrogen receptor, Gper (34, 56, 57).

In conclusion, the results achieved in this study contributed to a better characterization of Gpr30 function *in vivo*, disproving its involvement in glucose tolerance, adiposity and body weight regulation and soliciting further experiments aimed at clarifying a potential role of Gpr30 in T cell regulation, lipid and muscular metabolism, as well as in hepatic protection under a high fat diet regimen.

References

1. **Jacoby E, Bouhelal R, Gerspacher M, Seuwen K** 2006 The 7 TM G-protein-coupled receptor target family. ChemMedChem 1:761-782
2. **Strader CD, Fong TM, Tota MR, Underwood D, Dixon RA** 1994 Structure and function of G protein-coupled receptors. Annu Rev Biochem 63:101-132
3. **Nakagawa T, Sakurai T, Nishioka T, Touhara K** 2005 Molecular mechanisms underlying sex-pheromone reception in insects. Tanpakushitsu Kakusan Koso 50:1563-1570
4. **Das SS, Banker GA** 2006 The role of protein interaction motifs in regulating the polarity and clustering of the metabotropic glutamate receptor mGluR1a. J Neurosci 26:8115-8125
5. **Gloriam DE, Schioth HB, Fredriksson R** 2005 Nine new human Rhodopsin family G-protein coupled receptors: identification, sequence characterisation and evolutionary relationship. Biochim Biophys Acta 1722:235-246
6. **Prabhu Y, Eichinger L** 2006 The Dictyostelium repertoire of seven transmembrane domain receptors. Eur J Cell Biol 85:937-946
7. **Vassilatis DK, Hohmann JG, Zeng H, Li F, Ranchalis JE, Mortrud MT, Brown A, Rodriguez SS, Weller JR, Wright AC, Bergmann JE, Gaitanaris GA** 2003 The G protein-coupled receptor repertoires of human and mouse. Proc Natl Acad Sci U S A 100:4903-4908
8. **Wilkie TM, Gilbert DJ, Olsen AS, Chen XN, Amatruda TT, Korenberg JR, Trask BJ, de Jong P, Reed RR, Simon MI, et al.** 1992 Evolution of the mammalian G protein alpha subunit multigene family. Nat Genet 1:85-91
9. **Sprang SR** 1997 G protein mechanisms: insights from structural analysis. Annu Rev Biochem 66:639-678
10. **Oldham WM, Hamm HE** 2008 Heterotrimeric G protein activation by G-protein-coupled receptors. Nat Rev Mol Cell Biol 9:60-71
11. **Congreve M, Marshall F** 2009 The impact of GPCR structures on pharmacology and structure-based drug design. Br J Pharmacol
12. **Palczewski K, Kumasaka T, Hori T, Behnke CA, Motoshima H, Fox BA, Le Trong I, Teller DC, Okada T, Stenkamp RE, Yamamoto M, Miyano M** 2000 Crystal structure of rhodopsin: A G protein-coupled receptor. Science 289:739-745
13. **Salom D, Lodowski DT, Stenkamp RE, Le Trong I, Golczak M, Jastrzebska B, Harris T, Ballesteros JA, Palczewski K** 2006 Crystal structure of a photoactivated deprotonated intermediate of rhodopsin. Proc Natl Acad Sci U S A 103:16123-16128
14. **Clapham DE, Neer EJ** 1997 G protein beta gamma subunits. Annu Rev Pharmacol Toxicol 37:167-203
15. **Graf R, Mattera R, Codina J, Evans T, Ho YK, Estes MK, Birnbaumer L** 1992 Studies on the interaction of alpha subunits of GTP-binding proteins with beta gamma dimers. Eur J Biochem 210:609-619
16. **Kristiansen K** 2004 Molecular mechanisms of ligand binding, signaling, and regulation within the superfamily of G-protein-coupled receptors: molecular modeling and mutagenesis approaches to receptor structure and function. Pharmacol Ther 103:21-80
17. **Tolkovsky AM, Levitzki A** 1978 Mode of coupling between the beta-adrenergic receptor and adenylate cyclase in turkey erythrocytes. Biochemistry 17:3795
18. **Hein P, Frank M, Hoffmann C, Lohse MJ, Bunemann M** 2005 Dynamics of receptor/G protein coupling in living cells. Embo J 24:4106-4114
19. **Gales C, Van Durm JJ, Schaak S, Pontier S, Percherancier Y, Audet M, Paris H, Bouvier M** 2006 Probing the activation-promoted structural rearrangements in preassembled receptor-G protein complexes. Nat Struct Mol Biol 13:778-786
20. **Javitch JA** 2004 The ants go marching two by two: oligomeric structure of G-protein-coupled receptors. Mol Pharmacol 66:1077-1082
21. **Milligan G** 2004 G protein-coupled receptor dimerization: function and ligand pharmacology. Mol Pharmacol 66:1-7
22. **Pin JP, Galvez T, Prezeau L** 2003 Evolution, structure, and activation mechanism of family 3/C G-protein-coupled receptors. Pharmacol Ther 98:325-354
23. **Mukhopadhyay S, Howlett AC** 2005 Chemically distinct ligands promote differential CB1 cannabinoid receptor-Gi protein interactions. Mol Pharmacol 67:2016-2024
24. **Azpiazu I, Gautam N** 2001 G protein gamma subunit interaction with a receptor regulates receptor-stimulated nucleotide exchange. J Biol Chem 276:41742-41747
25. **Birnbaumer L, Birnbaumer M** 1995 Signal transduction by G proteins: 1994 edition. J Recept Signal Transduct Res 15:213-252

26. **Offermanns S** 2003 G-proteins as transducers in transmembrane signalling. Prog Biophys Mol Biol 83:101-130
27. **Hutchinson DS, Summers RJ, Bengtsson T** 2008 Regulation of AMP-activated protein kinase activity by G-protein coupled receptors: potential utility in treatment of diabetes and heart disease. Pharmacol Ther 119:291-310
28. **Hopkins AL, Groom CR** 2002 The druggable genome. Nat Rev Drug Discov 1:727-730
29. **Carmeci C, Thompson DA, Ring HZ, Francke U, Weigel RJ** 1997 Identification of a gene (GPR30) with homology to the G-protein-coupled receptor superfamily associated with estrogen receptor expression in breast cancer. Genomics 45:607-617
30. **O'Dowd BF, Nguyen T, Marchese A, Cheng R, Lynch KR, Heng HH, Kolakowski LF, Jr., George SR** 1998 Discovery of three novel G-protein-coupled receptor genes. Genomics 47:310-313
31. **Owman C, Blay P, Nilsson C, Lolait SJ** 1996 Cloning of human cDNA encoding a novel heptahelix receptor expressed in Burkitt's lymphoma and widely distributed in brain and peripheral tissues. Biochem Biophys Res Commun 228:285-292
32. **Takada Y, Kato C, Kondo S, Korenaga R, Ando J** 1997 Cloning of cDNAs encoding G protein-coupled receptor expressed in human endothelial cells exposed to fluid shear stress. Biochem Biophys Res Commun 240:737-741
33. **Filardo E, Quinn J, Pang Y, Graeber C, Shaw S, Dong J, Thomas P** 2007 Activation of the novel estrogen receptor G protein-coupled receptor 30 (GPR30) at the plasma membrane. Endocrinology 148:3236-3245
34. **Revankar CM, Cimino DF, Sklar LA, Arterburn JB, Prossnitz ER** 2005 A transmembrane intracellular estrogen receptor mediates rapid cell signaling. Science 307:1625-1630
35. **Joost P, Methner A** 2002 Phylogenetic analysis of 277 human G-protein-coupled receptors as a tool for the prediction of orphan receptor ligands. Genome Biol 3:RESEARCH0063
36. **Filardo EJ** 2002 Epidermal growth factor receptor (EGFR) transactivation by estrogen via the G-protein-coupled receptor, GPR30: a novel signaling pathway with potential significance for breast cancer. J Steroid Biochem Mol Biol 80:231-238
37. **Filardo EJ, Quinn JA, Bland KI, Frackelton AR, Jr.** 2000 Estrogen-induced activation of Erk-1 and Erk-2 requires the G protein-coupled receptor homolog, GPR30, and occurs via trans-activation of the epidermal growth factor receptor through release of HB-EGF. Mol Endocrinol 14:1649-1660
38. **Razandi M, Pedram A, Park ST, Levin ER** 2003 Proximal events in signaling by plasma membrane estrogen receptors. J Biol Chem 278:2701-2712
39. **Kanda N, Watanabe S** 2003 17beta-estradiol inhibits oxidative stress-induced apoptosis in keratinocytes by promoting Bcl-2 expression. J Invest Dermatol 121:1500-1509
40. **Kanda N, Watanabe S** 2004 17beta-estradiol enhances the production of granulocyte-macrophage colony-stimulating factor in human keratinocytes. J Invest Dermatol 123:329-337
41. **Maggiolini M, Vivacqua A, Fasanella G, Recchia AG, Sisci D, Pezzi V, Montanaro D, Musti AM, Picard D, Ando S** 2004 The G protein-coupled receptor GPR30 mediates c-fos up-regulation by 17beta-estradiol and phytoestrogens in breast cancer cells. J Biol Chem 279:27008-27016
42. **Vivacqua A, Bonofiglio D, Albanito L, Madeo A, Rago V, Carpino A, Musti AM, Picard D, Ando S, Maggiolini M** 2006 17beta-estradiol, genistein, and 4-hydroxytamoxifen induce the proliferation of thyroid cancer cells through the g protein-coupled receptor GPR30. Mol Pharmacol 70:1414-1423
43. **Vivacqua A, Bonofiglio D, Recchia AG, Musti AM, Picard D, Ando S, Maggiolini M** 2006 The G protein-coupled receptor GPR30 mediates the proliferative effects induced by 17beta-estradiol and hydroxytamoxifen in endometrial cancer cells. Mol Endocrinol 20:631-646
44. **Levin ER** 2009 G protein-coupled receptor 30: estrogen receptor or collaborator? Endocrinology 150:1563-1565
45. **Otto C, Fuchs I, Kauselmann G, Kern H, Zevnik B, Andreasen P, Schwarz G, Altmann H, Klewer M, Schoor M, Vonk R, Fritzemeier KH** 2009 GPR30 does not mediate estrogenic responses in reproductive organs in mice. Biol Reprod 80:34-41
46. **Pedram A, Razandi M, Levin ER** 2006 Nature of functional estrogen receptors at the plasma membrane. Mol Endocrinol 20:1996-2009
47. **Madak-Erdogan Z, Kieser KJ, Kim SH, Komm B, Katzenellenbogen JA, Katzenellenbogen BS** 2008 Nuclear and extranuclear pathway inputs in the regulation of global gene expression by estrogen receptors. Mol Endocrinol 22:2116-2127
48. **Sukocheva O, Wadham C, Holmes A, Albanese N, Verrier E, Feng F, Bernal A, Derian CK, Ullrich A, Vadas MA, Xia P** 2006 Estrogen transactivates EGFR via the sphingosine 1-phosphate receptor Edg-3: the role of sphingosine kinase-1. J Cell Biol 173:301-310
49. **Albanito L, Madeo A, Lappano R, Vivacqua A, Rago V, Carpino A, Oprea TI, Prossnitz ER, Musti AM, Ando S, Maggiolini M** 2007 G protein-coupled receptor 30 (GPR30) mediates gene

expression changes and growth response to 17beta-estradiol and selective GPR30 ligand G-1 in ovarian cancer cells. Cancer Res 67:1859-1866

50. **Kleuser B, Malek D, Gust R, Pertz HH, Potteck H** 2008 17-Beta-estradiol inhibits transforming growth factor-beta signaling and function in breast cancer cells via activation of extracellular signal-regulated kinase through the G protein-coupled receptor 30. Mol Pharmacol 74:1533-1543
51. **Otto C, Rohde-Schulz B, Schwarz G, Fuchs I, Klewer M, Brittain D, Langer G, Bader B, Prelle K, Nubbemeyer R, Fritzemeier KH** 2008 G protein-coupled receptor 30 localizes to the endoplasmic reticulum and is not activated by estradiol. Endocrinology 149:4846-4856
52. **Gobeil F, Fortier A, Zhu T, Bossolasco M, Leduc M, Grandbois M, Heveker N, Bkaily G, Chemtob S, Barbaz D** 2006 G-protein-coupled receptors signalling at the cell nucleus: an emerging paradigm. Can J Physiol Pharmacol 84:287-297
53. **Funakoshi T, Yanai A, Shinoda K, Kawano MM, Mizukami Y** 2006 G protein-coupled receptor 30 is an estrogen receptor in the plasma membrane. Biochem Biophys Res Commun 346:904-910
54. **Thomas P, Pang Y, Filardo EJ, Dong J** 2005 Identity of an estrogen membrane receptor coupled to a G protein in human breast cancer cells. Endocrinology 146:624-632
55. **Hamza A, Sarma MH, Sarma RH** 2003 Plausible interaction of an alpha-fetoprotein cyclopeptide with the G-protein-coupled receptor model GPR30: docking study by molecular dynamics simulated annealing. J Biomol Struct Dyn 20:751-758
56. **Bologa CG, Revankar CM, Young SM, Edwards BS, Arterburn JB, Kiselyov AS, Parker MA, Tkachenko SE, Savchuck NP, Sklar LA, Oprea TI, Prossnitz ER** 2006 Virtual and biomolecular screening converge on a selective agonist for GPR30. Nat Chem Biol 2:207-212
57. **Dennis MK, Burai R, Ramesh C, Petrie WK, Alcon SN, Nayak TK, Bologa CG, Leitao A, Brailoiu E, Deliu E, Dun NJ, Sklar LA, Hathaway HJ, Arterburn JB, Oprea TI, Prossnitz ER** 2009 In vivo effects of a GPR30 antagonist. Nat Chem Biol 5:421-427
58. **Rieck GC, Freites ON, Williams S** 2005 Is tamoxifen associated with high-risk endometrial carcinomas? A retrospective case series of 196 women with endometrial cancer. J Obstet Gynaecol 25:39-41
59. **Senkus-Konefka E, Konefka T, Jassem J** 2004 The effects of tamoxifen on the female genital tract. Cancer Treat Rev 30:291-301
60. **Isensee J, Meoli L, Zazzu V, Nabzdyk C, Witt H, Soewarto D, Effertz K, Fuchs H, Gailus-Durner V, Busch D, Adler T, de Angelis MH, Irgang M, Otto C, Noppinger PR** 2009 Expression pattern of G protein-coupled receptor 30 in LacZ reporter mice. Endocrinology 150:1722-1730
61. **Martensson UE, Salehi SA, Windahl S, Gomez MF, Sward K, Daszkiewicz-Nilsson J, Wendt A, Andersson N, Hellstrand P, Grande PO, Owman C, Rosen CJ, Adamo ML, Lundquist I, Rorsman P, Nilsson BO, Ohlsson C, Olde B, Leeb-Lundberg LM** 2009 Deletion of the G protein-coupled receptor 30 impairs glucose tolerance, reduces bone growth, increases blood pressure, and eliminates estradiol-stimulated insulin release in female mice. Endocrinology 150:687-698
62. **Wang C, Dehghani B, Magrisso IJ, Rick EA, Bonhomme E, Cody DB, Elenich LA, Subramanian S, Murphy SJ, Kelly MJ, Rosenbaum JS, Vandenbark AA, Offner H** 2008 GPR30 contributes to estrogen-induced thymic atrophy. Mol Endocrinol 22:636-648
63. **Hsieh YC, Yu HP, Frink M, Suzuki T, Choudhry MA, Schwacha MG, Chaudry IH** 2007 G protein-coupled receptor 30-dependent protein kinase A pathway is critical in nongenomic effects of estrogen in attenuating liver injury after trauma-hemorrhage. Am J Pathol 170:1210-1218
64. **Kimura M, Mizukami Y, Miura T, Fujimoto K, Kobayashi S, Matsuzaki M** 2001 Orphan G protein-coupled receptor, GPR41, induces apoptosis via a p53/Bax pathway during ischemic hypoxia and reoxygenation. J Biol Chem 276:26453-26460
65. **Wang C, Prossnitz ER, Roy SK** 2008 G protein-coupled receptor 30 expression is required for estrogen stimulation of primordial follicle formation in the hamster ovary. Endocrinology 149:4452-4461
66. **Das SK, Tan J, Raja S, Halder J, Paria BC, Dey SK** 2000 Estrogen targets genes involved in protein processing, calcium homeostasis, and Wnt signaling in the mouse uterus independent of estrogen receptor-alpha and -beta. J Biol Chem 275:28834-28842
67. **Hou X, Tan Y, Li M, Dey SK, Das SK** 2004 Canonical Wnt signaling is critical to estrogen-mediated uterine growth. Mol Endocrinol 18:3035-3049
68. **Haas E, Bhattacharya I, Brailoiu E, Damjanovic M, Brailoiu GC, Gao X, Mueller-Guerre L, Marjon NA, Gut A, Minotti R, Meyer MR, Amann K, Ammann E, Perez-Dominguez A, Genoni M, Clegg DJ, Dun NJ, Resta TC, Prossnitz ER, Barton M** 2009 Regulatory role of G protein-coupled estrogen receptor for vascular function and obesity. Circ Res 104:288-291
69. **Wang C, Dehghani B, Li Y, Kaler LJ, Proctor T, Vandenbark AA, Offner H** 2009 Membrane estrogen receptor regulates experimental autoimmune encephalomyelitis through up-regulation of programmed death 1. J Immunol 182:3294-3303

70. **Morales LB, Loo KK, Liu HB, Peterson C, Tiwari-Woodruff S, Voskuhl RR** 2006 Treatment with an estrogen receptor alpha ligand is neuroprotective in experimental autoimmune encephalomyelitis. J Neurosci 26:6823-6833
71. **Sicotte NL, Liva SM, Klutch R, Pfeiffer P, Bouvier S, Odesa S, Wu TC, Voskuhl RR** 2002 Treatment of multiple sclerosis with the pregnancy hormone estriol. Ann Neurol 52:421-428
72. **Soldan SS, Alvarez Retuerto AI, Sicotte NL, Voskuhl RR** 2003 Immune modulation in multiple sclerosis patients treated with the pregnancy hormone estriol. J Immunol 171:6267-6274
73. **Lu CL, Hsieh JC, Dun NJ, Oprea TI, Wang PS, Luo JC, Lin HC, Chang FY, Lee SD** 2009 Estrogen rapidly modulates 5-hydroxytrytophan-induced visceral hypersensitivity via GPR30 in rats. Gastroenterology
74. **Kuhn J, Dina OA, Goswami C, Suckow V, Levine JD, Hucho T** 2008 Estrogen Gpr30 estrogen receptors agonists induce mechanical hyperalgesia in the rat: Eur J Neurosci 27:1700-1709
75. **Jaenisch R** 1977 Germ line integration of moloney leukemia virus: effect of homozygosity at the m-mulV locus. Cell 12:691-696
76. **Jaenisch R, Mintz B** 1974 Simian virus 40 DNA sequences in DNA of healthy adult mice derived from preimplantation blastocysts injected with viral DNA. Proc Natl Acad Sci U S A 71:1250-1254
77. **Gordon JW, Scangos GA, Plotkin DJ, Barbosa JA, Ruddle FH** 1980 Genetic transformation of mouse embryos by microinjection of purified DNA. Proc Natl Acad Sci U S A 77:7380-7384
78. **Giraldo P, Montoliu L** 2001 Size matters: use of YACs, BACs and PACs in transgenic animals. Transgenic Res 10:83-103
79. **Porret A, Merillat AM, Guichard S, Beermann F, Hummler E** 2006 Tissue-specific transgenic and knockout mice. Methods Mol Biol 337:185-205
80. **Lo CW** 1986 Localization of low abundance DNA sequences in tissue sections by in situ hybridization. J Cell Sci 81:143-162
81. **Muller U** 1999 Ten years of gene targeting: targeted mouse mutants, from vector design to phenotype analysis. Mech Dev 82:3-21
82. **Pfeifer A** 2004 Lentiviral transgenesis. Transgenic Res 13:513-522
83. **Evans MJ, Kaufman MH** 1981 Establishment in culture of pluripotential cells from mouse embryos. Nature 292:154-156
84. **Martin GR** 1981 Isolation of a pluripotent cell line from early mouse embryos cultured in medium conditioned by teratocarcinoma stem cells. Proc Natl Acad Sci U S A 78:7634-7638
85. **Kawase E, Suemori H, Takahashi N, Okazaki K, Hashimoto K, Nakatsuji N** 1994 Strain difference in establishment of mouse embryonic stem (ES) cell lines. Int J Dev Biol 38:385-390
86. **Doetschman T, Gregg RG, Maeda N, Hooper ML, Melton DW, Thompson S, Smithies O** 1987 Targetted correction of a mutant HPRT gene in mouse embryonic stem cells. Nature 330:576-578
87. **Thomas KR, Capecchi MR** 1987 Site-directed mutagenesis by gene targeting in mouse embryo-derived stem cells. Cell 51:503-512
88. **Mansour SL, Thomas KR, Capecchi MR** 1988 Disruption of the proto-oncogene int-2 in mouse embryo-derived stem cells: a general strategy for targeting mutations to non-selectable genes. Nature 336:348-352
89. **Schwartzberg PL, Goff SP, Robertson EJ** 1989 Germ-line transmission of a c-abl mutation produced by targeted gene disruption in ES cells. Science 246:799-803
90. **Thompson S, Clarke AR, Pow AM, Hooper ML, Melton DW** 1989 Germ line transmission and expression of a corrected HPRT gene produced by gene targeting in embryonic stem cells. Cell 56:313-321
91. **Ramirez-Solis R, Liu P, Bradley A** 1995 Chromosome engineering in mice. Nature 378:720-724
92. **Santerre RF, Allen NE, Hobbs JN, Jr., Rao RN, Schmidt RJ** 1984 Expression of prokaryotic genes for hygromycin B and G418 resistance as dominant-selection markers in mouse L cells. Gene 30:147-156
93. **von Melchner H, DeGregori JV, Rayburn H, Reddy S, Friedel C, Ruley HE** 1992 Selective disruption of genes expressed in totipotent embryonal stem cells. Genes Dev 6:919-927
94. **Yagi T, Ikawa Y, Yoshida K, Shigetani Y, Takeda N, Mabuchi I, Yamamoto T, Aizawa S** 1990 Homologous recombination at c-fyn locus of mouse embryonic stem cells with use of diphtheria toxin A-fragment gene in negative selection. Proc Natl Acad Sci U S A 87:9918-9922
95. **Donehower LA, Harvey M, Vogel H, McArthur MJ, Montgomery CA, Jr., Park SH, Thompson T, Ford RJ, Bradley A** 1995 Effects of genetic background on tumorigenesis in p53-deficient mice. Mol Carcinog 14:16-22
96. **Hasty P, Rivera-Perez J, Bradley A** 1991 The length of homology required for gene targeting in embryonic stem cells. Mol Cell Biol 11:5586-5591
97. **Deng C, Capecchi MR** 1992 Reexamination of gene targeting frequency as a function of the extent of homology between the targeting vector and the target locus. Mol Cell Biol 12:3365-3371

98. **Friedrich G, Soriano P** 1991 Promoter traps in embryonic stem cells: a genetic screen to identify and mutate developmental genes in mice. Genes Dev 5:1513-1523
99. **Crawley JN** 2000 What´s wrong with my mouse? Behavioural phenotyping of transgenic and knockout mice. Wiley-Liss. New York
100. **Askew GR, Doetschman T, Lingrel JB** 1993 Site-directed point mutations in embryonic stem cells: a gene-targeting tag-and-exchange strategy. Mol Cell Biol 13:4115-4124
101. **Stacey A, Schnieke A, McWhir J, Cooper J, Colman A, Melton DW** 1994 Use of double-replacement gene targeting to replace the murine alpha-lactalbumin gene with its human counterpart in embryonic stem cells and mice. Mol Cell Biol 14:1009-1016
102. **Lathe R** 1996 Mice, gene targeting and behaviour: more than just genetic background. Trends Neurosci 19:183-186; discussion 188-189
103. **Erickson RP** 1996 Mouse models of human genetic disease: which mouse is more like a man? Bioessays 18:993-998
104. **Crawley JN, Belknap JK, Collins A, Crabbe JC, Frankel W, Henderson N, Hitzemann RJ, Maxson SC, Miner LL, Silva AJ, Wehner JM, Wynshaw-Boris A, Paylor R** 1997 Behavioral phenotypes of inbred mouse strains: implications and recommendations for molecular studies. Psychopharmacology (Berl) 132:107-124
105. **Dymecki SM** 1996 Flp recombinase promotes site-specific DNA recombination in embryonic stem cells and transgenic mice. Proc Natl Acad Sci U S A 93:6191-6196
106. **Meyers EN, Lewandoski M, Martin GR** 1998 An Fgf8 mutant allelic series generated by Cre- and Flp-mediated recombination. Nat Genet 18:136-141
107. **Gu H, Marth JD, Orban PC, Mossmann H, Rajewsky K** 1994 Deletion of a DNA polymerase beta gene segment in T cells using cell type-specific gene targeting. Science 265:103-106
108. **Metzger D, Clifford J, Chiba H, Chambon P** 1995 Conditional site-specific recombination in mammalian cells using a ligand-dependent chimeric Cre recombinase. Proc Natl Acad Sci U S A 92:6991-6995
109. **Schonig K, Schwenk F, Rajewsky K, Bujard H** 2002 Stringent doxycycline dependent control of CRE recombinase in vivo. Nucleic Acids Res 30:e134
110. **Matsuda I, Aiba A** 2004 Receptor knock-out and knock-in strategies. Methods Mol Biol 259:379-390
111. **Rohrer DK, Kobilka BK** 1998 G protein-coupled receptors: functional and mechanistic insights through altered gene expression. Physiol Rev 78:35-52
112. **Karasinska JM, George SR, O'Dowd BF** 2003 Family 1 G protein-coupled receptor function in the CNS. Insights from gene knockout mice. Brain Res Brain Res Rev 41:125-152
113. **Frendeus B, Godaly G, Hang L, Karpman D, Lundstedt AC, Svanborg C** 2000 Interleukin 8 receptor deficiency confers susceptibility to acute experimental pyelonephritis and may have a human counterpart. J Exp Med 192:881-890
114. **Hang L, Frendeus B, Godaly G, Svanborg C** 2000 Interleukin-8 receptor knockout mice have subepithelial neutrophil entrapment and renal scarring following acute pyelonephritis. J Infect Dis 182:1738-1748
115. **Conquet F, Bashir ZI, Davies CH, Daniel H, Ferraguti F, Bordi F, Franz-Bacon K, Reggiani A, Matarese V, Conde F, et al.** 1994 Motor deficit and impairment of synaptic plasticity in mice lacking mGluR1. Nature 372:237-243
116. **Matsusaka T, Nishimura H, Utsunomiya H, Kakuchi J, Niimura F, Inagami T, Fogo A, Ichikawa I** 1996 Chimeric mice carrying 'regional' targeted deletion of the angiotensin type 1A receptor gene. Evidence against the role for local angiotensin in the in vivo feedback regulation of renin synthesis in juxtaglomerular cells. J Clin Invest 98:1867-1877
117. **Sugaya T, Nishimatsu S, Tanimoto K, Takimoto E, Yamagishi T, Imamura K, Goto S, Imaizumi K, Hisada Y, Otsuka A, et al.** 1995 Angiotensin II type 1a receptor-deficient mice with hypotension and hyperreninemia. J Biol Chem 270:18719-18722
118. **Zambrowicz BP, Sands AT** 2003 Knockouts model the 100 best-selling drugs-will they model the next 100? Nat Rev Drug Discov 2:38-51
119. **Hoit BD** 2004 Murine physiology: measuring the phenotype. J Mol Cell Cardiol 37:377-387
120. **German Mouse Clinicn** 2008 Report for Gpr30-T181 Deltagen mice. Helmotz Zentrum, Deutsches Forshung Centrum für Gesundheit und Umwelt, Institut für Experimentelle Genetik. München
121. **Kautzky-Willer A, Handisurya A** 2009 Metabolic diseases and associated complications: sex and gender matter! Eur J Clin Invest
122. **Auryan S, Itamar R** 2008 Gender-specific care of diabetes mellitus: particular considerations in the management of diabetic women. Diabetes Obes Metab 10:1135-1156
123. **Ding EL, Song Y, Malik VS, Liu S** 2006 Sex differences of endogenous sex hormones and risk of type 2 diabetes: a systematic review and meta-analysis. JAMA 295:1288-1299

124. **Regitz-Zagrosek V, Lehmkuhl E, Mahmoodzadeh S** 2007 Gender aspects of the role of the metabolic syndrome as a risk factor for cardiovascular disease. Gend Med 4:S162-177
125. **Heine PA, Taylor JA, Iwamoto GA, Lubahn DB, Cooke PS** 2000 Increased adipose tissue in male and female estrogen receptor-alpha knockout mice. Proc Natl Acad Sci U S A 97:12729-12734
126. **Ohlsson C, Hellberg N, Parini P, Vidal O, Bohlooly YM, Rudling M, Lindberg MK, Warner M, Angelin B, Gustafsson JA** 2000 Obesity and disturbed lipoprotein profile in estrogen receptor-alpha-deficient male mice. Biochem Biophys Res Commun 278:640-645
127. **Takeda K, Toda K, Saibara T, Nakagawa M, Saika K, Onishi T, Sugiura T, Shizuta Y** 2003 Progressive development of insulin resistance phenotype in male mice with complete aromatase (CYP19) deficiency. J Endocrinol 176:237-246
128. **Barros RP, Machado UF, Warner M, Gustafsson JA** 2006 Muscle GLUT4 regulation by estrogen receptors ERbeta and ERalpha. Proc Natl Acad Sci U S A 103:1605-1608
129. **Ropero AB, Alonso-Magdalena P, Quesada I, Nadal A** 2008 The role of estrogen receptors in the control of energy and glucose homeostasis. Steroids 73:874-879
130. **Ding EL, Song Y, Manson JE, Rifai N, Buring JE, Liu S** 2007 Plasma sex steroid hormones and risk of developing type 2 diabetes in women: a prospective study. Diabetologia 50:2076-2084
131. **Alonso-Magdalena P, Morimoto S, Ripoll C, Fuentes E, Nadal A** 2006 The estrogenic effect of bisphenol A disrupts pancreatic beta-cell function in vivo and induces insulin resistance. Environ Health Perspect 114:106-112
132. **Ropero AB, Soria B, Nadal A** 2002 A nonclassical estrogen membrane receptor triggers rapid differential actions in the endocrine pancreas. Mol Endocrinol 16:497-505
133. **Valverde MA, Rojas P, Amigo J, Cosmelli D, Orio P, Bahamonde MI, Mann GE, Vergara C, Latorre R** 1999 Acute activation of Maxi-K channels (hSlo) by estradiol binding to the beta subunit. Science 285:1929-1931
134. **Pan WH, Cedres LB, Liu K, Dyer A, Schoenberger JA, Shekelle RB, Stamler R, Smith D, Collette P, Stamler J** 1986 Relationship of clinical diabetes and asymptomatic hyperglycemia to risk of coronary heart disease mortality in men and women. Am J Epidemiol 123:504-516
135. **Lundberg V, Stegmayr B, Asplund K, Eliasson M, Huhtasaari F** 1997 Diabetes as a risk factor for myocardial infarction: population and gender perspectives. J Intern Med 241:485-492
136. **Vaccarino V, Parsons L, Every NR, Barron HV, Krumholz HM** 1999 Sex-based differences in early mortality after myocardial infarction. National Registry of Myocardial Infarction 2 Participants. N Engl J Med 341:217-225
137. **Barrett-Connor E** 1997 Sex differences in coronary heart disease. Why are women so superior? The 1995 Ancel Keys Lecture. Circulation 95:252-264
138. **Mendelsohn ME, Karas RH** 1999 The protective effects of estrogen on the cardiovascular system. N Engl J Med 340:1801-1811
139. **Herrington DM, Howard TD, Hawkins GA, Reboussin DM, Xu J, Zheng SL, Brosnihan KB, Meyers DA, Bleecker ER** 2002 Estrogen-receptor polymorphisms and effects of estrogen replacement on high-density lipoprotein cholesterol in women with coronary disease. N Engl J Med 346:967-974
140. **Almeida S, Franken N, Zandona MR, Osorio-Wender MC, Hutz MH** 2005 Estrogen receptor 2 and progesterone receptor gene polymorphisms and lipid levels in women with different hormonal status. Pharmacogenomics J 5:30-34
141. **Bourassa PA, Milos PM, Gaynor BJ, Breslow JL, Aiello RJ** 1996 Estrogen reduces atherosclerotic lesion development in apolipoprotein E-deficient mice. Proc Natl Acad Sci U S A 93:10022-10027
142. **Couse JF, Korach KS** 1999 Estrogen receptor null mice: what have we learned and where will they lead us? Endocr Rev 20:358-417
143. **Zhang SH, Reddick RL, Piedrahita JA, Maeda N** 1992 Spontaneous hypercholesterolemia and arterial lesions in mice lacking apolipoprotein E. Science 258:468-471
144. **Haynes MP, Russell KS, Bender JR** 2000 Molecular mechanisms of estrogen actions on the vasculature. J Nucl Cardiol 7:500-508
145. **Simoncini T, Hafezi-Moghadam A, Brazil DP, Ley K, Chin WW, Liao JK** 2000 Interaction of oestrogen receptor with the regulatory subunit of phosphatidylinositol-3-OH kinase. Nature 407:538-541
146. **Stefano GB, Prevot V, Beauvillain JC, Cadet P, Fimiani C, Welters I, Fricchione GL, Breton C, Lassalle P, Salzet M, Bilfinger TV** 2000 Cell-surface estrogen receptors mediate calcium-dependent nitric oxide release in human endothelia. Circulation 101:1594-1597
147. **Surwit RS, Kuhn CM, Cochrane C, McCubbin JA, Feinglos MN** 1988 Diet-induced type II diabetes in C57BL/6J mice. Diabetes 37:1163-1167
148. **Speakman J, Hambly C, Mitchell S, Krol E** 2007 Animal models of obesity. Obes Rev 8 Suppl 1:55-61

149. **Nishikawa S, Yasoshima A, Doi K, Nakayama H, Uetsuka K** 2007 Involvement of sex, strain and age factors in high fat diet-induced obesity in C57BL/6J and BALB/cA mice. Exp Anim 56:263-272
150. **Winzell MS, Ahren B** 2004 The high-fat diet-fed mouse: a model for studying mechanisms and treatment of impaired glucose tolerance and type 2 diabetes. Diabetes 53 Suppl 3:S215-219
151. **Huang PL** 2009 A comprehensive definition for metabolic syndrome. Dis Model Mech 2:231-237
152. **Lembo G, Vecchione C, Iaccarino G, Trimarco B** 1996 The crosstalk between insulin and the sympathetic nervous system: possible implications in the pathogenesis of essential hypertension. Blood Press Suppl 1:38-42
153. **Sowers JR** 2003 Obesity as a cardiovascular risk factor. Am J Med 115 Suppl 8A:37S-41S
154. **Barouch LA, Berkowitz DE, Harrison RW, O'Donnell CP, Hare JM** 2003 Disruption of leptin signaling contributes to cardiac hypertrophy independently of body weight in mice. Circulation 108:754-759
155. **Carroll JF, Braden DS, Cockrell K, Mizelle HL** 1997 Obese hypertensive rabbits develop concentric and eccentric hypertrophy and diastolic filling abnormalities. Am J Hypertens 10:230-233
156. **Carroll JF, Dwyer TM, Grady AW, Reinhart GA, Montani JP, Cockrell K, Meydrech EF, Mizelle HL** 1996 Hypertension, cardiac hypertrophy, and neurohumoral activity in a new animal model of obesity. Am J Physiol 271:H373-378
157. **Carroll JF, Zenebe WJ, Strange TB** 2006 Cardiovascular function in a rat model of diet-induced obesity. Hypertension 48:65-72
158. **Okere IC, Chandler MP, McElfresh TA, Rennison JH, Sharov V, Sabbah HN, Tserng KY, Hoit BD, Ernsberger P, Young ME, Stanley WC** 2006 Differential effects of saturated and unsaturated fatty acid diets on cardiomyocyte apoptosis, adipose distribution, and serum leptin. Am J Physiol Heart Circ Physiol 291:H38-44
159. **Ouwens DM, Boer C, Fodor M, de Galan P, Heine RJ, Maassen JA, Diamant M** 2005 Cardiac dysfunction induced by high-fat diet is associated with altered myocardial insulin signalling in rats. Diabetologia 48:1229-1237
160. **Park SY, Cho YR, Kim HJ, Higashimori T, Danton C, Lee MK, Dey A, Rothermel B, Kim YB, Kalinowski A, Russell KS, Kim JK** 2005 Unraveling the temporal pattern of diet-induced insulin resistance in individual organs and cardiac dysfunction in C57BL/6 mice. Diabetes 54:3530-3540
161. **de Angelis MH, Chambon P, Brown S** 2006 Standards of mouse phenotyping. WILEY-VCH ed. Weinheim
162. **Rogers DC, Fisher EM, Brown SD, Peters J, Hunter AJ, Martin JE** 1997 Behavioral and functional analysis of mouse phenotype: SHIRPA, a proposed protocol for comprehensive phenotype assessment. Mamm Genome 8:711-713
163. **Tinsley FC, Taicher GZ, Heiman ML** 2004 Evaluation of a quantitative magnetic resonance method for mouse whole body composition analysis. Obes Res 12:150-160
164. **Schittmayer M, Birner-Gruenberger R** 2009 Functional proteomics in lipid research: Lipases, lipid droplets and lipoproteins. J Proteomics
165. **Collins KA, Korcarz CE, Lang RM** 2003 Use of echocardiography for the phenotypic assessment of genetically altered mice. Physiol Genomics 13:227-239
166. **Collins KA, Korcarz CE, Shroff SG, Bednarz JE, Fentzke RC, Lin H, Leiden JM, Lang RM** 2001 Accuracy of echocardiographic estimates of left ventricular mass in mice. Am J Physiol Heart Circ Physiol 280:H1954-1962
167. **Hoit BD, Khoury SF, Kranias EG, Ball N, Walsh RA** 1995 In vivo echocardiographic detection of enhanced left ventricular function in gene-targeted mice with phospholamban deficiency. Circ Res 77:632-637
168. **Liao Y, Ishikura F, Beppu S, Asakura M, Takashima S, Asanuma H, Sanada S, Kim J, Ogita H, Kuzuya T, Node K, Kitakaze M, Hori M** 2002 Echocardiographic assessment of LV hypertrophy and function in aortic-banded mice: necropsy validation. Am J Physiol Heart Circ Physiol 282:H1703-1708
169. **Pollick C, Hale SL, Kloner RA** 1995 Echocardiographic and cardiac Doppler assessment of mice. J Am Soc Echocardiogr 8:602-610
170. **Tanaka N, Dalton N, Mao L, Rockman HA, Peterson KL, Gottshall KR, Hunter JJ, Chien KR, Ross J, Jr.** 1996 Transthoracic echocardiography in models of cardiac disease in the mouse. Circulation 94:1109-1117
171. **Yang XP, Liu YH, Rhaleb NE, Kurihara N, Kim HE, Carretero OA** 1999 Echocardiographic assessment of cardiac function in conscious and anesthetized mice. Am J Physiol 277:H1967-1974
172. **Scherrer-Crosbie M, Steudel W, Hunziker PR, Liel-Cohen N, Ullrich R, Zapol WM, Picard MH** 1999 Three-dimensional echocardiographic assessment of left ventricular wall motion abnormalities in mouse myocardial infarction. J Am Soc Echocardiogr 12:834-840

173. **Zhou YQ, Foster FS, Nieman BJ, Davidson L, Chen XJ, Henkelman RM** 2004 Comprehensive transthoracic cardiac imaging in mice using ultrasound biomicroscopy with anatomical confirmation by magnetic resonance imaging. Physiol Genomics 18:232-244
174. **Arras M, Autenried P, Rettich A, Spaeni D, Rulicke T** 2001 Optimization of intraperitoneal injection anesthesia in mice: drugs, dosages, adverse effects, and anesthesia depth. Comp Med 51:443-456
175. **Scherrer-Crosbie M, Steudel W, Hunziker PR, Foster GP, Garrido L, Liel-Cohen N, Zapol WM, Picard MH** 1998 Determination of right ventricular structure and function in normoxic and hypoxic mice: a transesophageal echocardiographic study. Circulation 98:1015-1021
176. **Edwards DP** 2005 Regulation of signal transduction pathways by estrogen and progesterone. Annu Rev Physiol 67:335-376
177. **Sambrook, Russel** 2001 Molecular cloning: a laboratory manual. Cold Spring Harbor laboratory press
178. **Vandesompele J, De Preter K, Pattyn F, Poppe B, Van Roy N, De Paepe A, Speleman F** 2002 Accurate normalization of real-time quantitative RT-PCR data by geometric averaging of multiple internal control genes. Genome Biol 3:RESEARCH0034
179. **Hegde P, Qi R, Abernathy K, Gay C, Dharap S, Gaspard R, Hughes JE, Snesrud E, Lee N, Quackenbush J** 2000 A concise guide to cDNA microarray analysis. Biotechniques 29:548-550, 552-554, 556 passim
180. **AppliedBiosystems** Guide to performing relative quantitation of gene expression using Real Time Quantitative PCR: Applied Biosystems
181. **Vollmar AM, Lang RE, Hanze J, Schulz R** 1990 The rat thymus-a site of atrial natriuretic peptide synthesis. Peptides 11:33-37
182. **Maggiolini M, Picard D** 2009 The unfolding stories of GPR30, a new membrane-bound estrogen receptor. J Endocrinol
183. **Pham CT, MacIvor DM, Hug BA, Heusel JW, Ley TJ** 1996 Long-range disruption of gene expression by a selectable marker cassette. Proc Natl Acad Sci U S A 93:13090-13095
184. **Langer G, Bader B, Meoli L, Isensee J, Delbeck M, Noppinger PR, Otto C** 2009 A critical review of fundamental controversies in the field of GPR30 research. Steroids
185. **Blais ME, Brochu S, Giroux M, Belanger MP, Dulude G, Sekaly RP, Perreault C** 2008 Why T cells of thymic versus extrathymic origin are functionally different. J Immunol 180:2299-2312
186. **Samson WK** 1992 Natriuretic peptides A family of hormones. Trends Endocrinol Metab 3:86-90
187. **Nishikimi T, Maeda N, Matsuoka H** 2006 The role of natriuretic peptides in cardioprotection. Cardiovasc Res 69:318-328
188. **Vollmar AM** 1997 Influence of atrial natriuretic peptide on thymocyte development in fetal thymic organ culture. J Neuroimmunol 78:90-96
189. **Vollmar AM, Schmidt KN, Schulz R** 1996 Natriuretic peptide receptors on rat thymocytes: inhibition of proliferation by atrial natriuretic peptide. Endocrinology 137:1706-1713
190. **Vollmar AM, Schulz R** 1988 Evidence for the presence of ANP-precursor material in the rat thymus. Biochem Biophys Res Commun 155:700-708
191. **Deng H, Liu R, Ellmeier W, Choe S, Unutmaz D, Burkhart M, Di Marzio P, Marmon S, Sutton RE, Hill CM, Davis CB, Peiper SC, Schall TJ, Littman DR, Landau NR** 1996 Identification of a major co-receptor for primary isolates of HIV-1. Nature 381:661-666
192. **Liu R, Paxton WA, Choe S, Ceradini D, Martin SR, Horuk R, MacDonald ME, Stuhlmann H, Koup RA, Landau NR** 1996 Homozygous defect in HIV-1 coreceptor accounts for resistance of some multiply-exposed individuals to HIV-1 infection. Cell 86:367-377
193. **Floto RA, MacAry PA, Boname JM, Mien TS, Kampmann B, Hair JR, Huey OS, Houben EN, Pieters J, Day C, Oehlmann W, Singh M, Smith KG, Lehner PJ** 2006 Dendritic cell stimulation by mycobacterial Hsp70 is mediated through CCR5. Science 314:454-458
194. **Liu J, Albers MW, Wandless TJ, Luan S, Alberg DG, Belshaw PJ, Cohen P, MacKintosh C, Klee CB, Schreiber SL** 1992 Inhibition of T cell signaling by immunophilin-ligand complexes correlates with loss of calcineurin phosphatase activity. Biochemistry 31:3896-3901
195. **MacLennan DH, Brandl CJ, Korczak B, Green NM** 1985 Amino-acid sequence of a Ca2+ + Mg2+-dependent ATPase from rabbit muscle sarcoplasmic reticulum, deduced from its complementary DNA sequence. Nature 316:696-700
196. **Saggioro D, Silic-Benussi M, Biasiotto R, D'Agostino DM, Ciminale V** 2009 Control of cell death pathways by HTLV-1 proteins. Front Biosci 14:3338-3351
197. **Bai J, Rodriguez AM, Melendez JA, Cederbaum AI** 1999 Overexpression of catalase in cytosolic or mitochondrial compartment protects HepG2 cells against oxidative injury. J Biol Chem 274:26217-26224
198. **Sandstrom PA, Buttke TM** 1993 Autocrine production of extracellular catalase prevents apoptosis of the human CEM T-cell line in serum-free medium. Proc Natl Acad Sci U S A 90:4708-4712

199. **Tome ME, Baker AF, Powis G, Payne CM, Briehl MM** 2001 Catalase-overexpressing thymocytes are resistant to glucocorticoid-induced apoptosis and exhibit increased net tumor growth. Cancer Res 61:2766-2773
200. **Pratt JA** 1992 The neuroanatomical basis of anxiety. Pharmacol Ther 55:149-181
201. **Cunha TM, Peterson RG, Gobbett TA** 2005 Differing sources of dietary fat alter the character of metabolic syndrome induced in the C75BL/6 mouse. Purina Mills Test Diet study
202. **Vincelette J, Martin-McNulty B, Vergona R, Sullivan ME, Wang YX** 2006 Reduced cardiac functional reserve in apolipoprotein E knockout mice. Transl Res 148:30-36
203. **Kwiterovich PO, Jr.** 2000 The metabolic pathways of high-density lipoprotein, low-density lipoprotein, and triglycerides: a current review. Am J Cardiol 86:5L-10L
204. **Hachem SB, Mooradian AD** 2006 Familial dyslipidaemias: an overview of genetics, pathophysiology and management. Drugs 66:1949-1969
205. **Castle CK, Colca JR, Melchior GW** 1993 Lipoprotein profile characterization of the KKA(y) mouse, a rodent model of type II diabetes, before and after treatment with the insulin-sensitizing agent pioglitazone. Arterioscler Thromb 13:302-309
206. **Subah Packer C** 2007 Estrogen protection, oxidized LDL, endothelial dysfunction and vasorelaxation in cardiovascular disease: New insights into a complex issue. Cardiovasc Res 73:6-7
207. **Wallimann T, Wyss M, Brdiczka D, Nicolay K, Eppenberger HM** 1992 Intracellular compartmentation, structure and function of creatine kinase isoenzymes in tissues with high and fluctuating energy demands: the 'phosphocreatine circuit' for cellular energy homeostasis. Biochem J 281 (Pt 1):21-40
208. **Amin KA, Nagy MA** 2009 Effect of Carnitine and herbal mixture extract on obesity induced by high fat diet in rats. Diabetol Metab Syndr 1:17
209. **Helge JW, Fraser AM, Kriketos AD, Jenkins AB, Calvert GD, Ayre KJ, Storlien LH** 1999 Interrelationships between muscle fibre type, substrate oxidation and body fat. Int J Obes Relat Metab Disord 23:986-991
210. **Hickey MS, Carey JO, Azevedo JL, Houmard JA, Pories WJ, Israel RG, Dohm GL** 1995 Skeletal muscle fiber composition is related to adiposity and in vitro glucose transport rate in humans. Am J Physiol 268:E453-457
211. **Janssen E, Terzic A, Wieringa B, Dzeja PP** 2003 Impaired intracellular energetic communication in muscles from creatine kinase and adenylate kinase (M-CK/AK1) double knock-out mice. J Biol Chem 278:30441-30449
212. **Ahmed K, Tunaru S, Langhans CD, Hanson J, Michalski CW, Kolker S, Jones PM, Okun JG, Offermanns S** 2009 Deorphanization of GPR109B as a receptor for the beta-oxidation intermediate 3-OH-octanoic acid and its role in the regulation of lipolysis. J Biol Chem 284:21928-21933
213. **Bell MA, Scarrow WG** 1984 Staining for microvascular alkaline phosphatase in thick celloidin sections of nervous tissue: morphometric and pathological applications. Microvasc Res 27:189-203
214. **Anstrom JA, Thore CR, Moody DM, Brown WR** 2007 Immunolocalization of tight junction proteins in blood vessels in human germinal matrix and cortex. Histochem Cell Biol 127:205-213
215. **MPD** Mouse Phenome Database-Blood Chemistry. http://phenome.jax.org/pub-cgi/phenome/mpdcgi?rtn=docs/home
216. **Barros RP, Machado UF, Gustafsson JA** 2006 Estrogen receptors: new players in diabetes mellitus. Trends Mol Med 12:425-431
217. **Powell DR** 2006 Obesity drugs and their targets: correlation of mouse knockout phenotypes with drug effects in vivo. Obes Rev 7:89-108
218. **Ribas V, Nguyen MT, Henstridge DC, Nguyen AK, Beaven SW, Watt MJ, Hevener AL** 2009 Impaired Oxidative Metabolism and Inflammation are Associated with Insulin Resistance in ER alpha Deficient Mice. Am J Physiol Endocrinol Metab
219. **Walker VR, Korach KS** 2004 Estrogen receptor knockout mice as a model for endocrine research. Ilar J 45:455-461
220. **Windahl SH, Andersson N, Chagin AS, Martensson UE, Carlsten H, Olde B, Swanson C, Moverare-Skrtic S, Savendahl L, Lagerquist MK, Leeb-Lundberg LM, Ohlsson C** 2009 The role of the G protein-coupled receptor GPR30 in the effects of estrogen in ovariectomized mice. Am J Physiol Endocrinol Metab 296:E490-496
221. **Kurtz TW, Griffin KA, Bidani AK, Davisson RL, Hall JE** 2005 Recommendations for blood pressure measurement in humans and experimental animals: part 2: blood pressure measurement in experimental animals: a statement for professionals from the Subcommittee of Professional and Public Education of the American Heart Association Council on High Blood Pressure Research. Arterioscler Thromb Vasc Biol 25:e22-33
222. **Kolovou G, Anagnostopoulou K, Mikhailidis DP, Cokkinos DV** 2008 Apolipoprotein E knockout models. Curr Pharm Des 14:338-351

Table of Figures

Figure 1.1: GPCRs in pharmacology 6
Figure 1.2: Schema of a KO mouse generation 20
Figure 1.3: RT-PCR analysis (Deltagen) 24
Figure 3.1: Targeting vector used to generate Gpr30-T181 Deltagen mice. 38
Figure 3.2: Workflow at the German Mouse Clinic 48
Figure 3.3: Echocardiography in mice, mouse preparation 56
Figure 3.4: Echocardiography in mice, mouse orientation and its spatial relation with the transducer. 57
Figure 3.5: Echocardiography in mice, obtaining a left ventricle short axis view. 58
Figure 3.6: Echocardiography in mice, simplified schema of the mouse aortic arch. 59
Figure 3.7: Echocardiography in mice, left ventricle short axis view 60
Figure 3.8: Echocardiography in mice 61
Figure 3.9: Echocardiography in mice 62
Figure 3.10: Echocardiography in mice 63
Figure 3.11: Echocardiography in mice 63
Figure 3.12: ECG in mice 65
Figure 3.13: ECG recording over 1 minute: example of one R-R peaks distance. 65
Figure 4.1: Gpr30-T181 Deltagen mouse genotyping 68
Figure 4.2: Southern blotting 69
Figure 4.3: Real Time PCR quantification of the fusion transcripts 70
Figure 4.4: Gpr30 mRNA relative expression 71
Figure 4.5: SHG17 Artemis mice genotyping 72
Figure 4.6: Primary screen of Gpr30-T181 Deltagen mice. 76
Figure 4.7: HFD workflow. 80
Figure 4.8: Gpr30-T181 Deltagen mice, body weight (BW). 81
Figure 4.9: Gpr30-T181 mice, nuclear magnetic resonance (NMR) 82
Figure 4.10: Gpr30-T181 mice, intraperitoneal-glucose tolerance test (IPGTT) 83
Figure 4.11: Gpr30-T181 Deltagen mice intraperitoneal glucose tolerance test (IPGTT), area under the curve (AUC). 84
Figure 4.12: Gpr30-T181 Deltagen mice, echocardiography. 85
Figure 4.13: Blood chemistry of Gpr30-T181 Deltagen mice: cholesterol (Ch) levels 89
Figure 4.14: Blood chemistry of Gpr30-T181 Deltagen mice: high density lipoprotein (HDL) levels. 90
Figure 4.15: Blood chemistry of Gpr30-T181 Deltagen mice: creatine kinase (CK) levels 90
Figure 4.16: Blood chemistry of Gpr30-T181 Deltagen mice: alkaline phosphatase (AP) levels 91
Figure 4.17: SHG17 Artemis mice, body weight (BW). 94
Figure 4.18: SHG17 Artemis mice, nuclear magnetic resonance (NMR) 95
Figure 4.19: SHG17 Artemis mice, IPGTT 96

List of Tables

Table 1.1: Gpr30 *in vivo* function 12
Table 3.1: Primers 40
Table 3.2: Genotyping PCR reaction 41
Table 3.3: Reverse transcription 45
Table 3.4: Real-Time PCR 46
Table 3.5: Animal groups 52
Table 3.6: Rodents purified diets: nutritional profile 53
Table 3.7: Rodents purified diet: energetic profile 53
Table 3.8: Intraperitoneal Glucose Tolerance Test Matrix 55
Table 4.1: Immunology screen of Gpr30-T181 Deltagen mice 74
Table 4.2: Behavioural observations of Gpr30-T181 Deltagen mice 75
Table 4.3: Gene ontology annotation of deregulated genes in the thymus of Gpr30-T181$^{-/-}$ Deltagen mice 78
Table 4.4: Validation of microarray data 79
Table 4.5: Echocardiography of Gpr30-T181 Deltagen female mice 85
Table 4.6: Echocardiography of Gpr30-T181 Deltagen male mice 86
Table 4.7: Blood chemistry of Gpr30-T181 Deltagen female mice 87
Table 4.8: Blood chemistry of Gpr30-T181 Deltagen male mice 88
Table 4.9: Validation of microarray data 93
Table 4.10: Echocardiography of SHG17 mice 97
Table 5.1: Results summary 111

Acknowledgements

I want to thank all the people who supported and encouraged me in these nice and challenging PhD years spent at the CCR-sometimes difficult, never boring.

My first thanks go to Prof. Patricia Ruiz Noppinger for giving me the fantastic opportunity to make a PhD in her laboratory, in this wonderful town, Berlin! Thanks for all her precious teachings for always trusting in my work, and for being able like few others to transmit enthusiasm and motivation.

My thanks go also to Dr. Christiane Otto and the members of German Mouse Clinic for the fruitful collaboration.

I would like to thank all the colleagues and friends I met "on my way" in Prof. Ruiz Noppinger's lab for their professionalism and friendship: the "Gpr30er", Jörg and Valeria, for their precious support in sharing the same scientific "adventure" over these years; Henning ("Mr. Microarray") and Christoph for their invaluable help; Daniel, Ana and Markus for the fruitful discussions, and Jutta, Dian, Aydah, Beata, Carola and Carsta for the excellent technical assistance.

Thanks to the "mensa group" for the companionship and relaxing lunch break!

And of course a special thanks goes to Anne. Without her everything would have been much more difficult! Thanks for helping and supporting me, always so "*liebevoll*".
And thanks to my family despite being so far away I felt it always close to me. It is also thanks to my beloved parents, Antonio and Maria, and my siblings, Graziella and Rocco, that I was able to achieve such an important goal of my professional life.

The study was funded by the European Commission in the frame of Marie Curie Early Stage Research Training Programme "Cardiovasc" MEST-CT-2005-02026.

Eidesstattliche Erklärung

Hiermit versichere ich, dass ich die vorliegende Arbeit selbständig und nur unter Verwendung der angegebenen Hilfsmittel erarbeitet und verfasst habe. Diese Arbeit hat keiner anderen Prüfungsbehörde vorgelegen.

Berlin, den 15.04.2010

Luca Meoli

Publications

Comprehensive phenotyping of two mouse mutants reveals a potential novel role of G protein-coupled receptor 30
Meoli L, Isensee J, Zazzu V, Nabzdyk C, Soewarto D, Witt H, Otto C, Ruiz-Noppinger P
In preparation

A critical review of fundamental controversies in the field of Gpr30 research
Langer G, Bader B, **Meoli L**, Isensee J, Delbeck M, Ruiz-Noppinger P, Otto C
Steroids 2009

Expression pattern of G-protein coupled receptor 30 in LacZ reporter mice
Isensee J, **Meoli L**, Zazzu V, Nabzdyk C, Witt H, Soewarto D, Effertz K, Fuchs H, Gailus-Durner V, Busch D, Adler T, de Angelis MH, Irgang M, Otto C, Ruiz-Noppinger P
Endocrinology 2009

Abstracts

Deciphering the function of the G-protein Coupled Receptor 30
Isensee J, **Meoli L**, Zazzu V, Effertz K, Ruiz Noppinger P
XX international congress of genetics
12th-17th July 2008
Berlin, Germany

G Protein-Coupled Receptor 30 (Gpr30) mutant mice: towards an exhaustive phenotype analysis
Meoli L, Isensee J, Nabzdyk C, Zazzu V, Soewarto D, Ruiz Noppinger P
Keystone Symposium
18th May-23th May 2008
Killarney, Ireland

The estrogen receptor Gpr30: New insights in cardiovascular and metabolic diseases
Meoli L, Isensee J, Nabzdyk C, Soewarto D, Zazzu V, Ruiz-Noppinger P
12th Meeting of the European Council for Cardiovascular Research (ECCR)
12th-14th October 2007
La Colle sur Loup, Nice, France.

Towards Deciphering the Function of the G-Protein coupled receptor 30
Isensee J, Zazzu V, **Meoli L**, Effertz K and Ruiz-Noppinger P
11th Meeting of the European Council for Cardiovascular Research (ECCR)
29th September-1st October 2006
La Colle sur Loup, Nice, France.

The E2DISP Antigen Display Sistem
Lauman DN, Caivano A, Doria-Rose N, Domingo G, **Meoli L** , Buelow B, Sutton WF, Haigwood NL, De Berardinis P
AIDS vaccines
6th-9th September, 2005
Montreal, Quebec, Canada.

Berlin, den 15.04.2010

Luca Meoli